Università degli Studi di Milano

FACOLTÀ DI SCIENZE E TECNOLOGIE
Corso di Laurea Magistrale in Fisica

Tesi di Laurea Magistrale

A Constrained-Minimization Method for the Solution of the Inverse Kohn-Sham Problem in Nuclei

Relatore:
Prof. Gianluca Colò

Candidato:
Giacomo Accorto
Matricola 884296

Correlatore:
Dott. Xavier Roca-Maza

Anno Accademico 2017–2018

Contents

List of Figures

Introduction

Density functional theory (DFT) represents one of the most successful theoretical approaches to the study of both electronic [4] and nuclear structure [5,6]. In particular, DFT is the only theory that allows exploring systematically both medium-mass and heavy nuclei, and it is by far the model that permits to study the highest number of elements of the nuclear chart (all of them, at least in principle). The theory states a one-to-one correspondence between the correct ground state density $n(\vec{r})$ of a fermion system and the minimum value of an energy density functional (EDF) $E[n]$. Also, given the ground state density of a specific many-body system, one has access to its one-body ground state properties, such as charge and neutron radii, electric and magnetic moments, and so on [7].

The original formulation of density functional theory, provided by P. Hohenberg and W. Kohn in 1964 [8], is based on proof-by-contradiction theorems about the existence of an exact energy density functional, but do not point to any constructive method to get its form. Instead, the theory can be exploited as a rule, for precise calculations, in the Kohn-Sham scheme [9], that consists in a clever mathematical reorganization of the energy density functional. An auxiliary, non-interacting, Kohn-Sham system is uniquely defined once its density, that can be written in terms of single-particle orbitals, is set equal to that of the original system. When the equality is established, the energy density functional of the fictitious system coincides with that of the original one, as well as the ground state properties related to one-body operators. In such framework, one is able to write down the terms composing the EDF, namely a non-interacting kinetic energy term and a contribution given by an effective Kohn-Sham potential, coupled to the density. Although the formalism highly recalls that typical of mean-field methods, such as Hartree-Fock, it is remarkable that Kohn-Sham DFT provides, at least in principle, a fully exact formalism. A given level of approximation, such as local density approximation (LDA), must be applied only for practical calculations, in order to establish the form of the Kohn-Sham potential.

The present thesis addresses the solution of the inverse problem [10, 11] in Kohn-Sham density functional theory (KSDFT), in relation to nuclear systems. The problem consists in deducing the form of the Kohn-Sham potential once the density function of a nucleus is given. The aim is indeed pioneering in the field of Nuclear Physics, where the knowledge of the Kohn-Sham potential could provide an useful benchmark to the state-of-art approximate energy density functionals. In fact, the literature on the argument is almost entirely due to works that have been done in the field of Atomic and Condensed Matter Physics, or in Quantum Chemistry. The Milan Nuclear Physics research group has begun being interested in the inverse Kohn-Sham problem in 2015. Since then, three bachelor's theses, [12–14], have been devoted to the argument.

Many methods, seemingly independent of one another, have been developed

over the last thirty years to solve the inverse Kohn-Sham problem in DFT. These methods emerge from different ways of formulating the inverse problem. Some of them are based on the optimization of a functional [15, 16], while others are iterative [17–21]. The purpose of the present master's thesis is to try developing a constrained-minimization inversion algorithm, independent of, and more formal than, the one that has been used in the previous works. Our algorithm is inspired by the so-called Constrained-Variational method, that has been proposed in a recent paper by S. Jensen and A. Wasserman [22]; however, the article provides tests with analytic unidimensional densities, only. It is our scope to generalize such method to render it applicable to nuclear densities. In particular, we are interested to study of spherical symmetric magic nuclei, in which specific nuclear effects, such as the pairing, are negligible.

Chapter one of the thesis is devoted to a general review of nuclear phenomenology and to the exposition of the theoretical details concerning density functional theory.

Chapter two begins discussing the argument of inverse problems and how they require a more careful treatment than direct ones. In particular, we deepen the differences in the implementation of the the direct and inverse Kohn-Sham problem. Afterwards, we present the details of our inversion method, its theoretical assumptions, and its application to spherical symmetric systems. Finally, we discuss the methods through which the input data of the inverse problem, that is nuclear densities, are provided by the experimental literature.

The third chapter consists of a discussion of the numerical methods and libraries we used to implement the inverse problem solution and of the analysis of the results of the numerical tests we have benchmarked our software against. First, a set of unidimensional analytic tests, then a three-dimensional isotropic analytic test. The last section discusses the results we have obtained in applying the density-to-potential inversion method to the density of four magic nuclei: ^{4}He, ^{16}O, ^{40}Ca and ^{208}Pb. Finally, our conclusions will be drawn.

Chapter 1

Nuclear Density Functional Theory

1.1 Introduction to Nuclear Phenomenology and to Basic Concepts of Quantum Mechanics

1.1.1 Nuclear forces and Bulk Properties of Nuclei

Nuclei are self-bound systems, made by two types of fermions: *protons* and *neutrons*. Together, they are called *nucleons*. The forces that keep them bound are the *nuclear forces*, a general set of interactions comprising nucleon-nucleon, pionic and heavy mesons interactions. In general, a standard feature of the interactions of the many-body nuclear problem is that the forces acting between each pair of fermions involve the interplay of all hadrons, at least to some extent. In fact, depending on the scale of energy at which phenomena of interest happen, there is a different probability of producing a variety of strongly interacting particles. As we will remark below, the distance between nucleons in nuclei is large enough for the strong repulsive core of the interaction not to be felt at full by nucleons. Instead, nucleons mainly experience the softer tail of the interaction. Consider that the energy scale for removing a nucleon from a nucleus is $S_{(n,p)} \approx 10$ MeV, while the kinetic energy of nucleons in nuclei is $T \approx 40$ MeV; in contrast, the rest mass of the nucleons is $m_{(n,p)}c^2 \approx 1$ GeV, and that of the lightest existing hadron, the pion, is $m_\pi c^2 \approx 137$ MeV. A reasonable first approximation is to consider nuclei as being composed by non-relativistic nucleons. The exchange of mesons between neutrons or protons can be taken into account through the action of effective forces. Thereby, the full complexity of the nuclear forces does not come into play.

In addition to the nuclear interactions, the influence of other weaker forces cannot be neglected. For instance, protons indeed feel, and generate, electromagnetic fields. Also, the presence of weak interactions manifests itself in processes such as β-decays. Albeit such minor forces are not fundamental for establishing the main bulk properties of the nuclear structure, they play an important role in determining the stability of bound states.

Because of the short range of the nuclear forces, all nuclei are characterized, in

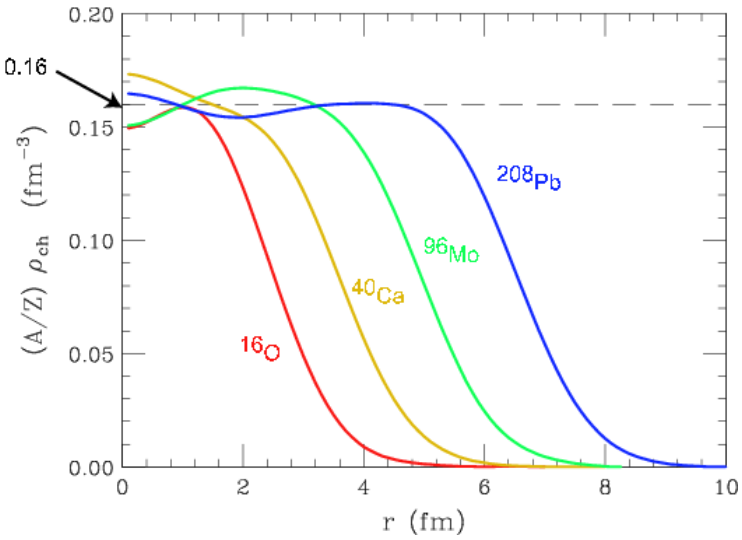

Figure 1.1: The nuclear density, in the inner part of nuclei, is in good approximation constant and independent of the mass number.

their interior part, by an approximately constant density (see figure 1.1) with value

$$n(0) = 0.16 \text{ fm}^{-3} \tag{1.1}$$

and by a volume that grows qualitatively in proportion with the mass number A. The density typically decay to zero over a distance of 2 fm; therefore the surface thickness of nuclei is rather small if compared to their radial extent R, defined as the distance at which the density has become half of its interior value $n(0)$. An empirical value for this quantity is given by

$$R = r_0 A^{\frac{1}{3}}; \tag{1.2}$$

electron elastic scattering data determine $r_0 = \left(\frac{3}{4\pi n(0)}\right)^{\frac{1}{3}} \approx 1.15$ fm.

The available data about nuclear matter distributions almost entirely consists of proton densities [1]. The neutron density of few isotopes of lead and tin have been obtained via proton scattering [2]. In heavy nuclei, the excess of neutrons with respect to protons gives rise to differences between the densities of the two types of nucleons.

Another important feature of nuclei is the value of the mean free path for the collision between the constituent nucleons. Many are the evidences that the mean free path in a nucleus is large in comparison with the nuclear size. Such long mean free path of the nucleons entails that the interactions, in first approximation, result in a smooth average potential, in which the particles move almost independently one of each other.

A simple way to understand the main trends characterizing the nuclear structure is to analyse the well-known semi-empirical expression provided by Weizsäcker in 1935 for the total nuclear binding energy. Such quantity is defined as the difference between the observed total nuclear energy in the ground state and the rest masses of the separeted nucleons. Based on the rough features we have discussed above, it is

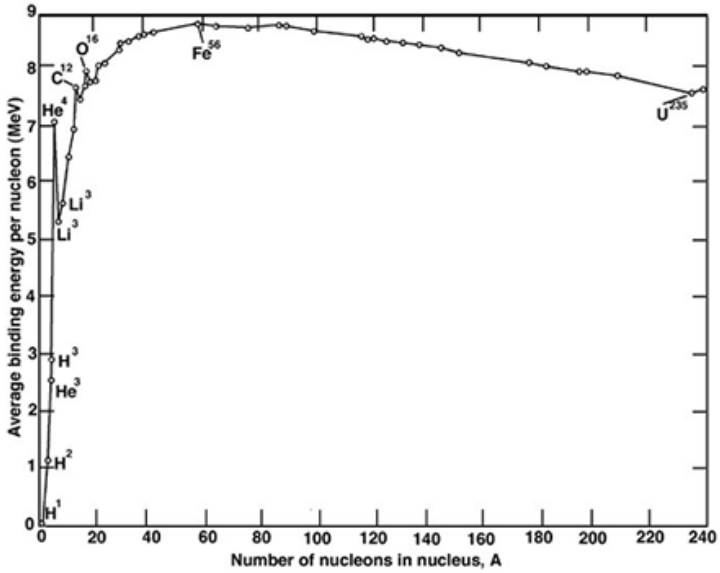

Figure 1.2: The binding energy per nucleon is, in first approximation, a constant function.

possible to write down a simple mass formula for the binding energy:

$$\mathscr{B} = b_{\text{vol}} A - b_{\text{surf}} A^{\frac{2}{3}} - \frac{1}{2} b_{\text{sym}} \frac{(N-Z)^2}{A} - \frac{3}{5} \frac{Z^2 e^2}{R_{\text{c}}} \tag{1.3}$$

- $b_{\text{vol}} A$ is the main, always present, volume energy term. It represents the limit of the binding energy for large A, $N = Z$ nuclei, in absence of Coulomb forces. The bulk binding energy of a nucleus is proportional to A and not to $A(A-1)/2$ because of the short range of the interaction: each nucleon interacts with its neighbours, only.

- $b_{\text{surf}} A^{\frac{2}{3}}$ is the surface energy, a contribution typical of finite systems, that reflecs the fact that particles are less bound at the surface, for they have less neighbours.

- The third term takes into account the fact that symmetric configurations of nuclei are energetically preferred. The Pauli principle enforces protons and neutrons to occupy energy levels with increasing energy. An inbalance of one type of fermion with respect to the other implies higher energy levels to be occupied.

- The last term represents the Coulomb energy of a uniform sphere with radius R_{c} and it is responsible for the slight, gradual, decrease of the binding energy per particle that can be observed in heavy nuclei. Also, it causes the excess of neutrons in heavy stable nuclear systems.

Figure 1.2 clearly shows the above trends. Although the Weizsäcker formula is subject to improvements by the addition of extra terms, such as a pairing, it does remain an empirical, qualitative tool, that completely neglects quantum effects.

However, it is a noteworthy example of how different effects interplay in nuclear systems and it accounts for their relative relevance.

From the observed binding energies, one can deduce the order of magnitude of the average potential energy that a single nucleon feels in a nucleus. The energy that is required to remove a neutron from a nucleus, namely the neutron separation energy, is

$$\mathscr{B}(N,Z) - \mathscr{B}(N-1,Z) \approx 10 \text{ MeV} \approx -(\mathrm{V_n} + \epsilon_\mathrm{F}). \tag{1.4}$$

Since $\epsilon_F \approx 40$ MeV, we expect such average potential, felt by a single nucleon, to be characterized by a depth of $V_n \approx -50$ MeV.

Just as in the electronic structure of atoms, the degeneracy of single-particle orbitals entails marked discontinuities, namely shell effects, in many nuclear properties. Therefore, nuclear configurations based on energy levels of nucleons in nuclei can be developed. Those constitute the nuclear shell structure.

1.1.2 Basic Concepts of Quantum Mechanics

Before explaining in detail how to develop the Nuclear Shell Model, let us recall some basic concepts of quantum mechanics. This will be useful in order to set the notation, a proper enviroment for the theoretical models exposed in the rest of the chapter and to define some relevant quantities.

The investigation of nuclei in their ground state concerns the solution of the time-independent *Schrödinger equation*. In fact, time-reversal symmetry holds in many cases of interests, namely in the study of even-even nuclei. For an A-particle system in the non-relativistic approximation, the Schrödinger equation has the structure of an eigenvalue problem,

$$\hat{H}\Psi = E\Psi, \tag{1.5}$$

where E is the energy of the nucleus, $\Psi = \Psi(\vec{x}_1, \ldots, \vec{x}_N)$ is the total *wave function* of the system, $\hat{H}$ is the *Hamiltonian operator*,

$$\hat{H} = \hat{T} + \hat{V} + \hat{W} = -\sum_{i=1}^{A} \frac{\hbar^2}{2m_i}\nabla_i^2 + \sum_{i=1}^{A} v(\vec{x}_i) + \sum_{i\neq j} w(\vec{x}_i, \vec{x}_j), \tag{1.6}$$

and the coordinates $\vec{x}_i$ comprise both the space coordinates $\vec{r}_i$ and the spin coordinates σ_i. The form of such Hamiltonian is pretty general. The idea is to provide an interdisciplinary notation, valid for the study of different fermionic system. It is clear that, for instance, in the nuclear case no external potential is present. On the other hand, as we have discussed above, the relevance of three-body interactions is quantitative. However, equation (1.6) is adequate to the purpose of presenting, in the next sections, the background theory that is fundamental to understand the scopes of the work of thesis.

Boundary conditions are required to make the problem solvable. In particular, the wave function Ψ must be well-behaved, that is smooth, everywhere. For the case of a finite nucleus, the wave function must decay to zero at infinity; if one investigates infinite nuclear matter, it must respect periodic boundary conditions. Because of the fermionic nature of the nucleons, the wave function Ψ must be antisymmetric with respect to the interchange of two particles.

Consider the set of the eigenvectors Ψ_k of $\hat{H}$, associated to the energy eigenvalues E_k. It follows from basic algebraic theorems that the set $\{\Psi_k\}_k$ is complete, and its elements can be chosen as orthogonal and normalized. Among all of the eigenvectors,

there is one that is related to the lowest energy eigenvalue E_0: the ground state wave function Ψ_0.

Each property of the system in some state can be calculated via an integration over $3N$ spatial coordinates and a summation over N spin coordinates. For instance, the expectation value of an observable, linked to a Hermitian linear operator $\hat{A}$, is given by

$$\langle \hat{A} \rangle = \frac{\int_\Omega d\vec{x}\, \Psi^* \hat{A} \Psi}{\int_\Omega d\vec{x}\, \Psi^* \Psi} = \frac{\langle \Psi | \hat{A} | \Psi \rangle}{\langle \Psi | \Psi \rangle}. \tag{1.7}$$

One can read the equation above in the sense that $\langle \hat{A} \rangle$ is a *functional* of the state Ψ,

$$\langle \hat{A} \rangle = A[\Psi]. \tag{1.8}$$

Consider the measurement of the energy expectation value

$$E[\Psi] = \frac{\langle \Psi | \hat{H} | \Psi \rangle}{\langle \Psi | \Psi \rangle}; \tag{1.9}$$

each measurement of the energy gives as a result a linear combination of the eigenvalues E_k of $\hat{H}$. The ground state energy is the global lower bound of the energy, as computed from any Ψ. A full minimization of the functional $E[\Psi]$ with respect to all the allowed A-nucleons wave functions is therefore the ground state energy

$$E[\Psi_0] = E_0 = \min_\Psi E[\Psi]. \tag{1.10}$$

In fact, it is indeed always possible to decompose any state Ψ on the complete set of the eigenstates of the Hamiltonian

$$\Psi = \sum_{k=1}^{N} C_k \Psi_k. \tag{1.11}$$

This decomposition can be explicitely inserted into the energy functional

$$E[\Psi] = \frac{\sum_{k=1}^N |C_k|^2 E_k}{\sum_{k=1}^N |C_k|^2}. \tag{1.12}$$

Since it is always possible to establish an ordering of the energy spectrum as $E_0 \leq E_1 \leq E_2 \leq \cdots \leq E[\Psi]$, $E[\Psi]$ will be greater than the eigenvalue E_0 and the minimum will be reached if and only if $\Psi = C_0 \Psi_0$. Every eigenstate of the Schrödinger equation is a local extremum of $E[\Psi]$, and it is therefore possible to replace the Schrödinger equation itself with the variational principle

$$\delta E[\Psi] = 0. \tag{1.13}$$

It is possible to reformulate the variational principle in such a way that the final state Ψ will be automatically normalized; one extremizes the quantity $\langle \Psi | \hat{H} | \Psi \rangle$ subject to the constraint $\langle \Psi | \Psi \rangle = 1$. According to the Lagrange multipliers method (see appendix A) this can be done by imposing

$$\delta [\langle \Psi | \hat{H} | \Psi \rangle - E \langle \Psi | \Psi \rangle] = 0. \tag{1.14}$$

The above procedure prescibes a method for moving from the piece of information about N and $v(\vec{r})$, to the ground state wave function Ψ_0, and hence to the ground-state properties of interest. It is very remarkable that the kinetic term and the inter-particle potential, depending only on the numeber N of nucleons, are not mentioned at all by the procedure: they are universal, in a sense that will be deepened below, by means of the Hohenberg and Kohn theorems. We highlight again that the energy $E[\Psi]$ is a functional of N and $v(\vec{r})$, alone.

1.1.3 Nuclear Shell Model

It is easy to understand that finding an exact solution of the Schrödinger equation for finite systems, such as nuclei, often reveals to be highly difficult. Luckily, most of the properties of finite nuclei can be well predicted within models that make use of approximate single-particle potentials. We remark again that the usage of single-particle potentials is thoretically justified by the long mean free path of nucleons in nuclei. The simplest forms of the single-particle potential one can consider are the infinite square-well potential and the harmonic potential, in spherical symmetry. Those provide the starting point for introducing the single-particle *Nuclear Shell Model* at its roughest approximation.

In the former case, the eigenfunctions of the Schrödinger equation, respecting proper boundary conditions, read

$$\Psi_{nlm_l}(\vec{r}) = N_{nl}\, j_l(kr)\, Y_{lm_l}(\theta,\phi), \tag{1.15}$$

where N_{nl} is a normalization constant, j_l are Bessel functions and Y_{lm_l} are the well-known spherical harmonics. Such eigenfunctions must vanish at the boundary of the well, which means that $k_{nl}R = X_{nl}$ must be the n^{th} zero of the l^{th} Bessel function. Their corresponding energy eigenvalues are

$$\epsilon_{nl} = \frac{\hbar^2 k_{nl}^2}{2m} - v_0. \tag{1.16}$$

The ordering of those eigenvalues produces the energy levels.

A second solvable single-particle potential is the three-dimentional isotropic harmonic oscillator

$$v(r) = -v_0 + \frac{1}{2} m\omega^2 r^2. \tag{1.17}$$

Consider an *Ansatz* of the eigenfunctions in the form

$$\Psi_{nlm_l}(\vec{r}) = \frac{u_{nl}}{r} Y_{lm_l}(\theta,\phi). \tag{1.18}$$

When those are inserted into the Schrödinger equation, they give rise to a radial differential equation

$$\Big[-\frac{\hbar^2}{2m}\frac{d^2}{dr^2} + v(r) + \frac{\hbar^2}{2m}\frac{l(l+1)}{r^2} - (\epsilon_{nl} + v_0)\Big], \tag{1.19}$$

that is solved by

$$u_{nl}(r) = N_{nl}\, q^{l+1} e^{-\frac{q^2}{2}} L_{n-1}^{l+\frac{1}{2}}(q^2) \tag{1.20}$$

$$L_p^a(z) = \frac{\Gamma(a+p+1)}{\Gamma(p+1)} \frac{e^z}{z^a} \frac{d^p}{dz^p}(z^{a+p} e^{-z}) \tag{1.21}$$

$$N_{nl} = \frac{2(n-1)!}{b[\Gamma(n+l+\frac{1}{2})]^3}; \tag{1.22}$$

where $q = \frac{r}{b}$, $b^2 = \frac{\hbar}{m\omega}$ and $L_p^a(z)$ are the generalized Laguerre polynomials. The spectrum of energies is obviously that of a harmonic oscillator

$$\epsilon_{nl} = \hbar\omega(N + \frac{3}{2}) - v_0, \tag{1.23}$$

$$N = 2(n-1) + l = 0, 1, 2, \ldots, \tag{1.24}$$

and produce the *oscillator shells*, each spaced from the other by $\hbar\omega$. A proper semi-empirical value for the level spacing is $\hbar\omega \approx 41/A^{\frac{1}{3}}$ MeV. Such value is a rough estimate thought in order to fit to mean-square radii of nuclei.

Albeit the true nuclear single-particle potential should definitely have a finite depth, the two previous approximations yield to a rather acceptable prediction of low-lying levels, those with higher binding energy. The higher is the quantum number l, the closer the levels are to the edge of the true well. The square-well potential in general predicts stronger bindings than the harmonic oscillator potential.

Having defined such shell configuration of nucleons, one finds that a particular stability is reached for closed-shell configurations. In particular, the highest stability is found in correspondence of numbers of protons or neutrons equal to $2,8,20,28,50,82,126,\ldots$ (see figure 1.3). Nuclei with such number of protons or neutrons are called *magic* or *doubly magic nuclei* and they are characterized by spherical symmetry.

Both the harmonic oscillator and the square well shell model correctly predict only the first three shell clusures. In 1955 M. G. Meyer and J. H. D. Jensen [23] proposed to consider a single-particle spin-orbit interaction term

$$H'(r) = -\alpha(r)\hat{L}\cdot\hat{S}, \tag{1.25}$$

where $\alpha(r)$ is a coupling costant, while $\hat{L}$ and $\hat{S}$ are the angular momentum and the spin operators, respectively. Such term is much more relevant that in the atomic case, and its presence leads to the appearance of a splitting of levels characterized by different total angular momentum. In the case of nuclear bindings the spin-orbit levels with higher total angular momentum j at given l are found to lie lower in energy; To account for this evidence, the spin-orbit interaction must be attractive, that is the coupling constant must be positive. The best choice of quantum numbers to treat the spin-orbit term is indeed the coupled basis $|nl\frac{1}{2}jm_j\rangle$. The first order splitting is equal to

$$\epsilon_{l-\frac{1}{2}} - \epsilon_{l+\frac{1}{2}} = \alpha_{nl}\frac{2l+1}{2} > 0 \tag{1.26}$$

$$\alpha_{nl} = \int dr\; u_{nl}^2(r)\alpha(r). \tag{1.27}$$

The addition of this term allows to predict the correct magic numbers, since it can happen that high j and l levels may be pushed from one shell to the lower one.

Many developments of the shell model have been performed, such as the addition of new terms to the potential, or the choice of a different single-particle potential. For instance, a more realistic choice of the single-particle potential is the Woods-Saxon potential, corrected by including an asymmetric term accounting for neutrons excess in the nucleus,

$$V_{WS(p,n)}(r) = \left(-51 \pm 33\frac{N-Z}{A}\right)\frac{1}{1+e^{\frac{r-R}{a}}}. \tag{1.28}$$

It is not our scope to discuss further about the Shell Model; more details can be found in [24–26].

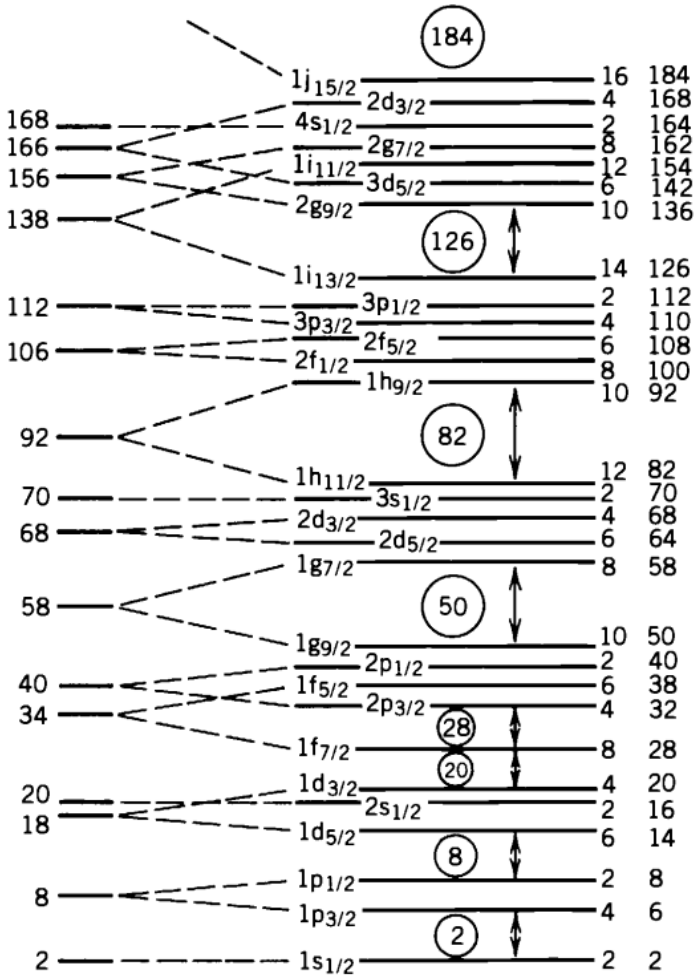

Figure 1.3: The nuclear shell structure; on the left the oscillator shells, on the right the spin-orbit interaction produces the j-splitting and predict the correct magic numbers.

1.2 Density Functional Theory

Theoretical many-body approaches to describe nuclear structure have been developed since the discovery of the neutron. Among those, an important role is played by nuclear energy density functionals (EDFs). Here, the energy of the system is a functional of the density. The functionals also contain a certain number of parameters, whose value is fitted to nuclear many-body data, such as binding energies or charge radii of few nuclei along the chart. There exist three main categories of nuclear energy density functionals: there are delta-shaped, zero-range (contact) forces, such as the so-called Skyrme-type interactions [27]; others rely on finite-range, Gaussian-shaped, forces and go under the name of Gogny-type interactions [28]; finally, relativistic nuclear energy density functionalss are covariant and yield to a natural inclusion of the spin degree of freedom to a unique parametrization of time-odd components of the mean-field [29].

Since the very first works on EDFs, it has been noticed that a density-dependence of the effective potentials is necessary to the aim of reproducing basic many-body properties of nuclear structure. Such semi-empirical feature has been explained in the framework of the nuclear density functional theory (DFT). The charm of the theory lies in the possibility of predicting, in principle exactly, the ground state properties of the system under investigation. Moreover, the computational cost that must be paid is incredibly low. The advantage of treating the density, a function of three space variables x, y, and z, as a basic variable, in contrast to the involved many-variable total wave function, is evident. DFT gives then access to the study of systems that can be very large in the sense of their degrees of freedom. Nowadays, DFT is the only theory that allows exploring systematically both medium-mass and heavy nuclei, and it is by far the model that permits to study the highest number of elements of the nuclear chart (all of them, at least in principle).

The density function is a quantity related to the wave function of the system. Such quantity is fundamental for the purposes of the thesis and it is the cornerstone of density functional theory and its inverse problem. The *nuclear density* is defined as the number of nucleons per unit of volume in a given state Ψ,

$$n(\vec{r}_1) = A \int \cdots \int |\Psi(\vec{x}_1, \ldots, \vec{x}_A)|^2 d\sigma_1 d\vec{x}_2 \ldots d\vec{x}_A, \tag{1.29}$$

and it integrates to the total number of nucleons in the system

$$\int d\vec{r}_1 \; n(\vec{r}_1) = A. \tag{1.30}$$

A more formal definition of the density function, thought as the local, one-body restriction of density matrices, is provided in the appendix B. In particular, it can be shown that such density matrices carry the very same piece of information as the total wave function, thus justifying the subtitution of basic variable we have mentioned above.

The Thomas-Fermi (TF) model, as it was proposed in the 1920s, was the first one to suggest the possibility of determining the energy of an electron system as an approximate functional of the density, only. The TF energy density functional reads

$$E_{TF}[n] = C_{TF} \int d\vec{r} [n(\vec{r})]^{\frac{5}{3}} - \int d\vec{r} \frac{n(\vec{r})}{|\vec{r}|} + \frac{1}{2} \int \int d\vec{r}_1 \, d\vec{r}_2 \frac{n(\vec{r}_1) n(\vec{r}_2)}{|\vec{r}_1 - \vec{r}_2|}. \tag{1.31}$$

For decades, the Thomas-Fermi model has been thought to be oversimplified, because of its very limited predictive power mainly due to its strong assumptions. The

idea of treating the properties of a system as functionals of the density alone was later developed by Hohenberg and Kohn; in 1964 [8] they provided three fundamental theorems, that showed that the Thomas-Fermi model may be thought as an approximation of a many-body exact theory: the density functional theory.

1.2.1 Hohenberg-Kohn Theorems

In general, the determination of the ground state energy and of the ground state wave function of a given fermion system would require both the knowledge of the number A of particles composing the system, *and* that of the external potential $v(\vec{r})$ to which the system is subject. The first Hohenberg and Kohn theorem justifies the usage of the local density $n(\vec{r})$, alone, as a basic variable, in place of A and $v(\vec{r})$. It is trivial that the density uniquely determines the number of particles A. It is much more remarkable the fact that the external potential $v(\vec{r})$ can be identified, up to an arbitrary constant, by the density $n(\vec{r})$. The inter-particle potential, as well as the kinetic term, are in principle fixed once one considers a given type and number of fermions.

The First Hohenberg and Kohn Theorem. *Given a system of A interacting particles, described by the Hamiltonian*

$$\hat{H} = \hat{T} + \hat{V} + \hat{W} = -\sum_{i=1}^{A} \frac{\nabla_i^2}{2m_i} + \sum_{i=1}^{A} v(\vec{r}_i) + \sum_{i \neq j} w(\vec{r}_i, \vec{r}_j), \tag{1.32}$$

its A-body wave function Ψ*, and the corresponding density* (1.29)*, the non-degenerate ground state wave function is a unique functional of the ground-state density:*

$$\Psi_0(\vec{r}_1 \ldots, \vec{r}_A) = \Psi[(n_0(\vec{r})]. \tag{1.33}$$

Thereby, the ground state expectation value of each observable is a functional of $n(\vec{r})$*, alone.*

Proof. The density trivially determines A by quadrature. It is then just necessary to show, as we have already mentioned, that it determines $v(\vec{r})$, too. Suppose there were two external potential v and v', differing by more than a constant, both related to the same ground state density n obtained as the solution of the Schrödinger equation. Then, there would exist two different Hamiltonians, $\hat{H}$ and $\hat{H}'$, whose ground state density were the same, even though the normalized wave functions Ψ and Ψ' would be different. Let Ψ' be a trial wave function for the $\hat{H}$ problem; then,

$$\begin{aligned} E_0 < \langle \Psi' | \hat{H} | \Psi' \rangle &= \langle \Psi' | \hat{H}' | \Psi' \rangle + \langle \Psi' | \hat{H} - \hat{H}' | \Psi' \rangle \\ &= E_0' + \int d\vec{r}\; n(\vec{r})[v(\vec{r}) - v'(\vec{r})] \end{aligned} \tag{1.34}$$

The same is indeed true if we interchange the dummy primed variables

$$\begin{aligned} E_0' < \langle \Psi | \hat{H}' | \Psi \rangle &= \langle \Psi | \hat{H} | \Psi \rangle + \langle \Psi' | \hat{H}' - \hat{H} | \Psi' \rangle \\ &= E_0 + \int d\vec{r}\; n(\vec{r})[v'(\vec{r}) - v(\vec{r})] \end{aligned} \tag{1.35}$$

By summing the two inequalities, one finds $E_0 + E_0' < E_0' + E_0$, which is absurd. There cannot therefore be two different potentials v providing the same ground state density n. □

In the same fashion of the Thomas-Fermi model, the total energy can be viewed as a functional of the density.

The Second Hohenberg and Kohn Theorem. *There exists a universal functional $F_{HK}[n]$, such that the total energy functional reads $E_v[n] = F_{HK}[n] + V[n] = T[n] + W[n] + V[n]$. The* Hohenberg and Kohn functional *$F_{HS}[n]$ is universal for a given particle-particle interaction and for a given number of particles in the system, since it does not depend on the external potential $v(\vec{r})$.*

Finally, a third theorem states an energy varational principle for the ground state energy, involving again the density alone.

The Third Hohenberg and Kohn Theorem. *Given some trial density $\widetilde{n}(\vec{r})$, such that*

$$\widetilde{n}(\vec{r}) \geq 0 \tag{1.36}$$

$$\int d\vec{r}\ \widetilde{n}(\vec{r}) = A \tag{1.37}$$

The ground state energy is a global minumum of the total energy,

$$E_0 = E_v[n] \leq E_v[\widetilde{n}] \tag{1.38}$$

Proof. Because of the first Hohenberg and Kohn theorem, $\widetilde{n}$ determines its own $\widetilde{v}$ and its $\widetilde{\Psi}$, up to a phase factor. Consider such wave function as a trial for the $\hat{H}$ problem,

$$\langle\widetilde{\Psi}|\hat{H}|\widetilde{\Psi}\rangle = \int d\vec{r}\ \widetilde{n}(\vec{r})\, v(\vec{r}) + F[\widetilde{n}] = E_v[\widetilde{n}] \geq E_v[n]. \tag{1.39}$$

□

If $E_v[n]$ is assumed to be differentiable, the third Hohenberg theorem can be written in the fashion of the method of Lagrange multipliers,

$$\delta\Big[E_v[n] - \mu\Big(\int d\vec{r}\ n(\vec{r}) - A\Big)\Big], \tag{1.40}$$

where μ is the *chemical potential*

$$\mu = \frac{\delta E_v[n]}{\delta n(\vec{r})} = v(\vec{r}) + \frac{\delta F_{HK}[n]}{\delta n(\vec{r})}. \tag{1.41}$$

The possibility to have an exact theory urges, and have urged, people to attempt determining an exact, or properly approximate, structure of the universal functional $F_{HK}[n]$. In fact, once we had its explicit form, we could apply density functional theory to any system. Unfortunately, this reveals to be an incredibly difficult task. The reason of that is indeed pretty clear, since all of the complications contained in the many-variable wave function Ψ could not have disappeared at once by moving to the usage of the simple density function as the basic variable of the many-body problem. Most of the attempts to provide approximate form of $F_{HK}[n]$ rely on drastic assumptions, but it is still very remarkable that we have a well-defined procedure for finding the ground state properties of a possibly huge amount of systems.

1.3 Levy-Lieb Constrained-Search Formulation of DFT

1.3.1 N-Representable and v-Representable Densities

The ground state wave function of a system described by a given Hamiltonian detemines the ground state density. The Hohenberg and Kohn theorems define then a one-to-one mapping between the density function and the external potential $v(\vec{r})$, up to an arbitrary constant. If one is able to provide a form of the universal functional $F_{HK}[n]$, the correct ground state density then determines uniquely the ground state energy.

We call a density *$v-$representable* if it is the related to the antisymmetric ground state wave function of a Hamiltonian of the type (1.6). It is important then to give a more precise fomulation of the first Hohenberg and Kohn theorem: *There exists a one-to-one map between the ground state wave function of each many-body quantum system and the v-representable density of such system.* The functionals composing the energy density functional are at this point defined for v-representable densities, only.

There is a major complication associated to v-representable densities: it is anything but straightforward that a given density is v-representable, since it seems there does not exist any condition for a trial density to be v-representable[1]. It has been shown that many given densities are not v-representable [31].

Here it comes the relevance of a new formulation of density functional theory, in terms of densities that satisfy a weaker condition, namely the N-representability condition. A density is *N-representable* if it can be obtained from an antisymmetric wave function. This condition is satisfied by any reasonable one-body local density and it is a necessary condition for v-representability. By reasonable density we mean that a density is N-representable if it satisfies the so-called Gilbert conditions:

$$n(\vec{r}) \geq 0, \tag{1.42}$$

$$\int d\vec{r}\; n(\vec{r}) = N, \tag{1.43}$$

$$\int d\vec{r}\; |\nabla\sqrt{n(\vec{r})}|^2 < \infty. \tag{1.44}$$

The last condition is a smoothness requirement on the density function form. For instance, wild oscillations of the density preclude N-representability. In other words, a N-representable density can be written in terms of N orthonormal orbitals, that generates $n(\vec{r})$ from a single-determinantal wave function [32]. Levy and Lieb independently provided such reformulation in 1980, and the next section is devoted to discuss that.

Before facing the details of the Levy-Lieb formulation of DFT, that implements N-representability into DFT, let us better comprehend how a N-representable density can be built in the one-dimensional case $x_1 \leq x \leq x_2$, starting from N smooth, continuous, and orthonormal orbitals. The constast with the non-constructive definition of the v-representable densities will be then fully perceptible.

Consider the orbitals

$$\phi_k(x) = \sqrt{\frac{n(x)}{N}}\, e^{i2\pi k \int_{x_1}^{x} dx\, \frac{n(x)}{N}}, \tag{1.45}$$

[1] Except for some simple dicrete systems [30]

where $k = 0, \pm 1, \pm 2, \ldots$ or $k = \pm\frac{1}{2}, \pm\frac{3}{2}, \ldots$; it holds that

$$|\phi_k(x)|^2 = \frac{n(x)}{N}, \tag{1.46}$$

and

$$\int_{x_1}^{x_2} dx\, \phi_k^*(x)\phi_l(x) = \delta_{kl}. \tag{1.47}$$

Any given one-dimensional density can represented as

$$n(x) = \sum_k^M \lambda_k |\phi_k|^2 \tag{1.48}$$

with $0 \leq \lambda_k \leq 1$ and $M \geq N$. This proves the sufficiency of the Gilbert condition in the one-dimentional case. Further details on the so-called N-representability problem can be found in [33].

1.3.2 Levy-Lieb Constrained-Search Formulation

By definition, there exists an infinite number of antisymmetric wave functions that reproduce the same correct ground-state density; thereby, one could ask how to distinguish the true ground state wave function Ψ_0 from some Ψ_{n_0} that also integrates to the correct ground state density n_0. In other words, the question is how to point, among the generic N-representable densities, to the v-representable density that comes from the true ground state wave function of the Hamiltonian.

This critical theoretical issue of the Hohenberg and Kohn formulation of density functional theory can be solved by extending the domain of the energy density functional $E_v[n]$ from v-representable densities to the larger set of N-representable densities. The idea, as suggested by Levy [34] and Lieb, is to exploit the minimum-energy principle, that uniquely identifies the true ground state wave function

$$\langle \Psi_{n_0} | \hat{H} | \Psi_{n_0} \rangle \geq \langle \Psi_0 | \hat{H} | \Psi_0 \rangle = E_0. \tag{1.49}$$

The expression above is given by the sum of the expectation value of the universal functional

$$F_{HK}[n_0] = \langle \Psi_0 | \hat{T} + \hat{W} | \Psi_0 \rangle, \tag{1.50}$$

$$= \min_{\Psi \to n_0} \langle \Psi | \hat{T} + \hat{W} | \Psi \rangle, \tag{1.51}$$

defined for any v-representable density, and that of the external potential term, coupled to the density. Levy and Lieb formulation writes the minimum energy principle in order to render more explicit the fact that the variational search is constrained (compare (1.50) and (1.51)); the trial space for the wave functions is restricted only to those that reproduce the requested v-representable density n_0 by quadrature. Using this clever reorganization, it is straighforward to extend the domain of the universal functional to N-representable densities n

$$F_{LL}[n] = \min_{\Psi \to n} \langle \Psi | \hat{T} + \hat{W} | \Psi \rangle. \tag{1.52}$$

Note that $F_{LL}[n_0] = F_{HK}[n_0]$.

A double hierarchy minimization for the ground state energy calculation stems then out,

$$E_0 = \min_{\Psi} \langle \Psi | \hat{T} + \hat{W} + \hat{V} | \Psi \rangle \tag{1.53}$$

$$= \min_{n} \Big\{ \min_{\Psi \to n} \Big[\langle \Psi | \hat{T} + \hat{W} + \hat{V} | \Psi \rangle \Big] \Big\} \tag{1.54}$$

$$= \min_{n} \Big\{ F_{LL}[n] + \int d\vec{r}\; n(\vec{r})\, v(\vec{r}) \Big] \Big\} \tag{1.55}$$

The existence of the minimum has been proved by Lieb in 1982 [35]. The Levy-Lieb constrained-search formulation of DFT removes the original issues associated to v-representability. The optimization procedure proceeds in two different steps; first one search the optimal wave function which reproduce a given density. The density trial space is explored, and at the end of the first minimization one has in its hands a set of local minima. The sense of the second minimization is simply to identify the global minimum among those.

1.4 Kohn-Sham Density Functional Theory

The Kohn-Sham scheme gives an insight on the Hohenberg-Kohn theorem, and especially on the structure of the universal functional $F_{HK}[n]$. In fact, Kohn and Sham, by mathematical reorganizing the energy density functional, reformulated density functional theory [9], turning a theory highly difficult to be handled into a practical tool for precise calculations.

A set of effective single-particle Kohn-Sham equations are introduced for an auxiliary *Kohn-Sham system* of N non-interacting particles, described by the Hamiltonian $\hat{H}_{KS} = \hat{T}_{KS} + \hat{V}_{KS}$. Exploiting the first Hohenberg-Kohn theorem, one asserts that for any interacting system there exists an unique, local, single-particle potential $v_{KS}(\vec{r})$ such that the exact ground state density of the interacting system equals that of a non-interacting reference system:

$$n(\vec{r}) = n_{KS}(\vec{r}) = \sum_{i=1}^{N} \sum_{\sigma} |\phi_i(\vec{r},\sigma)|^2 \tag{1.56}$$

For such reference system, the total ground-state wave function is determinantal

$$\Phi_{KS} = \frac{1}{\sqrt{N!}} |\phi_1 \phi_2 \dots \phi_N|, \tag{1.57}$$

and the ϕ_i can be found as the lowest eigenstates of the single-particle Hamiltonian H_{KS}:

$$H_{KS}\phi_i(\vec{r}) = \epsilon_i \phi_i(\vec{r},\sigma). \tag{1.58}$$

The orbitals are unique functionals of the density $\phi_i = \phi_i([n],\vec{r})$, too. The energy functional reads (let us drop the subscripts for the universal functional)

$$E[n] = F[n] + \int d^3r \; v_{KS}(\vec{r}) n(\vec{r}) \tag{1.59}$$

$$= T[n] + W[n] + \int d^3r \; v_{KS}(\vec{r}) n(\vec{r}) \tag{1.60}$$

$$= E_{KS}[n] = T_{KS}[n] + \int d^3r \; v_{KS}(\vec{r}) n(\vec{r}) \tag{1.61}$$

$$= -\frac{\hbar^2}{2m} \sum_i \langle \phi_i | \nabla^2 | \phi_i \rangle + \int d^3r \; v_{KS}(\vec{r}) n(\vec{r}) \tag{1.62}$$

and it is minimized by the correct ground state density of $\hat{H}_{KS}$. This scheme brings the universal functional to split into

$$F[n] = T_{KS}[n] + U[n] + E_{xc}[n], \tag{1.63}$$

where the first term is the non-interacting kinetic energy, the second term is the local Hartree term, while the third term is formally defined, throug the previous eqution, as $E_{xc} = T[n] + W[n] - U[n] - T_{KS}[n]$, and it gathers all the quantum many-body effects. Thereby, we have a structure for the Kohn-Sham potential

$$v_{KS}([n],\vec{r}) = v_H([n],\vec{r}') + v_{xc}([n],\vec{r}) \tag{1.64}$$

and the exchange-correlation potential is

$$v_{xc}(\vec{r}) = \frac{\delta E_{xc}}{\delta n}. \tag{1.65}$$

The Kohn-Sham density functional theory (KSDFT) framework has the advantage of being fully local. Its accuracy depends only on the approximation of the unknown exchange-correlation energy, which nevertheless is universal. The first level of approximation, consisting in fully neglecting E_{xc}, delivers the Hartree equations. Still, the scheme goes far beyond the Hartree mean-field approximation, even only because it takes into account all the correlation effects and it is, in principle, exact. Another possible approximation scheme is LDA, in which the exchange-correlation term is taken equal to that of an infinite uniform system:

$$E_{xc}^{\mathrm{LDA}} = \int d\vec{r}\; n(r)\epsilon_{xc}[n]. \tag{1.66}$$

Among the state-of-art beyond-LDA approximation schemes the most relevant is the generalized-gradient-approximation (GGA). See [36] for more details. However, since DFT is an exact non-perturbative theory, it results very difficult to find a clear direction for systematic improvements of the level accuracy of the calculations.

Chapter 2

Inverse Problem in Nuclear Kohn-Sham Density Functional Theory

2.1 Forward and Inverse Problems

The definition itself of inverse problems comes in opposition to that of direct, or forward, problems. A *direct problem* deals with the calculation of a quantity, e. g. the density of some system or its evolution in time, as a function of its causes, for instance the interaction between the constituent particles or the equation of motion. Direct problems can usually be expressed through a system of differential equations that fully determine their evolution. On the other hand, *inverse problems* typically arise whenever one tries to perform the indirect observation of some quantity of interest. Here, the knowledge of some observable is given, and one aims to calculate the causes that have resulted in that. It is a matter of fact that inverse problems often present features of non-locality and non-causality. Those features contributes generating instabilities of the solution of the problem [37].

For instance, consider the inverse heat equation problem, namely the attempt of estimating an initial temperature distribution, based on the measurement of the temperature distribution at some final time. It is easy to understand that an infinity of different initial conditions may have ended up into the same final state: small changes in the initial temperature could have smeared out in time. On the contrary, however complex the system could be, the corresponding forward problem is local and casual: it is guided by the well-known heat equation.

Another example is given by the calculation of the gravitational field of the Earth, given the knowledge of its density (direct problem) versus the estimate of the density the Earth given the knowledge of the generated gravitational field (inverse problem).

In the inverse problem case, one must incorporate all available information about the initial data that one may had prior to the measurement. It is not the scope of the present thesis to deepen the formalism within which this can be done; more details can be found, again, in [37].

In the next section we will focus on inverse problems seen as possibly *ill-posed problems* and on the regularization techniques one can apply to solve them.

2.2 Regularization techniques for Ill-posed Problems

The mathematical definition of *well-posed problem* was first stated by Jacques Hadamard. He pointed out three properties that any mathematical model, aiming to describe a physical system, should respect. They are:

- the existence of a solution of the problem;
- the uniqueness of the solution;
- the continuous dependence of the solution on the input data. This means that small enough changes in the initial conditions entail small changes in the solution.[1]

A problem is well-posed when the above three conditions are fulfilled, while it is said to be an *ill-posed problem* if any of those is defective.

Forward problems are in most of cases well-posed ones. Because of that there is a good chance of being able to implement stable algorithms to produce solutions. On the other hand, inverse problems are often ill-posed. The existence of an analytic solution is, in most cases, not guaranteed. It is then necessary to implement numerical methods to obtain results. When an inverse problem is formulated in terms of infinite-dimensional function spaces and then discretized for computational purposes, a discretization error appears. Finite precision easily leads to numerical instabilities and to unexpected, possibly non-physical, behaviours.

Numerical methods, because of their intrinsic rounding and approximations, can render inverse problems less ill-posed than they actually are and produce solutions containing more information than that carried by the input. To ignore the discretization errors results in excessively optimistic expectations about the performance of the method. Those numerical methods that yield to over-optimistic solutions go under the name of *inverse crimes* [39]. In those cases, one says that the model is over-fitting to the input data; that is, a wrong model is reproducing the data too well in comparison to the knowledge given by the input data.

2.2.1 Tikhonov Regularization

Regularization techniques are developed to get an estimate of the true solution of an ill-posed problem, as sound and as realistic as possible in relation to the knowledge of the data. Typically, those imply the inclusion in the algorithm of additional reasonable assumptions, such as the smoothness of the solution.

Let us linger on the details of one specific regularization technique, that will be later exploited in the definition of our inversion scheme. This is the so-called *Tikhonov regularization* [40]. The procedure is indeed a standard one to improve the solvability of the problem while preventing over-fitting features. The idea of the regularization method consists in controlling simultaneously both the norm of the residuals $r = \hat{A}x - y$ and the norm of the approximate solution x itself. Let $\delta > 0$ be a given constant, the so-called *regularization parameter*. The Tikhonov regularized solution x_δ is the minimum of the functional

$$F_\delta(x) = \|Ax - y\|^2 + \delta\|x\|^2, \tag{2.1}$$

[1] An entire mathematical theory is devoted to the study of *catastrophes* [38], that is sudden and abrupt changes in the response of the system to small, smooth changes of the initial conditions.

provided that such minimum exists. The regularization parameter represents a Lagrange multiplier and we may think that we are solving the original problem but constrained by $\|x\| = R$, for some $R > 0$. There exist theorems ensuring that the Tikhonov regularized solution exists and it is unique. The choice of the value of the regularization parameter δ is a pivotal issue. One idea is to make use of the *Morozov discrepancy principle* [41]. Imagine $\epsilon > 0$ is an estimate of the norm of the error in the input vector y; then, any x such that

$$\|Ax - y\| \leq \epsilon \tag{2.2}$$

can be considered acceptable as an approximate solution. If x_δ is the regularized solution, the residual are a function of the regularization parameter, too:

$$f_\delta = \|Ax_\delta - y\|. \tag{2.3}$$

The Morozov principle states that the parameter δ must be chosen in respect of the condition $f_\delta = \epsilon$. That means that the regularized solution should not give residuals smaller than the noise level of the input data.

The regularization technique we have just presented is strictly valid for linear problems, only. Nonetheless, the method is sometimes applicable to non-linear problems along the very same lines we have discussed here (see, again [37]).

2.3 The Inverse Problem In Nuclear Kohn-Sham Density Functional Theory

2.3.1 Comparing the Inverse and the Forward Problem

In the present thesis, we aim to deduce the form of the Kohn-Sham potential (1.64), given the knowledge of the density $\widetilde{n}$ of some nuclear system of interest. The solution of the inverse problem in DFT could reveal to be useful, for instance, to benchmark the approximate energy functionals available on the market. In this sense, it can represent an independent strategy to fine tune theoretical models describing the nuclear structure.

The direct problem in Kohn-Sham DFT, that is the potential-to-density problem, is widely considered to be well-posed, above all thanks to the Hohenberg and Kohn theorems and to the Levy-Lieb constrained-search formulation. On the other hand, although the inverse problem can also be well-posed for some special discretized systems [42], in most cases errors and lack of detailed information in the input density lead to the violations of the Hadamard conditions. The density (1.56) determines a set of single-particle wave functions, up to an overall phase factor; also, unitary transformations of the Kohn-Sham orbitals wind up in generating the same density, too. The orbitals in turn identify the form of the Kohn-Sham potential, up to an arbitrary constant, via the Kohn-Sham equations. Special attention must be paid then in developing an inversion method that converges to the true solution of the inverse problem, because non-uniqueness features are a matter of fact.

Let us deepen the detailed differences between the direct and the inverse problem in Kohn-Sham density functional theory. In general, both of them share the same set of equations, the Kohn-Sham equations. Still, there are some differences, that imply the need of developing completely independent algorithms to solve them. Let us recall the form of the Kohn-Sham equations. For a closed-shell, spin-saturated system of $2A$ nucleons,

$$\epsilon_j \phi_j(\vec{r}) = \Big[-\frac{\hbar^2 \nabla^2}{2m} + v_{KS}([n], \vec{r}) \Big] \phi_j(\vec{r}), \tag{2.4}$$

$$n(\vec{r}) = 2 \sum_{j=1}^{N_{\text{orbs}}} |\phi_j(\vec{r})|^2, \tag{2.5}$$

$$v_{KS}([n], \vec{r}) = v_{\text{H}}([n], \vec{r}) + v_{\text{xc}}([n], \vec{r}) \tag{2.6}$$

where the orbitals are considered to be orthonormal and the external potential is absent in the nuclear case. In the case of the direct problem, the unknowns are the set of the wave functions and the density; on the other hand, for the inverse problem the unknowns are the Kohn-Sham potential and the wave functions. In the forward problem one must deal with a non-linear eigenvalue problem, since assumptions for v_{KS} may contain powers of n, ∇n, and so on; instead, in the inverse problem the eigenvalue problem is fully linear, and non-linearity features are encoded in the definition of the density. Such subtle difference entails the necessity of using different methods for the solutions of the two problems. Moreover, the inverse problem is highly constrained, while the forward problem is free. In fact, in the former case the knowledge of the density defines several constraints to be respected by the Kohn-Sham orbitals. Those formal constraints will be made explicit below, in the definition of our specific inversion algorithm. In both cases, non-linearity requires the choice of

a smart starting guess of the solution, failing which convergence would not be always guaranteed.

The inversion problem solution is addressed both to finite and extended systems, once proper boundary conditions are applied. The main issue here is that in the framework of the inverse problem we miss a clear piece of information about the exact boundary conditions that must be applied *a priori* to the potential. We have only some phenomenological knowledge of the expected asymptotic behaviour. However, the density fine details fix somehow strictly the trend of the sum of the squared orbitals at boundaries. If boundaries are imposed, they should then be in full agreement with the density constraints. An alternative idea is to let the inversion method enforce the orbitals' boundaries to agree with density constraints. That is the so-called *no boundaries density constrained* strategy. Such strategy is applied, e.g., in the van Leeuwen and Baerends (vLB) method; further details on such method can be found below. Although in those methods no detailed knowledge of the boundaries is needed, it is quite common to stumble upon inverse crimes. In that case, the boundary values of the potential may have to be discarded *a posteriori*. Instead, we do believe our method could result in a potential more respectful of the real piece of information carried by the input density. On the other hand, we will make use of theoretically sound regularization tools, such as the Tikhonov's, in order to try reproducing physical results.

In the forward, well-posed, problem, the KS equations can be solved, e. g., self-consistently, let us say easily to some extent. The errors in the resulting density will mainly depend on the numerical discretization that will have been used in the algorithm, on the choice of the convergence condition, and on the particular input potential. Numerical precision in the inverse problem will also fairly depend on the discretization of the algorithm, but the quality of the target density represents in this case a very fundamental limit on the possibility of successfully performing the inversion. In fact, if the numerical error in a given density is not properly taken into account, the inversion can produce over-fitting issues or lead to unphysical features of the output potential. This may be caused by the fact that, in the framework of the direct problem, the assumed potential is known everywhere at the same level of detail; in contrast, the density of many system is known in some radial intervals and extrapolated elsewhere according to some more or less sound theoretical assumptions. Actually, results are mainly positive when one tests the algorithm with analytic formulas of the target density, for which we already know the expected potential, at least to some extent. On the other hand, when one deals with experimental densities and treats more-than-one-dimensional systems, much higher attention must be paid. That is, we believe, our major contribution to the literature, with respect, *e. g.* to [22] that deals only with one-dimensional, analytic systems, only.

2.3.2 Inversion methods

Over the last decades many different methods for the solution of the inversion problem have been proposed [15–22]. Most of them seems to be independent one of each other, at least to some extent. However, we may think to gather them into two categories. Some of the methods are based on the optimization of a certain energy functional, while others consist in a direct algebraic inversion of the Kohn-Sham equations. In the latter, the potential is recovered within some iterative self-consistent search of the solution and some density-based quantity is usually exploited to set the convergence rules. Such quantity also guides the update of the potential in

an iterative process. Instead, in the former the potential is usually defined as the derivative of the energy functional with respect to the density.

We briefly present now an inversion method that is a fair representative of the set of the iterative methods, namely the *Van Leeuwen and Baerends method* (vLB). The comparison of this method with ours will be very useful in order to deeply comprehend the advantages and the drawbacks of both. In vLB mehod, one multiplies equation (2.4) by ϕ_j^*,performs a summation over j, divides the result by the density and finds

$$v_{KS}(\vec{r}) = \frac{2}{n(\vec{r})} \sum_{j=1}^{A_{\text{orbs}}} \phi_j^*(\vec{r}) \frac{\hbar^2 \nabla^2}{2m} \phi_j(\vec{r}) + \epsilon_j |\phi_j|^2. \tag{2.7}$$

The formula can be rendered iterative by placing the input density at the denominator,

$$v_{KS}^{k+1}(\vec{r}) = \frac{n^k(\vec{r})}{\widetilde{n}(\vec{r})} v_{KS}^k(\vec{r}). \tag{2.8}$$

The $(k+1)$-step density is provided by the solution of the eigenvalue problem, given by the Kohn-Sham equations relative to the k-step potential. The method is almost self-explaining: the potential at the $(k+1)$-step is increased in regions where $n^k(\vec{r}) > \widetilde{n}(\vec{r})$ and vice versa. Normally, according to the usual presentation of the method, the iteration is successfully terminated

$$\max_{\vec{r}} \left| 1 - \frac{n^k(\vec{r})}{\widetilde{n}(\vec{r})} \right| < \epsilon, \tag{2.9}$$

where epsilon is some desired threshold. The method has been widely developed and applied to nuclear systems in [12–14]. Convergence is unreachable unless the starting guess for the potential is chosen to be very close to the solution. The trial space explored by the method is therefore quite small. In particular, those works have shown that the choice of of the convergence criterion is decisive. The criterion suggested by the literature seems not to be satisfied in most of cases. Further exploration of possible conditions for stopping the iterations must be then explored. For instance, in the works mentioned above, the criterion (2.9) is adjusted as

$$\frac{\max_{\vec{r}} \left| \widetilde{n}(\vec{r}) - n^k(\vec{r}) \right|}{\widetilde{n}(\vec{r})} < \epsilon, \tag{2.10}$$

to reach convergence. It is not entirely clear why such manual intervention on the convergence criterion should work better than others. In this method, the initial guess highly drives the potential behaviour, especially at the boundaries. In fact, the criterion (2.10) is easily satisfied at large radius, where the values of the density are infinitesimal. Here the potential profile follows almost perfectly the initial guess. This could be labelled as an inverse crime, since within the framework of experimental nuclear densities, we are aware that the values at the boundaries are extrapolated and quite unreliable. Over-fitting of the potential at large radius is then a real risk. On the other hand, this feature removes those unphysical behaviours that can appear when making use of methods that are more sensitive to the input. As we will see in next section, the vLB method is somehow complementary to the one we have chosen in the present work of thesis.

Although, from a theoretical point of view, the methods seem to be all well-defined, we retain that the detailed implementation gives rise to many different

advantages and drawbacks. We then promote and suggest a combined usage of different methods, in order to exploit at most simpler methods to complement the results of the more general and theoretically sound inversion scheme presented right below.

2.4 Constrained Variational Inversion Method

As presented in [22], the Constrained Variation (CV) method is indeed a promising inverse method to be applied in Nuclear Physics, especially because it does not involve the solution of an eigenvalue problem at each iteration. In fact, in many density-to-potential inversions, such as vLB method, the diagonalization of the Hamiltonian becomes one of the biggest computational limits whenever the size of the system increases. Not to solve any eigenvalue problem results in the fact that in the CV method one obtains wave functions that reproduce the correct target density, but are eventually an unitary transformation away from the eigenfunctions of the system. Moreover, with respect to other inversion methods, we believe that this method is better, since its starting point is not a direct, possibly biased, guess on the potential form; instead, the starting point for the inversion method is a guess on the Kohn-Sham orbitals, that are surely closer to the known input, the nuclear density, and share to some extent a similar functional behaviour. Thus, we avoid any inverse crime, possibly due to the usage in the inverse problem a piece of information on the potential coming from the direct problem.

The mathematical tool that is suitable for the implementation of a constrained optimization procedure is the method of Lagrange multipliers. In the fashion of the Kohn-Sham scheme, one performs a minimization of the total kinetic energy expectation value with respect to the orbitals, as if the system would be non-interacting:

$$\begin{aligned} f[\{\phi_j\}] &= -\frac{\hbar^2}{2m}\int d^3r \sum_{j=1}^{N} \phi_j^*(\vec{r})\nabla^2\phi_j(\vec{r}) \\ &= -\frac{\hbar^2}{2m}\int d^3r \sum_{j=1}^{N} \left[\nabla\cdot(\phi_j^*(\vec{r})\nabla\phi_j(\vec{r})) - |\nabla\phi_j(\vec{r})|^2\right] \\ &= \frac{\hbar^2}{2m}\int d^3r \sum_{j=1}^{N} |\nabla\phi_j(\vec{r})|^2, \end{aligned} \tag{2.11}$$

where N is the number of filled orbitals in the system. From now on, we will refer to this quantity as the objective function of the optimization. We made use of an integration by parts to rewrite the kinetic term, so that the dependence on the wave functions and on their gradients is more explicit. The first term in the second line gives no contribution if we apply boundary conditions at infinity on the wave functions.

Two types of constraints $c_i = 0$ are imposed: a density constraint and $\frac{N(N+1)}{2}$ orthonormality constraints.

$$c_0(\vec{r}) = \sum_{j=1}^{N} |\phi_j(\vec{r})|^2 - \tilde{n}(\vec{r}) = 0, \tag{2.12}$$

$$c_{jk} = \langle\phi_j|\phi_k\rangle - \delta_{jk} = \int d^3r'\, \phi_j^*(\vec{r}')\phi_k(\vec{r}') - \delta_{jk} = 0, \tag{2.13}$$

where $j = 1,\ldots,N$ and $k = j,\ldots,N$ are an adequate set of quantum numbers. The orbitals must integrate to the target density and respect orthonormality. Once those condition are fulfilled, the orbitals can generate a N-representable density (compare with the discussion in the previous chapter).

There are two equivalent paths we can follow in the development of the method. First, because the problem we address here is fully time-independent, we can take

the Kohn-Sham orbitals to be real. In the appendix C a formal justification of this statement is provided. We consider then real wave functions to define the non-interacting kinetic energy and the constraints, without any loss of generality. We will show below how, in the practice, this is the same as considering complex orbitals, since the methods naturally decouples into a real and an imaginary part.

We build then an auxiliary Lagrangian, as prescript by the Lagrange multiplier method, to turn the constrained minimization into a free one, with respect to the orbitals' set and to the Lagrange multipliers. The Lagrange multipliers are formally defined as

$$\lambda_i = \frac{\delta f[\{\phi_j\}]}{\delta c_i}. \tag{2.14}$$

The core of the inversion lies in the physical meaning of these quantities. The zeroth multiplier, related to the constraint (2.12), is directly linked to the Kohn-Sham potential

$$v_{KS}(\vec{r}) = \frac{\delta f[\{\phi_j\}]}{\delta \sum_{j=1}^{N} |\phi_j(\vec{r})|^2} = \frac{\delta}{\delta n} \left\langle \Phi_{KS} \middle| \hat{T}_{KS} \middle| \Phi_{KS} \right\rangle \tag{2.15}$$

at the minimum.

The multipliers associated to the constraints (2.13) have no plain physical meaning instead; those are the upper triangular part of a symmetric matrix. However, we could think to diagonalize the matrix containing those multipliers. In this case we would obtain the sequence of energies ϵ_j of the Kohn-Sham orbitals. The Kohn-Sham orbitals' energy have no physical meaning, except for the highest of them, $\epsilon_{\max}$, that is related to the first ionization energy of the system (DFT-Koopmans' theorem).

Let us define a cost functional J as the space integral of such auxiliary Lagrangian, and perform its minimization. Such procedure is totally similar to the fact that the minimization of the action functional in mechanical system is equivalent to the solution of the Euler-Lagrange equations

$$\frac{\partial \mathscr{L}}{\partial \phi_j(\vec{r})} - \nabla \cdot \frac{\partial \mathscr{L}}{\partial \nabla \phi_j(\vec{r})} = 0 \tag{2.16}$$

The main advantage is that in such a way we deal with the optimization of a functional instead of with a multidimensional function.

The cost functional and its associated density, that is the auxiliary Lagrangian, respectively read

$$\begin{aligned} J[\phi_j; v_{KS}(\vec{r}), \epsilon_{jk}] = \frac{\hbar^2}{2m} \int d^3r \sum_{j=1}^{N} |\nabla \phi_j(\vec{r})|^2 + \\ + \int d^3r \; v_{KS}(\vec{r}) \Big(\sum_{j=1}^{N} |\phi_j(\vec{r})|^2 - \tilde{n}(\vec{r}) \Big) + \\ + \int d^3r \sum_{j=1}^{N} \sum_{k=j}^{N} \epsilon_{jk} \Big(\int d^3r' \; \phi_j(\vec{r}') \phi_k(\vec{r}') - \delta_{jk} \Big), \end{aligned} \tag{2.17}$$

and

$$\mathscr{L}[\phi_j,\nabla\phi_j;v_{KS}(\vec{r}),\epsilon_{jk}] = \frac{\hbar^2}{2m}\sum_{j=1}^{N}|\nabla\phi_j(\vec{r})|^2 + \\ + v_{KS}(\vec{r})\Big(\sum_{j=1}^{N}|\phi_j(\vec{r})|^2-\tilde{n}(\vec{r})\Big) + \\ + \sum_{j=1}^{N}\sum_{k=j}^{N}\epsilon_{jk}\Big(\int d^3r'\,\phi_j(\vec{r}')\phi_k(\vec{r}')-\delta_{jk}\Big). \tag{2.18}$$

The minimum of the kinetic energy, plus the constraints, does coincide by definition with the minimum of the functional. A necessary condition for the presence of an extremum is that the Lagrangian satisfies the Euler-Lagrange equations. First, let us consider the kinetic term:

$$\Big(\frac{\delta}{\delta\phi_\alpha}-\nabla\cdot\frac{\delta}{\delta\nabla\phi_\alpha}\Big)\frac{\hbar^2}{2m}\sum_{j=1}^{N}\Big[(\nabla\phi_j(\vec{r}))^2\Big] \\ = -\frac{\hbar^2}{m}\nabla^2\phi_\alpha(\vec{r}). \tag{2.19}$$

The derivation of the constraint terms gives

$$\Big(\frac{\delta}{\delta\phi_\alpha}-\nabla\cdot\frac{\delta}{\delta\nabla\phi_\alpha}\Big)\Big\{v_{KS}(\vec{r})\Big[\sum_{j=1}^{N}\Big(\phi_j(\vec{r})\phi_j(\vec{r})\Big)-\tilde{n}(\vec{r})\Big] + \\ + \sum_{j=1}^{N}\sum_{k=j}^{N}\epsilon_{jk}\Big(\int d^3r'\,\phi_j(\vec{r}')\phi_k(\vec{r}')-\delta_{jk}\Big)\Big\} \\ = 2v_{KS}(\vec{r})\phi_\alpha(\vec{r}) + \Big[\sum_{j=1}^{\alpha}\phi_j(\vec{r})\epsilon_{j\alpha}+\sum_{k=\alpha}^{N}\epsilon_{\alpha k}\phi_k(\vec{r})\Big]. \tag{2.20}$$

While deriving the orthogonality term we used the fact that we have only defined the upper triangular part of the symmetric matrix ϵ_{jk}; the sum in this term proceeds as highlighted in (2.21), with a double counting of the diagonal elements.

$$\begin{bmatrix} \epsilon_{11} & & \epsilon_{1\alpha} & & \\ & \ddots & \downarrow & & \\ & & \epsilon^{x2}_{\alpha\alpha} & \rightarrow & \epsilon_{\alpha N} \\ & & & \ddots & \\ & & & & \epsilon_{NN} \end{bmatrix} \tag{2.21}$$

Equations (2.19) and (2.20) sum up to zero; then, the minimum is identified by the following set of Euler-Lagrange equations, obtained by artificially introducing $\phi_\beta(\vec{r})$ and integrating:

$$\frac{\hbar^2}{m}\int d^3r\,\phi_\beta(\vec{r})\nabla^2\phi_\alpha(\vec{r}) = 2\int d^3r\,\Big[\phi_\beta(\vec{r})v_{KS}(\vec{r})\phi_\alpha(\vec{r})\Big] + \\ + \int d^3r\,\phi_\beta(\vec{r})\Big[\sum_{j=1}^{\alpha}\phi_j(\vec{r})\epsilon_{j\alpha}+\sum_{k=\alpha}^{N}\epsilon_{\alpha k}\phi_k(\vec{r})\Big], \tag{2.22}$$

where $\alpha = 1,\dots,N$ and ,$\beta \geq \alpha$. One takes the orbitals coming from the free minimization of the functional, and uses them to get the potential by solving the linear equations above.

Let us come back to the definition of $f[\{\phi_j\}]$ and assume that the orbitals are fully complex. Then, the matrix ϵ_{jk} is not symmetric any more, but indeed it is hermitian. If we refuse to pick the orbitals to be real, a subtle difference stems out in the derivation of the Euler-Lagrange equations. In fact, we need to calculate both

$$\frac{\partial \mathscr{L}}{\partial \phi_j(\vec{r})} - \nabla \cdot \frac{\partial \mathscr{L}}{\partial \nabla \phi_j(\vec{r})} = 0, \tag{2.23}$$

$$\frac{\partial \mathscr{L}}{\partial \phi_j^*(\vec{r})} - \nabla \cdot \frac{\partial \mathscr{L}}{\partial \nabla \phi_j^*(\vec{r})} = 0. \tag{2.24}$$

The result is

$$\frac{\hbar^2}{2m}\nabla^2\phi_\alpha^*(\vec{r}) = v_{KS}(\vec{r})\phi_\alpha^*(\vec{r}) + \sum_{j=\alpha}^{N} \epsilon_{\alpha j}^* \phi_j^*(\vec{r}) \tag{2.25}$$

$$\frac{\hbar^2}{2m}\nabla^2\phi_\alpha(\vec{r}) = v_{KS}(\vec{r})\phi_\alpha(\vec{r}) + \sum_{k=\alpha}^{N} \epsilon_{\alpha k} \phi_k(\vec{r}). \tag{2.26}$$

The sum of the two equations produces

$$\begin{aligned}
\frac{\hbar^2}{m}\nabla^2\Re[\phi_\alpha(\vec{r})] &= 2v_{KS}(\vec{r})\Re[\phi_\alpha(\vec{r})] + 2\sum_{k=\alpha}^{N}\Re[\epsilon_{\alpha k}\phi_k(\vec{r})]. \\
&= 2v_{KS}(\vec{r})\Re[\phi_\alpha(\vec{r})] + \Big[\sum_{j=1}^{\alpha}\Re[\epsilon_{j\alpha}^*\phi_j^*(\vec{r})] + \sum_{k=\alpha}^{N}\Re[\epsilon_{\alpha k}\phi_k(\vec{r})]\Big] \\
&= 2v_{KS}(\vec{r})\Re[\phi_\alpha(\vec{r})] + \Big[\sum_{j=1}^{\alpha}\Re[\epsilon_{j\alpha}\phi_j(\vec{r})] + \sum_{k=\alpha}^{N}\Re[\epsilon_{\alpha k}\phi_k(\vec{r})]\Big],
\end{aligned} \tag{2.27}$$

that is equation (2.22). On the other hand, the difference of the two equations leads to the imaginary part of the equations

$$\begin{aligned}
&\frac{\hbar^2}{m}\nabla^2\Im[\phi_\alpha(\vec{r})] = 2v_{KS}(\vec{r})\Im[\phi_\alpha(\vec{r})] + 2\sum_{k=\alpha+1}^{N}\Im[\epsilon_{\alpha k}\phi_k(\vec{r})] \\
&= 2v_{KS}(\vec{r})\Im[\phi_\alpha(\vec{r})] + \Big[\sum_{j=1}^{\alpha-1}\Im[\epsilon_{j\alpha}^*\phi_j^*(\vec{r})] + \sum_{k=\alpha+1}^{N}\Im[\epsilon_{\alpha k}\phi_k(\vec{r})]\Big] \\
&= 2v_{KS}(\vec{r})\Im[\phi_\alpha(\vec{r})] + \Big[-\sum_{j=1}^{\alpha-1}\Im[\epsilon_{j\alpha}\phi_j(\vec{r})] + \sum_{k=\alpha+1}^{N}\Im[\epsilon_{\alpha k}\phi_k(\vec{r})]\Big]
\end{aligned} \tag{2.28}$$

that does not bring along further information if the system is time-independent.

2.4.1 Scaling

In the practice, one may suffer from numerical rounding errors, especially in those regions where the kinetic energy is small due to the exponential decay of the wave functions. Therefore, inspired by the density constraint, one rescales the wave functions as

$$\phi_j(\vec{r}) = \sqrt{\tilde{n}(\vec{r})}\, g_j(\vec{r}). \tag{2.29}$$

Such redefinition of the orbitals renders the terms in the sum of the kinetic energy all of the same order of magnitude.

Moreover, as we have already mentioned, there is an intrinsic non-uniqueness in the problem due to the definition of the density itself. Since the problem is ill-posed, the competition between orthogonality and density constraints can lead to non-physical orbitals, in particular when the starting point of the minimization is not wisely chosen. Typically, one applies a regularization scheme to solve this issue. We make use of a Tikhonov regularization. Let $\delta > 0$ be a given constant; the Tikhonov regularized solution is the one that minimizes the functional J plus the penalty functional

$$R[\{g_j\}] = \delta \int d^3r \sum_{j=1}^{N} |\nabla g_j(\vec{r})|^2. \tag{2.30}$$

In the Lagrange picture, the penalty functional can also be read as an extra constraint on the norm of the gradient of the scaled wave functions $\|\nabla g_j\|_{L_2} = R$, δ being the corresponding Lagrange multiplier. The orbitals characterized by strong variations are therefore penalized in the search for the minimum. The value of the penalty parameter has to be chosen via the Morozov discrepancy principle, which states that the approximated solution cannot satisfy the constraints more accurately than up to the numerical noise level of the input density. Thus, the scaled and regularized cost functional reads

$$\begin{aligned}
\widetilde{J}[\{g_j\}, v_{KS}, \epsilon_{jk}] = {} & \frac{\hbar^2}{2m} \int d^3r \sum_{j=1}^{N} |\nabla(\sqrt{\widetilde{n}(\vec{r})} g_j(\vec{r}))|^2 + \delta \int d^3r \sum_{j=1}^{N} |\nabla g_j(\vec{r})|^2 + \\
& + \int d^3r \; v_{KS}(\vec{r}) \widetilde{n}(\vec{r}) \Big(\sum_{j=1}^{N} |g_j(\vec{r})|^2 - 1 \Big) \\
& + \int d^3r \sum_{j=1}^{N} \sum_{k=j}^{N} \epsilon_{jk} \Big(\int d^3r' \; \widetilde{n}(\vec{r}') g_j(\vec{r}') g_k(\vec{r}') - \delta_{jk} \Big) \\
= {} & \frac{\hbar^2}{2m} \int d^3r \sum_{j=1}^{N} \Big[\frac{(\nabla \widetilde{n}(\vec{r}))^2}{4\widetilde{n}(\vec{r})} g_j^2(\vec{r}) + \Big(\nabla \widetilde{n}(\vec{r}) \cdot \nabla g_j(\vec{r}) \Big) g_j(\vec{r}) \\
& + (\widetilde{n}(\vec{r}) + \delta) |\nabla g_j(\vec{r})|^2 \Big] + \int d^3r \; v_{KS}(\vec{r}) \widetilde{n}(\vec{r}) \Big(\sum_{j=1}^{N} |g_j(\vec{r})|^2 - 1 \Big) \\
& + \int d^3r \sum_{j=1}^{N} \sum_{k=j}^{N} \epsilon_{jk} \Big(\int d^3r' \; \widetilde{n}(\vec{r}') g_j(\vec{r}') g_k(\vec{r}') - \delta_{jk} \Big).
\end{aligned} \tag{2.31}$$

Again, the solution of the Euler-Lagrange equations

$$\frac{\partial L}{\partial g_\alpha} - \nabla \cdot \frac{\partial L}{\partial \nabla(g_\alpha)} = 0, \tag{2.32}$$

optimizes the functional, and an explicit calculation of those gives

$$\begin{aligned}
& \frac{\hbar^2}{m} \Big[g_\alpha(\vec{r}) \Big(-\frac{(\nabla \widetilde{n}(\vec{r}))^2}{4\widetilde{n}(\vec{r})} + \frac{\nabla^2 \widetilde{n}(\vec{r})}{2} \Big) + \nabla \widetilde{n}(\vec{r}) \cdot \nabla g_\alpha(\vec{r}) + (\widetilde{n}(\vec{r}) + \delta) \nabla^2 g_\alpha(\vec{r}) \Big] \\
& = 2 v_{KS}(\vec{r}) \widetilde{n}(\vec{r}) g_\alpha(\vec{r}) + \widetilde{n}(\vec{r}) \Big(\sum_{k=\alpha}^{N} \epsilon_{\alpha k} g_k(\vec{r}) + \sum_{j=1}^{\alpha} g_j(\vec{r}) \epsilon_{j\alpha} \Big).
\end{aligned} \tag{2.33}$$

Once more, the artificial introduction of $g_\beta(\vec{r})$, plus an integration, provides a matrix form of those equations,

$$\frac{\hbar^2}{m}\int d^3r\; g_\beta(\vec{r})\Big[g_\alpha(\vec{r})\Big(-\frac{(\nabla\widetilde{n}(\vec{r}))^2}{4\widetilde{n}(\vec{r})}+\frac{\nabla^2\widetilde{n}(\vec{r})}{2}\Big)+\nabla\widetilde{n}(\vec{r})\cdot\nabla g_\alpha(\vec{r})+(\widetilde{n}(\vec{r})+\delta)\nabla^2 g_\alpha(\vec{r})\Big]$$
$$=\int d^3r\; g_\beta(\vec{r})\widetilde{n}(\vec{r})\Big[2v_{KS}(\vec{r})g_\alpha(\vec{r})+\Big(\sum_{k=\alpha}^{N}\epsilon_{\alpha k}g_k(\vec{r})+\sum_{j=1}^{\alpha}g_j(\vec{r})\epsilon_{j\alpha}\Big)\Big], \tag{2.34}$$

where $\alpha = 1,\ldots,N$, $\beta \geq \alpha$.

2.5 Insertion of Spherical Symmetry into the Constrained Variational Method

2.5.1 The Spherical Hamiltonian

In order to lay the ground for solving the inverse Kohn-Sham problem relative to nuclear densities, let us consider systems characterized by spherical symmetry. This means the Hamiltonian will be invariant under rotations, and the Kohn-Sham potential will be central.

The assumption of spherical symmetry implies that the Hamiltonian commutes with the squared angular momentum and with one of its components, say the projection along the z-axis,

$$[\hat{H}, \hat{L}^2] = [\hat{H}, \hat{L}_z] = 0. \tag{2.35}$$

Therefore, the Hamiltonian separates as

$$\hat{H}_r = \frac{\hat{p}_r^2}{2} + \frac{\hat{L}^2}{2r^2} + \hat{V}(r) \tag{2.36}$$

$$= -\frac{1}{2}\Big(\frac{\partial^2}{\partial r^2} + \frac{2}{r}\frac{\partial}{\partial r} - \frac{L^2}{r^2}\Big) + \hat{V}(r). \tag{2.37}$$

Since we are trying to generalize our inversion model as much as possible, let us consider systems characterized by a spin degree of freedom, too. We require the Hamiltonian to commute with the square of the spin operator S, together with one of its components

$$[\hat{H}, \hat{S}^2] = [\hat{H}, \hat{S}_z] = 0. \tag{2.38}$$

In such a way we have chosen the so-called $|nlm_l sm_s\rangle$ representation, namely the decoupled basis. The components of the wave functions on the decoupled basis, in the position space, read then

$$\varphi_{nlm_l sm_s}(\vec{r}, \sigma) = \frac{u_{nl}(r)}{r} Y_{lm_l}(\theta, \phi)\chi_{sm_s}(\sigma). \tag{2.39}$$

The functions $Y_{lm_l}(\theta, \phi)$ are the well known spherical harmonics, which form a complete orthonormal set on the sphere $\mathbb{S}^2$. They are defined by

$$Y_{lm_l}(\theta, \phi) = (-1)^m \sqrt{\frac{(2l+1)}{4\pi}\frac{(l-m_l)!}{(l+m_l)!}} P_l^{m_l}(\cos\theta) e^{im_l\phi}, \tag{2.40}$$

where $P_l^{m_l}(x)$ are the generalized Legendre polynomials, $l = 0, 1, \ldots$ and $m_l = -l, \ldots, l$. The requirement on the wave functions to be eigenfunctions of the angular momentum, characterized by definite values of the quantum numbers l and m_l, completely fixes their angular dependency.

In the following, it will be useful to write the orbitals in the coupled basis $|nlsjm_j\rangle$, the operator $J = L + S$ standing for the total angular momentum. Such alternative set of quantum numbers is more convenient than the other, because an overall rotational invariance (orbital momentum and spin) implies that that j and m_j are constants of motion. Moreover, the great importance of the spin-orbit coupling

$$H'(r) = -\alpha(r)\hat{L}\cdot\hat{S} = -\alpha(r)\frac{\hat{J}^2 - \hat{L}^2 - \hat{S}^2}{2}, \tag{2.41}$$

in nuclear systems guides our basis choice; the spin-orbit term is diagonal in the coupled representation.

We decide then to simultaneously diagonalize the angular momentum and the spin operator, together with the total angular momentum and one of its components

$$[\hat{H},\hat{L}^2]=[\hat{H},\hat{S}^2]=[\hat{H},\hat{J}^2]=[\hat{H},\hat{J}_z]=0. \tag{2.42}$$

The orbitals on this basis read

$$\varphi_{nlsjm_j}(\vec{r},\sigma)=\frac{u_{nlj}(r)}{r}[Y_l(\theta,\phi)\otimes\chi_s(\sigma)]_{jm_j}. \tag{2.43}$$

Either description, decoupled and coupled, is complete. Since the two bases are fully equivalent, they must be connected by a unitary transformation:

$$|nlsjm_j\rangle=\sum_{m_l m_s}\langle lm_l sm_s|lsjm_j\rangle\,|nlm_l sm_s\rangle\,. \tag{2.44}$$

The matrix bridging the two representations is composed by the Clebsch-Gordan coefficients; those coefficients are independent of the quantum number n, since the transformation regards the angular parts of the wave function, alone. In the following, we will make use of some of their properties:

$$\sum_{m_l m_s}\langle lsj'm'_j|lm_l sm_s\rangle\langle lm_l sm_s|lsjm_j\rangle=\delta_{jj'}\delta_{m_j m'_j} \tag{2.45}$$

$$\sum_{jm_j}\langle lm'_l sm'_s|lsjm_j\rangle\langle lsjm_j|lm_l sm_s\rangle=\delta_{m_l m'_l}\delta_{m_s m'_s}. \tag{2.46}$$

A detailed descussion about how the Clebsch-Gordan coefficients properties and how they can be explicitely caluclated can be found, e.g., in [24]. The Clebsch-Gordan coefficients are computed up to an overall phase; the standard convention is to pick them up as real and satisfying the following symmetry properties

$$\langle lm_l sm_s|lsjm_j\rangle=(-1)^{l+s-j}\langle l-m_l s-m_s|lsjm_j\rangle\,, \tag{2.47}$$

$$\langle lm_l sm_s|lsjm_j\rangle=(-1)^{l+s-j}\langle sm_s lm_l|lsjm_j\rangle\,, \tag{2.48}$$

$$\langle lm_l sm_s|lsjm_j\rangle=(-1)^{s-m_s}\sqrt{\frac{2j+1}{2l+1}}\langle s-m_s jm_j|sjlm_l\rangle\,. \tag{2.49}$$

The insertion of an identity resolution into the coupled decomposition allows to recover the well known structure, easy indeed to be treated, of the spherical harmonics. The cost to be paid in order to do that is the computation of the Clebsch-Gordan coefficients. Luckily, we will show that we can get rid of the CG coefficient through some manipulations and exploiting the symmetries we have assumed.

$$\varphi_{nlsjm_j}(\vec{r},\sigma)=\frac{u_{nlj}(r)}{r}[Y_l(\theta,\phi)\otimes\chi_s(\sigma)]_{jm_j} \tag{2.50}$$

$$=\frac{u_{nlj}(r)}{r}\sum_{m_l m_s}\langle\theta\phi\sigma|lm_l sm_s\rangle\langle lm_l sm_s|lsjm_j\rangle \tag{2.51}$$

$$=\frac{u_{nlj}(r)}{r}\sum_{m_l m_s}\langle lm_l sm_s|lsjm_j\rangle\,Y_{lm_l}(\theta,\phi)\chi_{sm_s}(\sigma). \tag{2.52}$$

2.5.2 The Spherical Form of the Cost Functional

We are ready to define the quantities of our inversion methods in terms of spherical coordinates. First, let us calculate the nuclear density:

$$
\begin{aligned}
n^{(q)}(\vec{r}) &= \sum_{nlsjm_j} |\varphi^{(q)}_{nlsjm_j}(\vec{r},\sigma)|^2 \\
&= \sum_{nljm_j} \frac{u^{2(q)}_{nlj}(r)}{r^2} \sum_{m_l m_s m'_l m'_s} \langle lsjm_j|lm'_l sm'_s\rangle \langle lm_l sm_s|lsjm_j\rangle \\
&\quad Y^*_{lm'_l}(\theta,\phi) Y_{lm_l}(\theta,\phi) \sum_s \chi^*_{sm'_s}(\sigma)\chi_{sm_s}(\sigma)] \\
&= \sum_{nlj} \frac{u^{2(q)}_{nlj}(r)}{r^2} \sum_{m_l m_s m'_l m'_s m_j} \frac{2j+1}{2l+1} \langle lslm'_l|jm_j s(-m'_s)\rangle \langle jm_j s(-m_s)|lslm_l\rangle \\
&\quad [Y^*_{lm'_l}(\theta,\phi) Y_{lm_l}(\theta,\phi)\delta_{m_s m'_s}] \\
&= \sum_{nlj} \frac{u^{2(q)}_{nlj}(r)}{r^2} \sum_{m_l m'_l} \frac{2j+1}{2l+1} \delta_{m_l m'_l} Y^*_{lm'_l}(\theta,\phi) Y_{lm_l}(\theta,\phi) \\
&= \sum_{nlj} \frac{u^{2(q)}_{nlj}(r)}{r^2} \frac{2j+1}{2l+1} \sum_{m_l} Y^*_{lm_l}(\theta,\phi) Y_{lm_l}(\theta,\phi) \\
&= \sum_{nlj} \frac{2j+1}{4\pi} \frac{u^{2(q)}_{nlj}(r)}{r^2}.
\end{aligned} \tag{2.53}
$$

In the second step we have used the completeness of the spinors; moreover, we have exploited the symmetry properties of the Clebsch-Gordan coefficients in order to make the m_j-degeneracy explicit. Finally, in the last step we have exploited a resolution of the identity and the following property of the spherical harmonics:

$$
\sum_{m_l=-l}^{l} Y^*_{lm}(\theta_1,\phi_1) Y_{lm}(\theta_2,\phi_2) = \frac{2l+1}{4\pi} P^0_l(\cos\omega), \tag{2.54}
$$

$$
\cos\omega = \cos\theta_1\cos\theta_2 + \sin\theta_1\sin\theta_2\cos(\phi_1-\phi_2), \tag{2.55}
$$

where $\cos\omega = 1$ for $\theta_1 = \theta_2$, $\phi_1 = \phi_2$, and $P^0_l(1) = 1$.

The calculation of the kinetic term passes through the transformation of the Laplace operator in spherical coordinates,

$$
\nabla^2 f = \frac{\partial^2 f}{\partial r^2} + \frac{2}{r}\frac{\partial f}{\partial r} + \frac{\Lambda^2 f}{r^2} \tag{2.56}
$$

$$
= \frac{1}{r}\frac{\partial^2}{\partial r^2}(rf) + \frac{\Lambda^2 f}{r^2}, \tag{2.57}
$$

whose angular dependence is entirely contained in the Legendre operator,

$$
\Lambda^2 f = \frac{1}{\sin\theta}\frac{\partial}{\partial\theta}\Big(\sin\theta\frac{\partial f}{\partial\theta}\Big) + \frac{\partial^2 f}{\partial\phi^2}. \tag{2.58}
$$

The eigenfunctions of the Legendre operator are exactly the spherical harmonics $Y_{lm}(\theta,\phi)$, with eigenvalues $-l(l+1)$. By comparing equations (2.37) and (2.56), it is

straightforward to notice that, from a physical point of view, the Legendre operator represents minus the angular momentum operator in the position space. The decomposition and the radial rescaling that we have applied to the wave functions are explicitly thought to simplify the way the Laplace operator acts on them. The total kinetic energy expectation value, that the first term of the cost functional, transforms as

$$
\begin{aligned}
J_{\mathrm{I}} &= \sum_q \Big(-\frac{\hbar^2}{2m_q}\Big) \int r^2 dr d\Omega \sum_\sigma \sum_{nljm_j} \varphi^{*(q)}_{nl\frac{1}{2}jm_j}(\vec{r},\vec{\sigma}) \Big(\frac{1}{r}\frac{\partial^2}{\partial r^2} r + \frac{\Lambda^2}{r^2}\Big) \varphi^{(q)}_{nl\frac{1}{2}jm_j}(\vec{r},\sigma) \\
&= \sum_q \Big(-\frac{\hbar^2}{2m_q}\Big) \int r^2 dr d\Omega \sum_\sigma \sum_{nljm_j} \frac{u^{(q)}_{nlj}(r)}{r} \sum_{m'_l m'_s} \langle l m'_l \frac{1}{2} m'_s | j m_j \rangle \, Y^*_{lm'_l}(\theta,\phi) \chi^*_{\frac{1}{2}m'_s}(\sigma) \\
&\quad \Big(\frac{1}{r}\frac{\partial^2}{\partial r^2} r + \frac{\Lambda^2}{r^2}\Big) \frac{u^{(q)}_{nlj}(r)}{r} \sum_{m_l m_s} \langle l m_l \frac{1}{2} m_s | j m_j \rangle \, Y_{lm_l}(\theta,\phi) \chi_{\frac{1}{2}m_s}(\sigma) \\
&= \sum_q \Big(-\frac{\hbar^2}{2m_q}\Big) \int r^2 dr \sum_{nlj} \sum_{m_j} \Big(\frac{u^{(q)}_{nlj}(r)}{r^2} \frac{\partial^2 u^{(q)}_{nlj}(r)}{\partial r^2} - u^{2(q)}_{nlj}(r) \frac{l(l+1)}{r^4} \Big) \\
&\quad \sum_{m_l m_s m'_l m'_s} \langle l m_l \frac{1}{2} m_s | j m_j \rangle \langle j m_j | l m'_l \frac{1}{2} m'_s \rangle \int d\Omega Y^*_{lm'_l}(\theta,\phi) Y_{lm_l}(\theta,\phi) \\
&\quad \sum_\sigma \chi^*_{\frac{1}{2}m'_s}(\sigma) \chi_{\frac{1}{2}m_s}(\sigma) \\
&= \sum_q \Big(-\frac{\hbar^2}{2m_q}\Big) \int dr \sum_{nlj} (2j+1) \Big(u^{(q)}_{nlj}(r) \frac{\partial^2}{\partial r^2} u^{(q)}_{nlj}(r) - u^{2(q)}_{nlj}(r) \frac{l(l+1)}{r^2} \Big) \\
&\quad \sum_{m_l m_s m'_l m'_s} \langle l m_l \frac{1}{2} m_s | j m_j \rangle \langle j m_j | l m'_l \frac{1}{2} m'_s \rangle \delta_{m_l m'_l} \delta_{m_s, m'_s} \\
&= \sum_q \frac{\hbar^2}{2m_q} \int dr \sum_{nlj} (2j+1) \Big(|\frac{\partial}{\partial r} u^{(q)}_{nlj}(r)|^2 + u^{2(q)}_{nlj}(r) \frac{l(l+1)}{r^2} \Big). \qquad (2.59)
\end{aligned}
$$

The key idea is that once the Laplace operator acts on the wave functions, we can exploit the orthogonality of the spinors, of the spherical harmonics, and that of the Clebsch-Gordan coefficients. We would like to remark that the coordinate transformation of the kinetic term gives rise to two contributions; the first is the proper radial kinetic term, while the second represent a centrifugal fictitious potential.

The potential term, that is the second term in the functional, reads

$$
\begin{aligned}
J_{\mathrm{II}} &= \sum_q \int r^2 dr d\Omega \sum_\sigma v^{(q)}_{KS}(r) \Big[\sum_{nljm_j} |\varphi^{(q)}_{nl\frac{1}{2}jm_j}(\vec{r},\sigma)|^2 - \widetilde{n}^{(q)}(r) \Big] \qquad (2.60) \\
&= \sum_q \int dr \; v^{(q)}_{KS}(r) \Big[\sum_{nlj} (2j+1) u^{2(q)}_{njl}(r) - 4\pi r^2 \widetilde{n}^{(q)}(r) \Big]. \qquad (2.61)
\end{aligned}
$$

Here we made use of the nuclear density expression (2.53). It is quite immediate to read out the density constraint from this term,

$$
\sum_{nlj} (2j+1) u^{2(q)}_{njl}(r) - 4\pi r^2 \widetilde{n}^{(q)}(r) \stackrel{!}{=} 0. \qquad (2.62)
$$

Finally, the orthonormality term is given by

$$
\begin{aligned}
J_{\mathrm{III}} &= \sum_q \int r^2 dr d\Omega \sum_\sigma \sum_{\alpha\alpha'} \epsilon^{(q)}_{\alpha\alpha'} \Big[\int r'^2 dr' d\Omega' \sum_{\sigma'} \varphi^*_{\alpha'}(\vec{r'},\sigma')\varphi_\alpha(\vec{r'},\sigma') - \delta_{\alpha\alpha'} \Big] \\
&= \sum_q \int r^2 dr d\Omega \sum_\sigma \sum_{nljm_j} \sum_{n'l'j'm'_j} \epsilon^{(q)}_{(nljm_j),(n'l'j'm'_j)} \\
&\quad \Big[\int dr'\, r'^2 \frac{u^{(q)}_{nlj}(r') u^{(q)}_{n'l'j'}(r')}{r'^2} \sum_{m_l m_s m'_l m'_s} \langle l m_l \tfrac{1}{2} m_s | j m_j \rangle \langle j' m'_j | l' m'_l \tfrac{1}{2} m'_s \rangle \\
&\quad \int d\Omega'\, Y^*_{l'm'_l}(\theta',\phi') Y_{lm_l}(\theta',\phi') \sum_{\sigma'} \chi^*_{\frac{1}{2}m'_s}(\sigma') \chi_{\frac{1}{2}m_s}(\sigma') - \delta_{nn'}\delta_{ll'}\delta_{jj'}\delta_{m_j m'_j} \Big] \\
&= \sum_q \int r^2 dr d\Omega \sum_\sigma \sum_{nljm_j} \sum_{n'l'j'm'_j} \epsilon^{(q)}_{(nljm_j),(n'l'j'm'_j)} \\
&\quad \Big[\int dr'\, u^{(q)}_{nlj}(r') u^{(q)}_{n'l'j'}(r') \sum_{m_l m_s m'_l m'_s} \langle l m_l \tfrac{1}{2} m_s | l \tfrac{1}{2} j m_j \rangle \langle j' m'_j | l' m'_l \tfrac{1}{2} m'_s \rangle \\
&\quad \delta_{ll'}\delta_{m_l m'_l}\delta_{m_s m'_s} - \delta_{nn'}\delta_{ll'}\delta_{jj'}\delta_{m_j m'_j} \Big] \\
&= \sum_q \int r^2 dr d\Omega \sum_\sigma \sum_{njm_j} \sum_{n'j'm'_j} \epsilon^{(q)}_{(njm_j),(n'j'm'_j)} \\
&\quad \Big[\int dr'\, u^{(q)}_{nlj}(r') u^{(q)}_{n'lj'}(r') \sum_{m_l m_s} \langle l m_l \tfrac{1}{2} m_s | j m_j \rangle \langle j' m'_j | l m_l \tfrac{1}{2} m_s \rangle - \delta_{nn'}\delta_{jj'}\delta_{m_j m'_j} \Big] \\
&= \sum_q \int r^2 dr d\Omega \sum_\sigma \sum_{nljm_j} \sum_{n'j'm'_j} \epsilon^{(q)}_{(nljm_j),(n'ljm'_j)} \delta_{jj'}\delta_{m_j m'_j} \\
&\quad \Big[\int dr'\, u^{(q)}_{nlj}(r') u^{(q)}_{n'lj'}(r') - \delta_{nn'} \Big] \\
&= \sum_q \int 4\pi r^2 dr \sum_{nn'} \epsilon^{(q)}_{nn'} \sum_{lj} (2j+1) \Big[\int dr'\, u^{(q)}_{nlj}(r') u^{(q)}_{n'lj}(r') - \delta_{nn'} \Big].
\end{aligned} \tag{2.63}
$$

In other words, the physical request of orthogonality of the wave functions involves just their radial part. In fact, the orthogonality of the angular and spin part is implicitly hidden in the decomposition we have made. Note that as well as in the general calculation, the matrix $\epsilon^{(q)}_{nn'}$ is symmetric, and we can pick the $n' \leq n$ case, only. The orthogonality constraints are therefore

$$
\sum_{lj} (2j+1) \Big[\int dr'\, u^{(q)}_{nlj}(r') u^{(q)}_{n'lj}(r') - \delta_{nn'} \Big] \stackrel{!}{=} 0 \tag{2.64}
$$

Thus, summing up these three terms we get the cost functional in spherical

symmetry

$$
\begin{aligned}
&J[\{u^{(q)}_{nlj}(r)\}, v_{KS}(r), \epsilon^{(q)}_{nn'}] = J_{\rm I} + J_{\rm II} + J_{\rm III} \\
&= \sum_q \Big\{ \frac{\hbar^2}{2m_q} \int dr \sum_{nlj} (2j+1) \Big(|\frac{\partial}{\partial r} u^{(q)}_{nlj}(r)|^2 + u^{2(q)}_{nlj}(r) \frac{l(l+1)}{r^2} \Big) \\
&+ \int dr\ v^{(q)}_{KS}(r) \Big[\sum_{nlj} (2j+1) u^{2(q)}_{njl}(r) - 4\pi r^2 \tilde{n}^{(q)}(r) \Big] \\
&+ \int 4\pi r^2 dr \sum_{nlj} \sum_{n'} (2j+1) \epsilon^{(q)}_{nn'} \Big[\int dr'\ u^{(q)}_{nlj}(r') u^{(q)}_{n'lj}(r') - \delta_{nn'} \Big] \Big\}. \qquad (2.65)
\end{aligned}
$$

The Euler-Lagrange equations produce the linear system whose solution minimize the cost functional and satisfies the imposed constraints. We apply the spherical symmetry to the linear system,

$$
\begin{aligned}
&\int dr\, u^{(q)}_{n'jl}(r) \frac{\hbar^2}{m_q} \Big[\frac{\partial^2 u^{(q)}_{nlj}(r)}{\partial r^2} - u^{(q)}_{nlj}(r) \frac{l(l+1)}{r^2} \Big] \\
&= 2 \int dr\, u^{(q)}_{n'jl}(r) v^{(q)}_{KS} u^{(q)}_{nlj}(r) \\
&+ \int dr\, u^{(q)}_{n'jl}(r) \Big[\sum_{s=1}^{n} \epsilon^{(q)}_{ns} u^{(q)}_{slj}(r) + \sum_{t=n}^{N_{\rm max}} \epsilon^{(q)}_{tn} u^{(q)}_{tlj}(r) \Big] \qquad (2.66)
\end{aligned}
$$

The rescaling of the wave functions and the insertion of a penalty functional are trivial and follow the very same procedure we have already done in the general calculation. In particular, the rescaling we have chosen is inspired by the form of the density constraint (2.62):

$$u_{nlj}(r) = \sqrt{4\pi r^2 \tilde{n}}\, g_{nlj}(r). \qquad (2.67)$$

Its substitution into the cost functional reads

$$
\begin{aligned}
&\widetilde{J}[\{g^{(q)}_{nlj}(r)\}, v_{KS}(r), \epsilon^{(q)}_{nn'}] = \\
&\sum_q \Big\{ \frac{\hbar^2}{2m_q} \int dr \sum_{nlj} (2j+1) 4\pi g^{(q)}_{nlj}(r) \Big[\Big(r \frac{\partial \tilde{n}(r)}{\partial r} + r^2 \frac{\partial^2 \tilde{n}(r)}{\partial r^2} - \frac{r^2}{4\tilde{n}(r)} \Big(\frac{\partial \tilde{n}(r)}{\partial r} \Big)^2 \Big) g^{(q)}_{nlj}(r) \\
&+ \Big(2r\tilde{n}(r) + r^2 \frac{\partial \tilde{n}(r)}{\partial r} \Big) \frac{\partial g^{(q)}_{nlj}(r)}{\partial r} + (r^2 \tilde{n}(r) + \delta) \frac{\partial^2 g^{(q)}_{nlj}(r)}{\partial r^2} - \frac{l(l+1)}{r^2} \tilde{n}(r) g^{(q)}_{nlj}(r) \Big) \\
&+ \int dr\ v^{(q)}_{KS}(r) \Big[\sum_{nlj} (2j+1) g^{(q)}_{nlj}(r) - 1 \Big] \\
&+ \int 4\pi r^2 dr \sum_{nlj} \sum_{n'} (2j+1) \epsilon^{(q)}_{nn'} \Big[\int dr'\ 4\pi r^2 \tilde{n}(r') g^{(q)}_{nlj}(r') g^{(q)}_{n'lj}(r') - \delta_{nn'} \Big] \Big\}. \qquad (2.68)
\end{aligned}
$$

2.5.3 Spherical Bondary Conditions

The reduction of the original three-dimensional problem to a unidimensional one, via the change to spherical coordinates, entails the appearance of extra boundary conditions that the solution must respect.

First, the wave functions have to be normalizable, and this imply that its integral has to converge in the origin. This is possible if

$$u(r \to 0) \sim r^{-\beta}, \tag{2.69}$$

with $\beta < 1/2$. However, one can prove that, if the potentials to which the system is subject to are not extremely pathological, the condition above gets more restrictive, that is

$$u(r \to 0) = 0. \tag{2.70}$$

With such a piece of information, a more detailed study of the behaviour of the wave functions in the origin can be done. As $r \to 0$, the centrifugal term is always dominating the Hamiltonian if we require the energy spectrum to be lower bounded. The Schrödinger equation close to the origin then behaves as

$$\frac{d^2u(r)}{dr^2} - \frac{l(l+1)}{r^2}u(r) = 0. \tag{2.71}$$

The equation is solved by polynomials of the type

$$u(r) = Ar^{l+1} + Br^{-l}. \tag{2.72}$$

It is clear that if we apply the integrability conditions we have just discussed above, the parameter $B = 0$, and $u(r \to 0) \sim r^{l+1}$.

At infinity, the behaviour of the wave functions depends on that of the potential. Indeed, if $V(r \to \infty) \to 0$, the asymptotic of the wave functions reflects that of a free particle. In fact, in this case the Schrödinger equation at infinity becomes

$$\frac{d^2u(r)}{dr^2} = -2\mathscr{E}u(r). \tag{2.73}$$

Bounded states ($\mathscr{E} < 0$) then behave as

$$u(r \to \infty) \sim e^{-\sqrt{2|\mathscr{E}|}r}. \tag{2.74}$$

Last but not least, note that in contrast with the unidimensional case, where the existence of at least one bound state is always guaranteed, this is not the case for three-dimensional systems. In fact, it is known that the ground state of a system subject to an one-dimensional system exists, is even, and the excited states alternate their parity. Nonetheless, even though we have seen that the Hamiltonian of a spherical symmetric system can be treated as one-dimensional (keeping into account the restriction $r > 0$), the boundary condition (2.72) implies that only odd solutions are acceptable, and a ground state may not exist. Finally, the repulsiveness of the centrifugal potential certainly involves that the number of possibly bound states decreases as l rises.

2.6 Parametrizations of Experimental Nuclear Densities

With the definition of a theoretically sound density-to-potential method at hand, we are left with the problem of how to obtain the input density for the inversion scheme.

Indeed, one can test the robustness of the model on analytic formulas of the density, as obtained by solving the Schrödinger equation for a given potential and inter-particle interaction. This is what we will discuss about in the first part of the next chapter of the thesis.

It is much more involving and interesting to use some realistic densities as inputs. Those can be obtained in seveveral ways. The second part of next chapter will be devoted to the analysis of the results of the derivation of a Kohn-Sham potential for realistic calculations or experimental data in magic, spherical, nuclei.

We must remark that it is not an easy task to get experimental data on nuclear densities; the literature is poor for which regards neutron densities, while proton densities must be obtained from charge proton density. Nuclear experimental densities are usually deduced by measuring the electron or proton elastic scattering by nuclei. The main reference that collects the experimental proton charge densities of nuclei is a paper by De Vries *et al.* [1]. Electron elastic scattering is the most easy-access method to study nuclear structure, thanks to the fact that the form of the electric force is known. The link between the differential cross section and the form factor of the target depends on the nature of the forces acting between the probe and the target. In Plane-Wave Born Approximation, valid for small atomic number Z, for the case of Coulomb forces, the relation is given by

$$\frac{d\sigma(q)}{d\Omega} = \sigma_{\text{Mott}}|F(q)|^2, \tag{2.75}$$

where σ_{Mott} is the Mott cross section [43], that is typical of the scattering of an electron beam from a target with the size of a nucleus. In the case of high Z, a more involved model (Distorted-Wave Born Approximation) must be used, and details of the proportion between the two quantities can be found in [44]. Then, the form factor of the nucleus depends on the charge density as

$$\hat{F}(q) = 4\pi \int_0^\infty r\, dr\, \frac{\sin(qr)}{q} n_{\text{charge}}(r), \tag{2.76}$$

The charge density can be obtained as the inverse Fourier transformation of the above equation. The energy scale of the electron-proton interaction is low enough to allow stopping perturbative calculations of cross sections at the first order. On the other hand, there are at least two evident drawbacks in such type of measurements of the density:

- electrons interact with protons only, not with neutrons. Therefore, via electronic scattering experiments, it is possible to get proton charge densities, only. A method to calculate the proton barionic density from the proton charge density is therefore needed. As it is shown in appendix D, since the proton form factor is known, this can be done through a deconvolution.

- the experimental analysis of the nuclear form factor is restricted to a finite interval of momentum transfers. It is thereby possible to get sound information only relatively to the exterior part of nuclei. The interior, as well as the long tail,

part of the densities can only be extrapolated through a fit, usually exploiting a minimum χ^2 method and an assumption of the form of the density. Those regions reveal then to be characterized by high uncertainties, and they are rather unreliable.

Zenihiro *et al.* [2] managed to provide the neutron density of few isotopes of lead and tin, through the analysis of elastic proton scattering. Due to the fact that the knowledge of the strong interactions in the mean is all but complete, differential cross sections measured by hadron scattering are in general characterized by much higher and systematic uncertainties than the correspondent electron cross sections. Here, it is necessary to rely on an effective interaction, in order to provide the relation between the form factor and the differential cross section. The energy of the proton beam in those experiments is around 300 MeV. This is a good value both to avoid the production of heavy mesons in the scattering reactions and to extract information about the shape of the surface of the nucleus. Again, the density IS extrapolated in the other regions.

Extrapolations are obtained by assuming a parametrization of the density, that allows for a fit to nuclear charge radii.

A possible choice is to fit the density to a two- or three- parameters Fermi (2pF, 3pF) function:

$$n^{(2pF)}(r) = n_0 \frac{1}{1+e^{\frac{r-c}{z}}}, \tag{2.77}$$

$$n^{(3pF)}(r) = n_0 \frac{1+\frac{w^2 r^2}{c^2}}{1+e^{\frac{r^2-c^2}{z^2}}}, \tag{2.78}$$

where c, z, and w are fit parameters. The main advantage of those kinds of fits is that the tails of the densities result more similar to those theoretically expected, and fall to zero with the correct rough behaviour. However, features of model-dependence are often present: results may highly differ according to the choice of the parameters.

At present, the majority of results are analysed are Fourier-Bessel (FB) analysis and sum of Gaussians (nSoG). Details on the possible choices of the parametrizations of nuclear densities, with their advantages and drawbacks, are available in [45].

In the present thesis we made use of the nSoG parametrizations, only. In fact FB analysis in not adequate for our purposes, since it present a cutoff to zero at some radial value. The discontinuity of the input would then preclude the usage of our method, for which quanties of interest must be at least twice continuous.

It must be highlighted that in the experimental literature, the term model independent is used to address those parametrization that are not highly dependent from the specific value of the parameters. For instance, if the number of Gaussian used in nSoG is large enough, results are independent from that. On the contrary, a given choice of the parametrization entails a specific, different, extrapolation of the densities in the outer regions. In nSoG, the width $\gamma/\sqrt{2}$ of the Gaussians is set to be equal to the smallest width of the radial wave functions, as obtained through Hartree-Fock calculations. The values of $n(r)$ at different values are decoupled; we mean that the rapid decrease of the Gaussians allows to assume that the density at

some point is parametrized, to some extent, by the closest Gaussian, only.

$$n_{(p.n)}^{(nSoG)}(r) = \sum_{i=1}^{n} \frac{A_i^{(p,n)}}{\gamma^3} \left\{ e^{-\frac{(r-R_i)^2}{\gamma^2}} + e^{-\frac{(r+R_i)^2}{\gamma^2}} \right\} \tag{2.79}$$

$$A_i^p = \frac{ZeQ_i}{2\pi^{\frac{3}{2}}(1+2\frac{R_i^2}{\gamma^2})} \tag{2.80}$$

$$A_i^n = \frac{NQ_i}{2\pi^{\frac{3}{2}}(1+2\frac{R_i^2}{\gamma^2})} \tag{2.81}$$

$$\tag{2.82}$$

For which regards De Vries' densities, this represents the parametrization of the proton charge density; it is necessary to apply the deconvolution we have mentioned above in order to obtain the proton density,

$$n_p^{(SoG)}(r) = \sum_{i=1}^{n} \frac{A_i}{e\beta r} \left\{ \left(\frac{r-R_i}{\beta^2} + \frac{R_i}{\gamma^2} \right) e^{-\frac{(r-R_i)^2}{\beta^2}} + \left(\frac{r+R_i}{\beta^2} - \frac{R_i}{\gamma^2} \right) e^{-\frac{(r+R_i)^2}{\beta^2}} \right\}. \tag{2.83}$$

Instead, in Zenihiro's article, parametrization (2.80) with (2.81) is obviously directly referred to neutron densities. The parameters R_i represent the centres of the Gaussian, while Q_i are related to the fraction of charge (or of particles) brought by each Gaussian. Indeed, $\sum_{i=1}^{n} Q_i = 1$.

The main drawback of such parametrization is that it assumes a completely wrong analytical shape for the tails of the densities. We will see how, within the nSoG parametrization, the extrapolated tail of the density will produce a potential that is known to produce Gassians wave function: the harmonic oscillator potential.

Chapter 3

Implementation of the Constrained Variational Method and Inversion Results

The chapter is devoted to present the results of the CV method for the solution of the inverse Kohn-Sham problem. The first section discusses the numerical implementation of the method. Then, a series of tests of increasing complexity is presented. Finally, we analyse and discuss the results of the inversion when the input density is a nuclear one.

3.1 Implementation of the Constrained Variational Method

The perspective we have followed during almost one year of developments has been to provide an algorithm applicable to inverse problems that are as general as possible. In the end, we managed to build a software that can be used for solving three-dimensional spherical problems. However, the formalism of the method, as well as its implementation, are explicitely thought in order to make further generalizations natural.

We make use of the IPOPT (Interior POint OPTimizer) library[1], projected to solve large-scale non-linear optimization problems of the kind

$$\min_{\vec{x}\in\mathbb{R}^n} f(\vec{x}) \tag{3.1}$$

$$\text{s.t. } g_i^L \leq g_i(\vec{x}) \leq g_i^U \tag{3.2}$$

$$x_j^L \leq x_j \leq x_j^U, \tag{3.3}$$

where x_j are the variables of the problem, f is the objective function to be optimized, and g_i are constraints. The functions can be linear or non-linear, convex or non-convex, but should be at least twice continuously differentiable. In general, the constraints have lower and upper bounds, but those can collapse one on the other to specify equality constraints. The software implements an interior-point filter line-search algorithm [46], that aims to find a local solution of the optimization problem.

[1] `https://projects.coin-or.org/Ipopt`

We make use of the software to perform the numerical constrained-minimization of the objective function. In our case, this would be (2.11) for a non-scaled, non-regularized cartesian problem, the first term of (2.31) for a scaled and regularized cartesian problem, and the first term in (2.68) for a spherical problem. The program requires, as a further input with respect to the target density, a starting guess for the set of the Kohn-Sham orbitals. In the section of the results, we will discuss, case by case, which has been the particular choice of the starting point for the optimization. The software begins modifying such initial guess for the orbitals, aiming to make new trials minimize the objective function and to respect the constraints of the problem. The routine computes then, at each step, the objective function and its gradient, that is used for the choice of the search direction. The program also calculates at each step the constraints (2.12) and (2.13), their violation with respect to zero and their gradient. Second derivatives of the quantities listed above are passed to the software by building the Hessian of the Lagrangian of the problem, that is

$$\mathscr{H}_{kl}[f(x), g_i(x); \lambda_i] = \frac{\partial^2 f(\vec{x})}{\partial x_k \partial x_l} + \sum_i \lambda_i \frac{\partial^2 g_i(\vec{x})}{\partial x_k \partial x_l}, \tag{3.4}$$

where λ_i are the Lagrange multipliers correspondent to the constraints g_i. Finally, the search must be restricted to a compact space, to guarantee the existence of an extremum and to satisfy the hypotheses of the Lagrange Multiplier Method. We will discuss the values of the intervals defining such compact space, case by case, in the following.

In general, if the new trial for the optimization improves the objective function value, or if it improves the violation of the constraints, the new guess is accepted; else, the iteration is restored to the previous step. The process is iterated up to when a local minimum is found, that is when small variations of the orbitals do not produce any decrease of the objective function, within a user-chosen tolerance. With such piece of information, the linear system of Euler-Lagrange equations, given by (2.22), can be solved.

As we have already mentioned, a discretization of the variables of the problem is required for the numerical implementation of the problem. Therefore, the space is divided into a grid of equidistant points. The variables of the problem, that is the Kohn-Sham orbitals, are defined, point by point, on the spatial grid. The choice of the methods for deriving and integrating becomes then crucial for the efficiency of the minimization.

More details on the implementation of numerical derivatives, integrals and on the implementation of the quantities mentioned above, are available in appendix E.

3.2 Unidimensional Numerical Tests

3.2.1 Harmonic Oscillator Density

As a first test, we apply our inversion scheme to a unidimensional system subject to an harmonic external field, that is

$$v_{\text{ext}}(x) = \frac{1}{2} m\omega^2 x^2, \tag{3.5}$$

For such a simple system we have an analytic expression for all of the eigenfunctions,

$$\phi_n(x) = c_n H_n\Big(\sqrt{\frac{m\omega}{\hbar}}x\Big) e^{-\frac{m\omega x^2}{2\hbar}} \tag{3.6}$$

$$c_n = \sqrt{\frac{1}{2^n n!}}\Big(\frac{m\omega}{\pi\hbar}\Big)^{\frac{1}{4}}. \tag{3.7}$$

The Hermite polynomials are formally defined as

$$H_n(x) = (-1)^n e^{x^2} \frac{d^n}{dx^n} e^{-x^2}, \tag{3.8}$$

and can be implemented according to the recurrence relation

$$\begin{aligned} &H_0(x) = 1, \\ &H_1(x) = 2x, \\ &H_n(x) = 2xH_{n-1}(x) - 2(n-1)H_{n-2}(x) \end{aligned} \tag{3.9}$$

for $n \geq 2$. Therefore, depending on the number of filled orbitals, we get an analytic expression of the target density by using equation (1.56).

One-orbital Inversion

We begin by considering a one-orbital system. The target density reads

$$\widetilde{n} = \phi_0^2(x) = \Big(\frac{m\omega}{\pi\hbar}\Big)^{\frac{1}{2}} e^{-\frac{m\omega x^2}{\hbar}}. \tag{3.10}$$

Thus, the system we must solve is

$$\begin{cases} \varphi_1^2(x) - \widetilde{n}(x) = 0 \\ \frac{\hbar^2}{m}\int dx\, \varphi_1(x)\nabla^2\varphi_1(x) = 2\int dx\, (v_{KS}(x) + \epsilon_{11})\varphi_1^2(x) \end{cases} \tag{3.11}$$

Since just one orbital is occupied, the requirement of normalization is hidden in the first equation. Also the only orbital is determined by $\varphi_1(x) = \pm\sqrt{\widetilde{n}(x)}$. This happens every time we consider one-orbital systems. Such feature renders one-orbital inversions somehow special: an analytical solution of the inversion is always possible and the inversion problem is actually well-posed (in particular, the solution is unique) if we discard the negative solution and forget the arbitrary constant of the potential. With the Kohn-Sham orbital at hand, one computes its Laplacian,

$$\begin{aligned} \nabla^2\varphi_1(x) &= \frac{d^2}{dx^2}\Big[\Big(\frac{m\omega}{\pi\hbar}\Big)^{\frac{1}{4}} e^{-\frac{m\omega x^2}{2\hbar}}\Big] \\ &= \varphi_1(x)\Big(\frac{m\omega}{\hbar}\Big)\Big[\Big(\sqrt{\frac{m\omega}{\hbar}}x\Big)^2 - 1\Big], \end{aligned}$$

and gets the Kohn-Sham potential by comparison of the two integrands in the second equation of (3.11),

$$\begin{aligned} v_{KS}(x)+\epsilon_{11} &= \frac{\hbar^2}{2m}\left(\frac{m\omega}{\hbar}\right)\left[\left(\sqrt{\frac{m\omega}{\hbar}}x\right)^2-1\right] \\ &= \frac{1}{2}m\omega^2x^2-\frac{1}{2}\hbar\omega \\ &= v_{\text{ext}}-E_0. \end{aligned} \tag{3.12}$$

Note that, as it is expected, the Kohn-Sham potential in absence of an inter-particle interaction is indeed equal to the external field. Moreover, the Kohn-Sham orbital is exactly the eigenfunction of the Hamiltonian. The Lagrange multiplier ϵ_{11} corresponds to minus the energy of the first orbital. Nevertheless, this is trifling, since the potential is defined up to a constant.

In the one-orbital case the only unitary transformation we can apply to the KS orbital is a change of sign. This is again unimportant, since this information is lost in the density computation. The explicit formula for the solution of the inversion problem in the one-orbital case [22] reads

$$v_{KS}(\vec{r}) = \frac{\nabla^2\varphi_1(\vec{r})}{2\varphi_1(\vec{r})} = \frac{\nabla^2\sqrt{\widetilde{n}(\vec{r})}}{2\sqrt{\widetilde{n}(\vec{r})}} \tag{3.13}$$

The first test of the routine takes such density of a one-orbital unidimensional quantum harmonic oscillator.

Based on the extent of the input density, we choose the compact space for the minimization as $[-8,8]$, with a mesh $h=0.1$. For the sake of simplicity we make use of natural units, $m=1$, $\omega=1$, and $\hbar=1$. We will restore those quantities to their physical values while studying three-dimensional systems.

If we do not take any precaution, the test immediately exhibits the numerical issues we have already discussed in the second chapter. In fact, while the minimizing orbital is properly constructed in the entire space (see figure 3.1) almost independently from the choice of the starting guess, figure 3.2 shows that the numerical errors in the Kohn-Sham potential become important already for $|x|>1$, where the potential starts not to follow the expected parabolic behaviour. Instead, the shape of the potential in the central region is reasonable.

If we make use of the one-orbital formula (3.13), instead of applying the CV method, the potential is better reproduced, but still it stubles into numerical errors in the outer regions, for $|x|>3.5$; this is shown in figure 3.3.

It is interesting to point out that indeterminately refining the spatial grid does not entail any sensitive improvement of the results; on the contrary, it does increase the number of variables to be treated, and weights on the computational cost of the routine.

The unsatisfactory results call for a new numerical approach; the scaling (2.29) of the wave functions comes at hand. In fact, the results of the inversion are definitely improved once we rescale all the terms in the cost functional. Such a remarkable improvement is due to the fact that the rescaling process renders the quantity to be minimized of the same order of magnitude in the entire space. This feature solves the problem of roundings in the summation of wave functions characterized by a rapid, exponential, decay to zero.

The program finds the right solution even for starting points that can be pretty far from the expected solution, e.g. for strongly non-localized guesses such as a

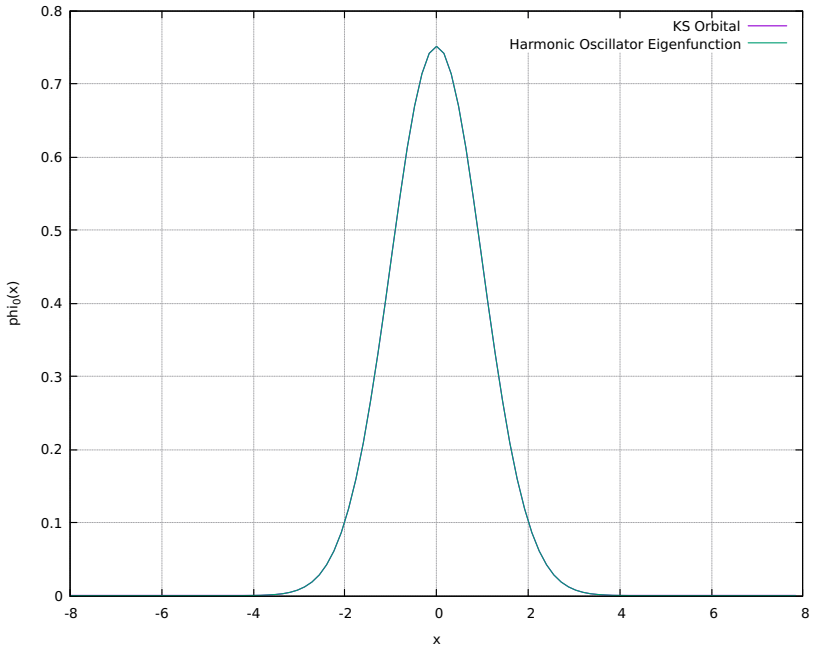

Figure 3.1: The Kohn-Sham orbital for a single particle, subject to a harmonic oscillator trap, is Gaussian and concide with the first eigenfunction of the harmonic oscillator.

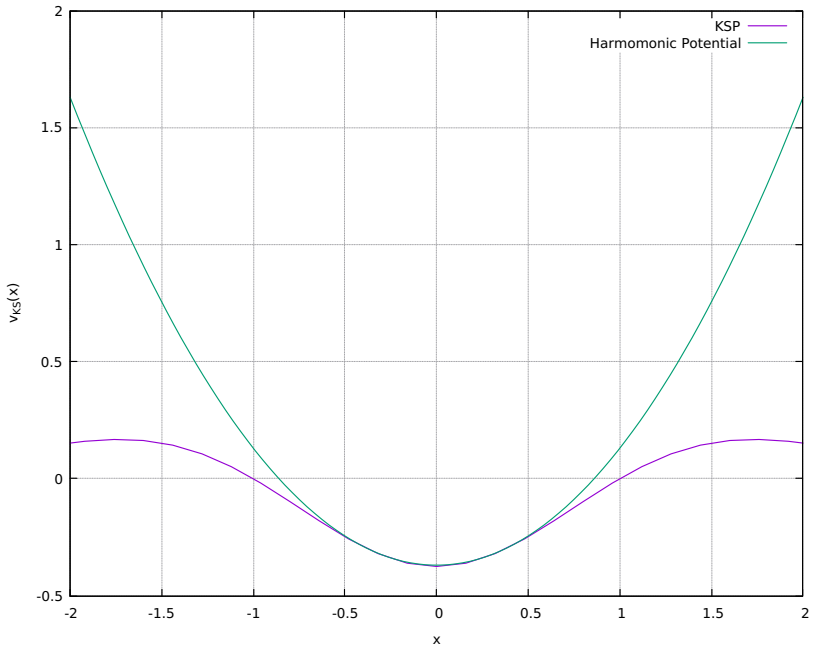

Figure 3.2: The Kohn-Sham potential as it results from a non-scaled one-orbital harmonic oscillator inversion.

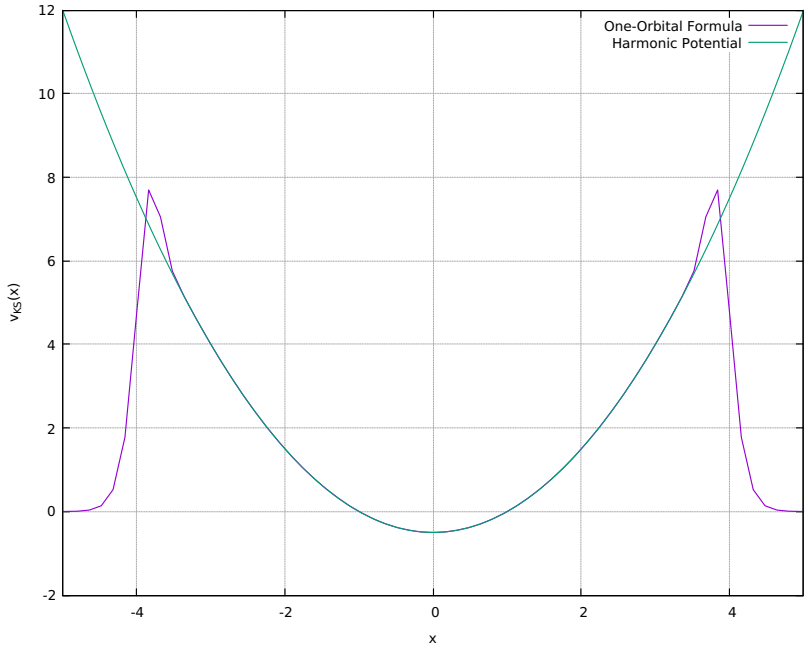

Figure 3.3: The Kohn-Sham potential, computed through the one-orbital anlaytic formula (3.13), compared with the expected potential.

sinusoidal wave function guess. The result is illustrated in figure 3.4, for a starting guess of a constant scaled wave function.

In the present test of the routine we provided the analytical structure of the first and of the second derivative of the density function, which are required by the program in the scaled scheme (compare equation (2.17) and (2.31); derivatives of the density appear in the latter), but the generalizing perspective brought us to a numerical automation of those calculations in the following tests.

Many-Orbital Harmonic Oscillator

The major addition coming along with the increasing number of filled orbitals is certainly the necessity of imposing orthonormality constraints. This is necessary also to avoid trivial solutions of the inversion, e.g. $\phi_i = \sqrt{\widetilde{n}(x)}$ and $\phi_{i\neq j} = 0$.

The insertion of a regularization scheme becomes more and more important, in order to prevent oscillating solutions. In fact, the two different types of constraints tend to compete in the search of the minimum, and may produce non-physical results. The reason of this behaviour is that when more than one degree of freedom is present, the inversion problem really becomes ill-posed. As we already discussed, the insertion of a non-vanishing regularization term put then an artificial upper bound to the norm of the gradient of the wave functions, it reduces the number of possible solutions and renders them smoother. The effect of the presence of the penalty functional, with a penalty parameter $\delta = 0.1$[2], is shown in figures 3.5 and 3.6 for the case of a two-orbital system. The effect is more marked if the number of filled

[2] Equal to the mesh, that is our estimate of the numerical noise of the input density.

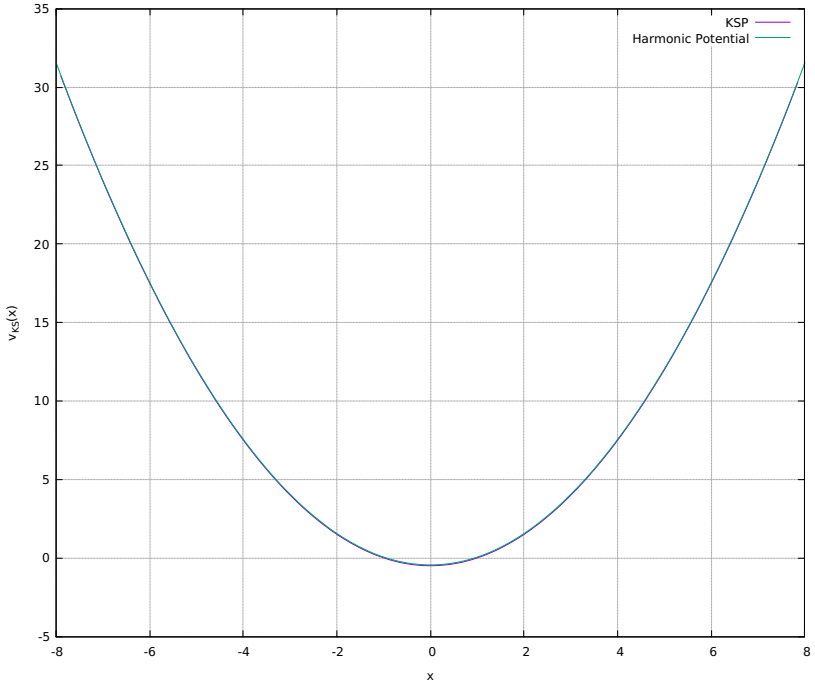

Figure 3.4: The Kohn-Sham potential as obtained from a scaled one-orbital harmonic oscillator inversion.

orbitals in the system increases.

The increased number of degrees of freedom of the system results in a higher number of possible unitary transformations of the wave functions to appear as solutions of the minimization. In particular, the wave functions tend to mingle and exchange one with each other, especially in the central region. Figure 3.7) shows the Kohn-Sham wave functions obtained in a run of the software with three filled orbitals, versus the eigenfunctions of a harmonic oscillator eigenvalue problem. It is interesting to notice that the Kohn-Sham wave functions follow the parity of the correspondent eigenfunctions. In other words, even (odd) Kohn-Sham orbitals are unitary transformation of even (odd) eigenfunctions. No mixing is present. However, those unitary transformations do not affect at all the Kohn-Sham potential structure; figure 3.8 shows this aspect.

It also becomes important not to pick up a very poor starting guess; still, the choice is quite free, once it respects some basic symmetries and properties of the solution. In these tests we have used monomials $(x/8)^j$[3] of rising degree as starting point of the minimization; they approximately follow the parity of the solution, but are satisfactorily far from it. It is necessary to be pretty specific in fixing the limits of the compact space. The space must obviously be big enough to host orbitals that respect the constraints. However, if such compact space is too big, the many trial options to be explored may render the convergence unreachable.

The routine is in principle able to solve the inversion problem for an arbitrary number of degrees of freedom, but with time and computational limits. In particular,

[3]The guess is normalized in order not to go out from the compact space in which the software works.

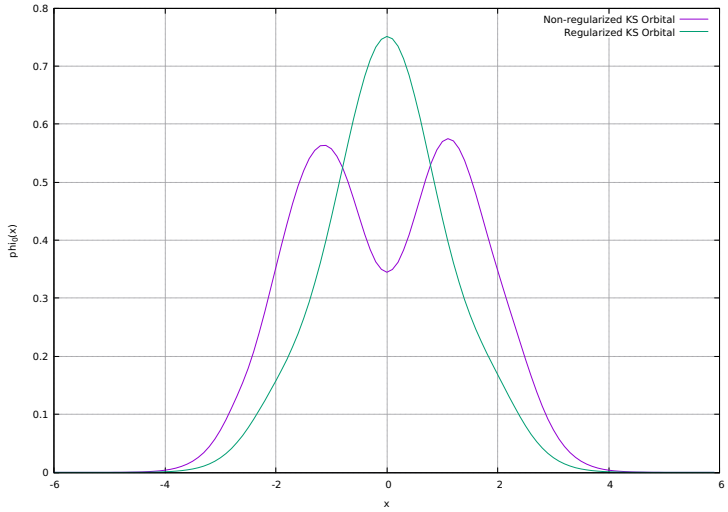

Figure 3.5: The first Kohn-Sham orbitals resulting from a two-orbital inversion in absence of a regularization scheme, compared with the same orbital calculated using the Tikhonov regularization. The number of inflexion points diminishes.

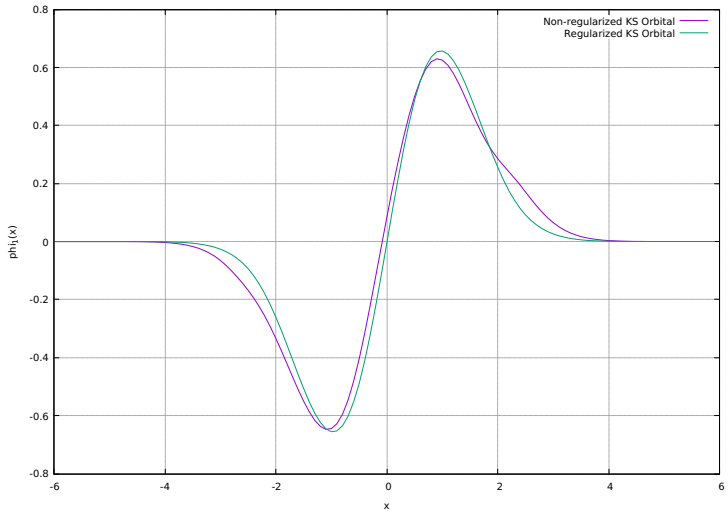

Figure 3.6: The second Kohn-Sham orbitals resulting from a two-orbital inversion in absence of a regularization scheme, compared with the same orbital calculated using the Tikhonov regularization. The asymmetries disappear.

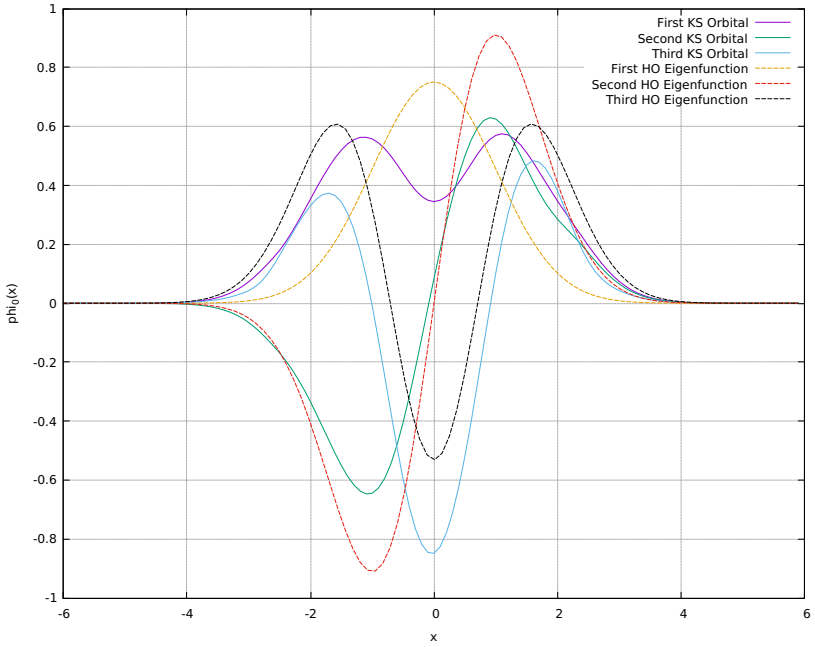

Figure 3.7: The Kohn-Sham orbitals resulting from a three-orbital inversion (solid lines) compared with the first three eigenfunction of the harmonic oscillator (dashed lines).

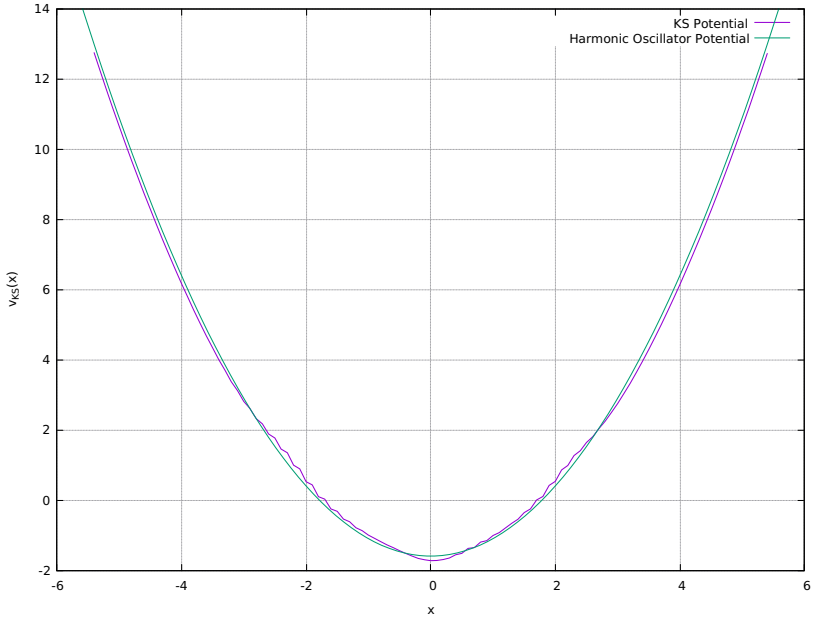

Figure 3.8: The Harmonic Kohn-Sham potential in a three-orbital system, as recovered from the Kohn-Sham orbitals shown in figure 3.7.

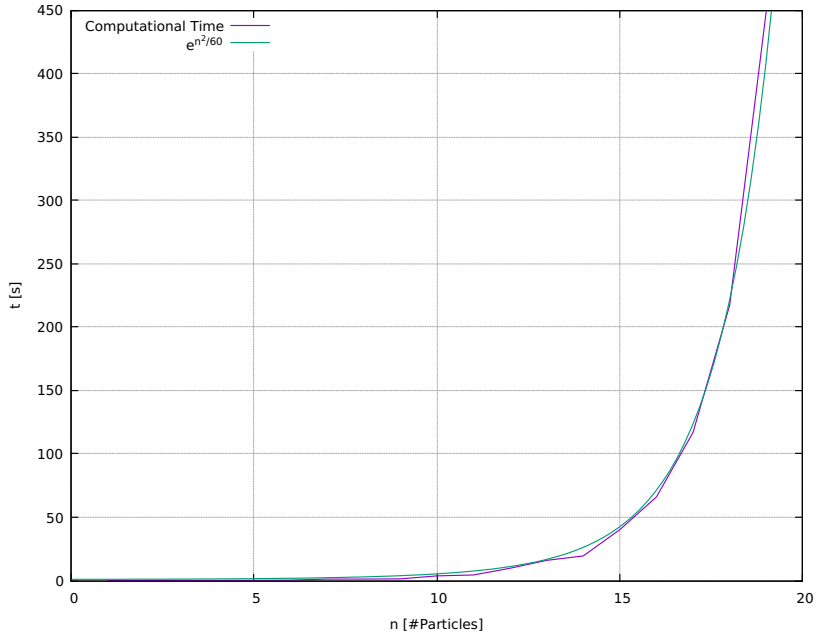

Figure 3.9: The computational time is a steep function of the number of filled orbital (degrees of freedom of the problem) in the harmonic oscillator inversion. A qualitative comparison of such function with $e^{n^2/60}$ is also illustrated in the figure.

we point out that the computational time increases exponentially with the number of degrees of freedom, and this is a great limitation especially when a poor starting guess is chosen. Figure 3.9 exhibits this feature. The number of variables and the amount of calculations done to evaluate the function in the routine are the main reasons explaining this type of growth. Still, this is a harsh limit only if we would want to use the software as a brute force tool, without taking into account the symmetries and the properties of the problem under investigation. Instead, the perspective for the usage of the program is good enough if we plan to face up problems in which we are able to provide good starting points, and in which we have a knowledge of features characterising the solution.

The spatial mesh is usually taken of the order of 10^{-1} fm, and the tolerance for the acceptance of the solution is set to 10^{-4} fm, roughly what we expect to be the numerical error correspondent to the chosen implementation of the numerical methods. The above tolerance is set both as the relative error in order to ensure that the iterations have effectively reached an optimal value and as the absolute value of the constraints violation.

3.2.2 Morse Oscillator Density

Another group of tests deals with the density typical of a Morse Oscillator [47]

$$v_{\text{ext}}(x) = D(1 - e^{-\alpha x})^2, \tag{3.14}$$

whose structure is depicted in figure 3.10. Variables x actually stands for $r - r_e$, r_e being some equilibrium value. This potential is often used to describe the energy

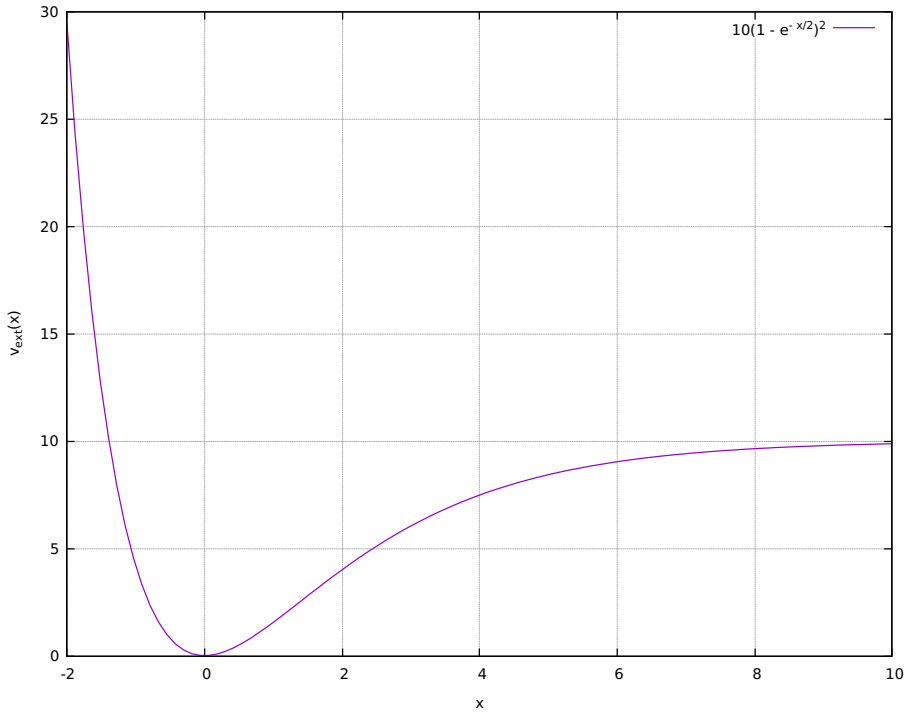

Figure 3.10: The Morse Oscillator for $D = 10$ and $\alpha = 1/2$.

spectrum of vibrating, non-rotating diatomic molecules. Also, it has been widely used in the study of collision theory and intra- or inter-molecular bindings. For detailed application of the Morse potential we address the reader to [48].

Our main interest in such potential, in comparison with the harmonic one, comes from the fact that it saturates at infinity. The same happens for the nuclear potential, that goes to zero at infinity. The system presents then a finite number of bound states and its density gets certainly closer to those we will be meant to treat at the end of the tests.

Before listing the eigenfunctions of a system subject to a Morse potential, we need a brief series of definitions. Let us define $\xi = e^{-\alpha x}$ and $\lambda = \sqrt{2D}/\alpha$; let $\Gamma(x)$ be the Euler's Gamma function,

$$\Gamma(x) = \int_0^\infty dt\ t^{x-1} e^{-t}, \tag{3.15}$$

and $L_n^{(\alpha)}(x)$ the so called associated Laguerre polynomials,

$$L_n^{(\alpha)}(x) = \frac{x^{-\alpha} e^x}{n!} \frac{d^n}{dx^n}(e^{-x} x^{n+\alpha}), \tag{3.16}$$

that satisfy the recurrence rule

$$nL_n^\alpha(x) = (-x + 2(n-1) + \alpha + 1)L_{n-1}^\alpha(x) - (n - 1 + \alpha)L_{n-2}^\alpha(x) \tag{3.17}$$

for $n \geq 2$. Note that for $\alpha = 0$, we recover the usual definition of the Laguerre polynomials. Then, the system presents $[\lambda + 1/2]$ normalized bound states, those that solve

the Schrödinger equation

$$-\frac{\hbar^2}{2m}\frac{d^2\psi}{dx^2} + D(1-e^{-\alpha x})^2\psi = \mathscr{E}\psi. \tag{3.18}$$

The explicit form of the eigenfunctions is found to be [49]

$$\psi_{\lambda,n}(\xi) = N(\lambda,n)\xi^{\lambda-n-\frac{1}{2}}e^{-\frac{\xi}{2}}L_n^{(2\lambda-2n-1)}(\xi), \tag{3.19}$$

$$N(\lambda,n) = \sqrt{\frac{(2\lambda-2n-1)\Gamma(n+1)}{\Gamma(2\lambda-n)}}, \tag{3.20}$$

for $n = 0,\ldots[\lambda-1/2]$.

We have chosen the potential parameters as $\alpha = 1/2$, $D = 10$, so that $\lambda \approx 8.9$ and the potential well offers room for nine bound states. The inversion process behaves for all of the possible degrees of freedom in the system. Here the interval of definition of the orbitals is chosen as $[-3,6]$, with a mesh equal to $h = 0.1$, and penalty parameter $\delta = 0.1$. The starting guess for the minimization is a set of rising monomials, as well as for the harmonic oscillator tests; this decision stems out from the fact that the Morse potential in the neighbours of its minimum can be approximated to a harmonic oscillator. Figure 3.11 exhibits the potential we have extracted for a seven-orbital system. Some numerical noise is present in the intermediate part of the potential. Those small oscillations, that can also be noticed in figure 3.8, have been present in many results of the tests until, while analysing the three-dimensional harmonic oscillator problem, we inserted a correction into the code, relatively to the implementation of the Simpson's integration method.

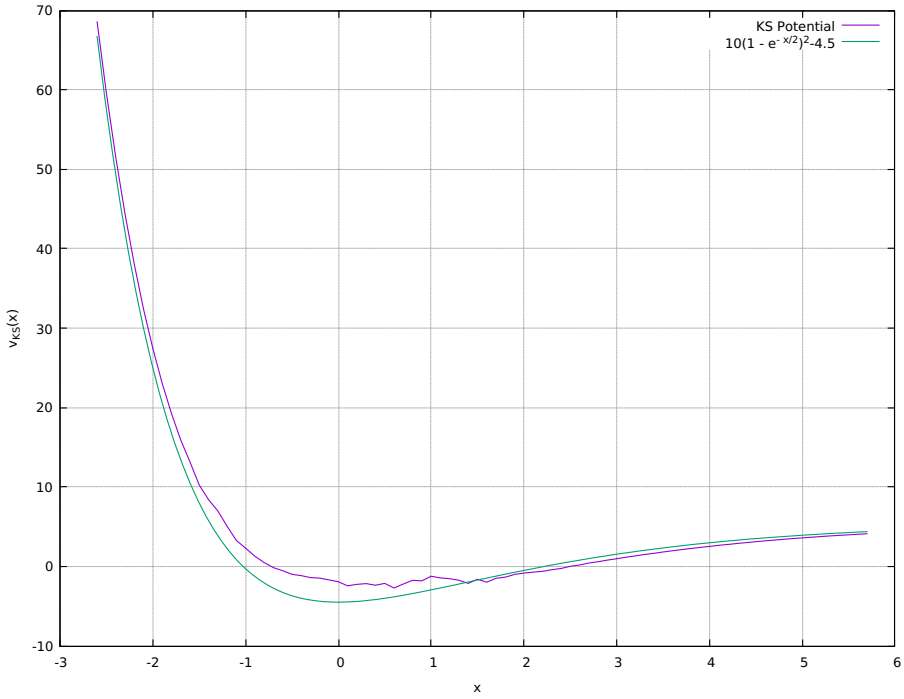

Figure 3.11: The Kohn-Sham potential from the density of seven-orbital in a Morse oscillator trap.

3.3 Three-dimensional Test

Harmonic Oscillator Inversion

The first application of the three-dimensional spherical version of Constrained Variational method has been done on a system characterized by the density typical of an isotropic harmonic three-dimentional oscillator,

$$v_{\text{ext}}(r) = \frac{1}{2} m\omega^2 r^2, \tag{3.21}$$

where $m = 939$ MeV is the approximate mass of a nucleon and $\omega = 41/A^{\frac{1}{3}}$ [24]. By chosing those values for the mass and the frequency of the oscillator, we mean to provide results that will be comparable, at least to some extent, to those we will obtain with nuclear densities. In fact, as we have discussed while presenting the Nuclear Shell Model, the harmonic oscillator is a first approximation of the nuclear average potential that acts on the individuals nucleons, especially adequate in the inner part of nuclei.

The solution of the Schödinger eigenvalue problem with an harmonic potential is the set of eigenfunctions

$$\psi_{nlm}(r,\theta,\phi) = R_{nl}(r)\,Y_{lm}(\theta,\phi) = N_{nl}\, r^l e^{-\nu r^2} L_{n-1}^{(l+\frac{1}{2})}(2\nu r^2)\, Y_{lm}(\theta,\phi), \tag{3.22}$$

$$N_{nl} = \sqrt{\sqrt{\frac{2\nu^3}{\pi}} \frac{2^{k+2l+2} k! \nu^l}{(2n+2l-1)!!}}, \tag{3.23}$$

$$\nu = \frac{m\omega}{2\hbar}, \tag{3.24}$$

where $L_{n-1}^{(l+\frac{1}{2})}(2\nu r^2)$ are the generalized Laguerre polynomials already defined in equation (3.16). The corresponding eigenvalues,

$$E_{nl} = \hbar\omega\Big(2(n-1) + l + \frac{3}{2}\Big), \tag{3.25}$$

set a clear energy order and define the degeneracy $d = \sum_l (2l+1) = \frac{(n+1)(n+2)}{2}$.

From the orbitals written in the decoupled basis, the density is obtained as

$$n(r) = \sum_{(nl)} \frac{2l+1}{4\pi} |R_{nl}(r)|^2. \tag{3.26}$$

We can always decide how many particles to put in the system, up to some numerical limit. The test was mainly developed to benchmark the application of the inversion schemes to nuclei. Results are mainly positive and do not present any new critical feature with respect to those we have already encountered in the one-dimensional tests. We choose the interval of definition as $[0, 12]$ fm, with mesh $h = 0.1$ fm and penalty parameter $\delta = 0.1$. The starting guess is taken as functions that are proportional to the eigenfunctions of the harmonic oscillator. We report the result of a succesful inversion, with the input of a four orbitals' harmonic oscillator density (see figure figure 3.12). In particular, the Kohn-Sham orbitals we obtain, shown in figure 3.13, respect the number of nodes of the eigenfunction of the direct problem. The Kohn-Sham potential relative to such density is illustrated in figure 3.14.

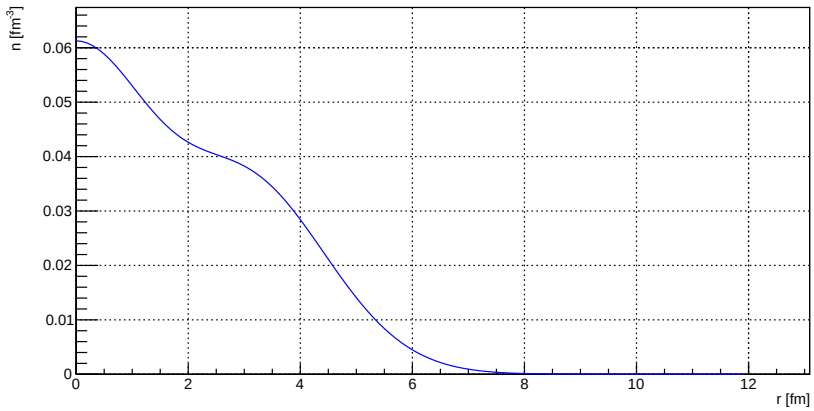

Figure 3.12: The density of a system composed by twenty particles, distributed in the four lowest-energy orbitals, in an isotropic harmonic oscillator trap.

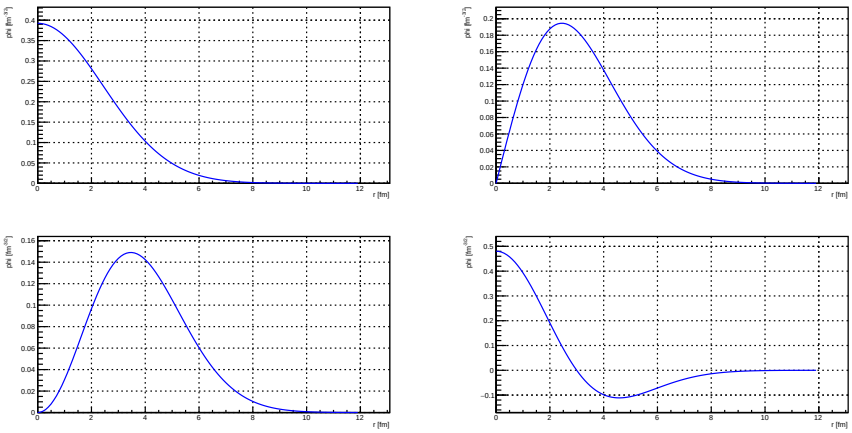

Figure 3.13: The Kohn-Sham orbitals that are obtained by minimizing the objective function highly resemble the $1s$, $1p$, $1d$, and $2s$ eigenfunctions (respectively from left to right, top to bottom) of the harmonic oscillator.

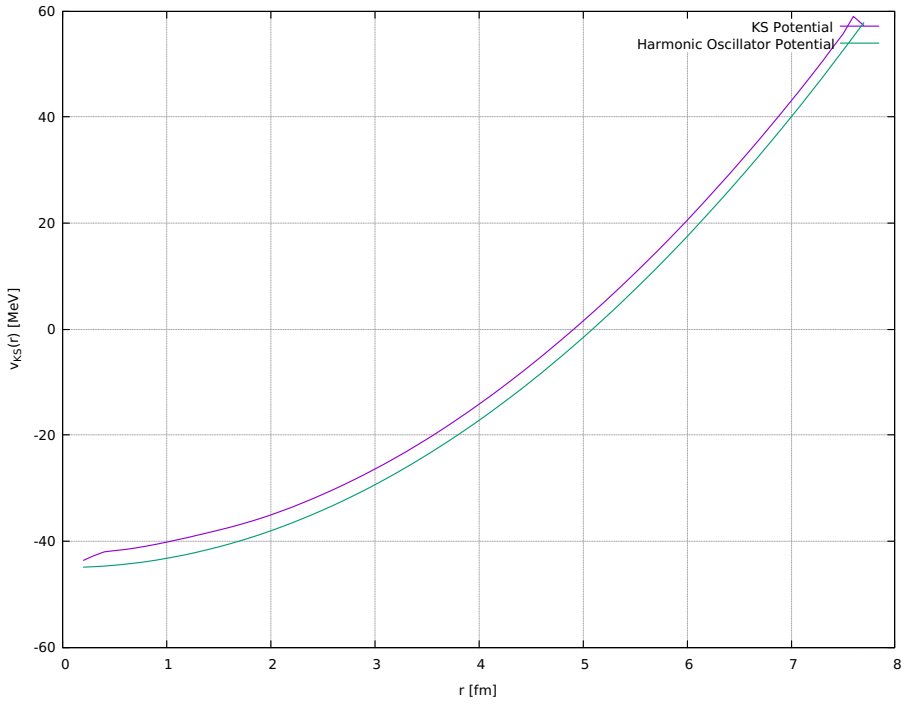

Figure 3.14: The Kohn-Sham potential of a system composed by twenty particles, distributed in the four lowest-energy orbitals, versus the expected result. The potentials are shifted to provide a better qualitative comparison.

3.4 Kohn-Sham Potential Deduced from Nuclear Densities

With the aid of the Constrained Variational method we proceed to deduce the Kohn-Sham potential from the experimental densities of magic nuclei. We have already discussed, in the first section of the manuscript, how those nuclei present a higher average binding energy than one would expect by analysing the semi-empirical mass formula (1.3) and how they are more stable against decay with respect to other configurations. Closed-shell systems are characterized by spherical symmetry, that leads to a complete cancellation of the angular dependence of the quantities of interest, the density (2.53) above all.

In the following, we will investigate four nuclei: ^{4}He, ^{16}O, ^{40}Ca, and ^{208}Pb. The choice of studying each nucleus is guided by particular reasons;

- ^{4}He is a one-orbital nucleus. We can then benchmark the results of our minimization method against the one-orbital analytic and exact formula (3.13).
- ^{16}O and ^{40}Ca are interesting cases of light and medium-mass nuclei. For each of them, the literature makes available both the nSoG and the 3pF parametrizations. We will especially focus on the investigation of model-dependence features. This will hopefully help us to understand what are the limitations of our procedure that do not depend on the physics of the system, but on the implementation of our inversion routine.
- ^{208}Pb is a heavy nucleus. We will address the study of this nucleus to propose possible solutions to the model-dependence features that characterize experimental densities. Moreover, the investigation of a theoretical Lead density, together with other techniques, will be exploited to qualitatively understand how errors propagate from the nuclear density to the Kohn-Sham potential.

We will organize the analysis of results concerning the study of each nuclear potential from the lighter to the heavier nucleus. Our objective is to let the reader understand which issues stem out when one deals with densities that are obtained through a model-dependent analysis, other than being characterized by numerical uncertainties. Also, the following exposition is thought in order to highlight the differences between model-dependent and numerical issues, to clarify their causes and to try proposing a solution to them.

3.4.1 The Helium Nucleus

The ^{4}He proton charge density is made available by [1] in the 10SoG parametrization. Figure 3.15 illustrates the proton density that has been used as the input of the inversion scheme. The results of this inversion are an application of the numerical method to a system that is characterized by one filled $1s_{1/2}$ orbital, only. A comparison of the Kohn-Sham potential can be therefore done with the analytic, exact result given by equation (3.13). The Helium nucleus represents a good laboratory in order to begin comprehending the limitations that the choice of the density parametrization has on the Kohn-Sham potential.

The Kohn-Sham potential of the numerical minimization coincides to that obtained analytically. We can assert that the inversion procedure works fine in the one-orbital case. In figure 3.16 we draw the result of the numerical inversion, only,

but the analytic potential would exactly coincide. Here and in the following inversions, the starting guess is the set of the eigenfunctions (3.22) of the harmonic oscillator. The domain of the orbital is chosen as $[0.1,7]$ fm, with a mesh $h = 0.1$ fm. Such values are chosen by looking at the input density, that can be considered to be decayed to zero at the position of $r \approx 6-7$ fm. We cannot explore the potential at $r = 0$ fm, since the de-convoluted proton density (2.83) is not defined for such value.

The knowledge of the density does not carry any piece of information about the value of the arbitrary constant of the Kohn-Sham potential, but since in the Helium case an asymptotic behaviour appears evident, we can shift the result to let it go to zero at large distance, as it should.

The potential has a reasonable depth of $V_p \approx -42$ MeV, that is 5 MeV away from the expected phenomenological value, according to the proton average potential (1.28). The difference is about 10 %. The radial extent of the potential is too long if compared to that expected, that is $R(^4\text{He}) = 1.6755(28)$ fm [4]. If we look at the position where the potential has reached half of its depth, this correspond approximately to $r = 3.5$ fm, that is almost twice the expectation. Such spread may be caused by the fact that we are considering a small finite nucleus within local density approximation; contributions due to the gradient of the density function may be decisive in determining the form of the Kohn-Sham potential.

If we extend the radial domain of the orbital to $[0.1,8]$, a non-physical behaviour appears (see figure 3.17): the tail of the potential is wrong and resembles a parabolic growth. This feature can be explained by the fact that the Gaussians used in the nSoG parametrization of the density extend up to 4.9 fm. The tail of the density is extrapolated as the tail of the last of the Gaussian of the parametrization. Indeed, the potential that produces a Gaussian-modulated density is an harmonic oscillator potential. We encounter here for the first time the strong limitation that characterizes the nSoG parametrization. The functional assumption for the extrapolation of the densities at large r in the experimental literature is found to be wrong.

This statement seems to collide with the results provided in [13], where apparently positive and physically meaningful results have been deduced from a 12SoG Lead neutron density of the Lead for the tail of the Kohn-Sham potential. We assert that such result must be labelled as an inverse crime. In fact, the inversion method (vLB) that has been used there is characterized by a great bias due to the fact that its starting guess is given by a Woods-Saxon potential. Because of its particular convergence criterion, the method does not modify the tail of the Woods-Saxon potential to let it agree with the nSoG density. While discussing the case of Lead neutron density, we will discuss a possible technique to proceed to a correct extrapolation of the tail.

[4] `https://www-nds.iaea.org/radii/`

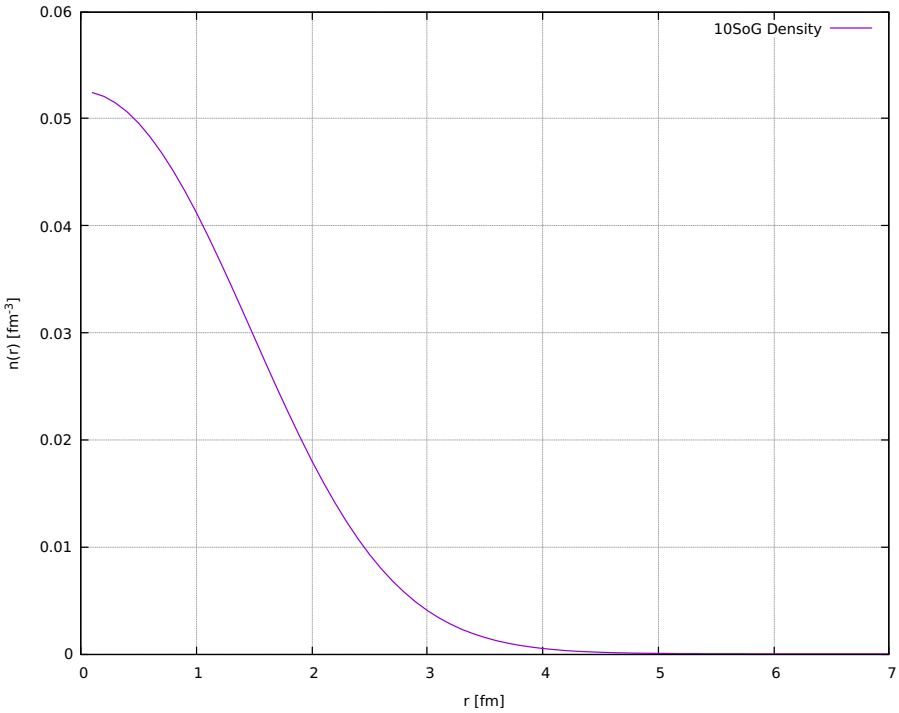

Figure 3.15: The ^{4}He proton density as obtained via a deconvolution from the proton charge densy provided by De Vries [1].

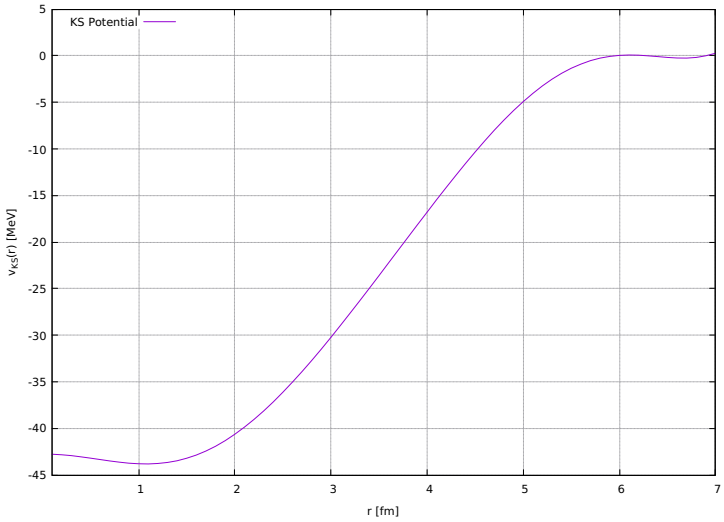

Figure 3.16: The Kohn-Sham potential deduced from the ^{4}He proton density.

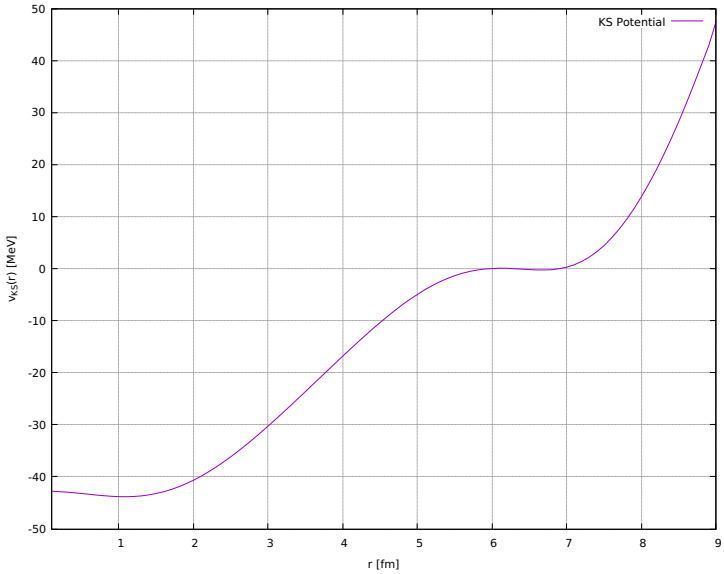

Figure 3.17: The Kohn-Sham potential, deduced from the ^{4}He proton density, presents a non-physical parabolic growth at large r.

3.4.2 The Oxygen Nucleus

Oxygen is a light, doubly magic, nucleus, with eight protons and eight neutrons, each of them filling the $1s_{1/2}$, $1p_{3/2}$ and $1p_{1/2}$ orbitals.

Literature [1] provides the proton density of Oxygen in two different parametrizations (3pF and 12SoG), shown in figure 3.18. Their form suggests to choose the interval of domain of the orbitals as $[0.1, 8]$ fm, with a mesh $h = 0.1$ fm and a penalty parameter $\delta = 0.1$. Different parametrizations of the density lead to surprisingly different densities:

- The 12SoG parametrization produces a density that is much more compact than the 3pF. The radial extent of the 12SoG density is acceptable ($R = 2.7$ fm) if compared to the charge radius of the Oxygen nucleus, that is $R(^{16}\mathrm{O}) = 2.6991(52)$ fm[5]; in contrast, the 3pF parametrization provides a wrong radius, that is about 3.6 fm. However, as it can be seen from figure 3.19, the tail of the latter parametrization is qualitatively correct (compare with the functional behaviour (3.19) of the Morse oscillator density, that saturates at large r), while the tail of the 12SoG decays to zero too fast, as discussed for the case of Helium.

- A marked dip characterizes the 12SoG proton density. The value of the density at the origin is due to the contribution of the orbital $1s_{1/2}$, only, since the centrifugal potential prevents other orbitals to explore the position $r = 0$. The dip may then be caused by an emptying of the orbital $1s_{1/2}$ in the target nucleus. On the other hand, the density parametrized by a Fermi function is, by construction, flat nearby the origin.

Figure 3.20 depicts the Kohn-Sham potential we have deduced from the 12SoG proton density of Oxygen.

Non-physical oscillations stem out in the intermediate radial interval. Let us recall that in scattering measurements the inner part of the density and its tail are extrapolated. It seems that, since the radial extent of the nucleus is not very large, the two critical radial intervals in which we extract the potential from the extrapolated density do overlap, thus tainting the intermediate part of the potential, too. Moreover, the potential seems to follow, at each point, the behaviour induced by the closest Gaussian, only, and is therefore characterized by a sequence of parabolic behaviours. This interpretation is enforced by the fact that the minimum of each parabola roughly corresponds to the centres R_i of one of the Gaussians in the parametrization.

The marked oscillation of the potential makes it impossible to determine the physical asymptotic behaviour of the potential. We assume that the last parabola with minimum at $r = 6.5$ fm is due to the last Gaussian of the parametrization ($R_i = 6.4$ fm). Beyond this value, we say the result to be fully model-dependent. A rough resemblance of the Kohn-Sham potential to a Woods-Saxon potential can then be noticed for smaller radii.

The inversion scheme for the 12SoG density provides meaningful results only in an intermediate radial interval, relatively to the depth ($V_p \approx -50$ Mev) and to the radial extent of the potential ($R \approx 3$ fm).

Whenever a dip of the target density at the origin is present, the inversion scheme reads it as a smaller probability for nucleons to occupy such position. The potential deduced from the 12SoG density presents therefore a raise at small r that reflects such physical interpretation.

[5] `https://www-nds.iaea.org/radii/`

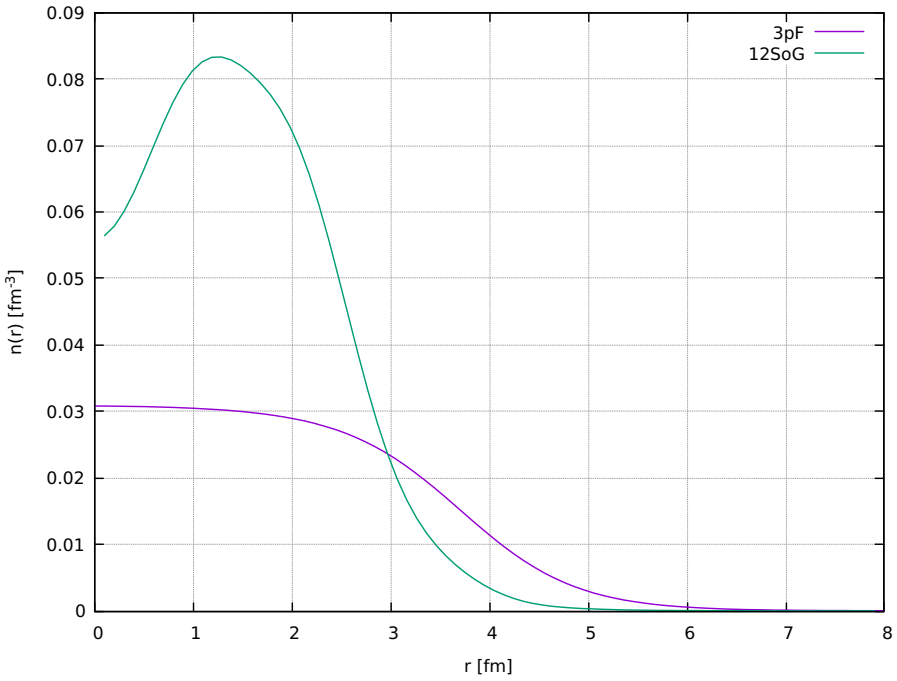

Figure 3.18: The ^{16}O proton density as obtained via a deconvolution from the proton charge density provided by De Vries [1] with a 3pF and a 12SoG parametrizations.

Figure 3.21 illustrates the Kohn-Sham potential deduced from the 3pF proton density of Oxygen. The depth of the potential well is acceptably predicted. With respect to the previous case, it is much easier to estimate it from the potential: $V_p \approx -50$ Mev. As we already noticed, the radial extent of the 3pF is wider than in the previous case. Consequently, the same happens for the potential.

The non-physical oscillations that characterized the inversion with the 12SoG density disappear in the 3pF case. This confirms our intuition; oscillations are caused by the individual Gaussians that are used in the Sum of Gaussian parametrizations and this effect is magnified in the density-to-potential inversion.

Except for some oscillations of the order of about 5 MeV, the asymptotic behaviour of the tail of the potential is here clear and correct. The Fermi parametrizations are characterized by a correct functional assumption for the behaviour of the tail of the nuclear densities. Also, such feature points to the fact that our inversion method extracts only the piece information that is carried by the experimental densities: neither it stumbles upon inverse crimes, nor it generates physically meaningful results on its own.

The potential at small r does not behave correctly and shows the same trend as in the previous case. This must be then labelled as a limitation of our code. In comparison with the 12SoG, the 3pF density has a lower value at the origin, but it is flat. The correspondent raise of the Kohn-Sham potential is more marked than before, but has no clear physical meaning.

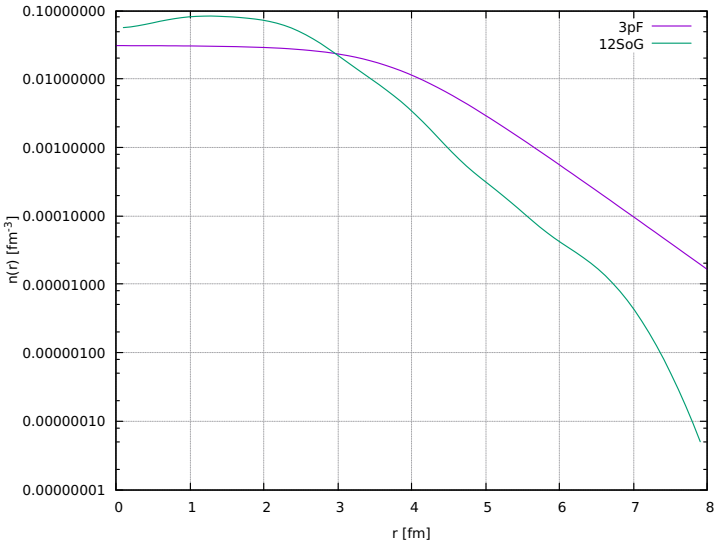

Figure 3.19: The ^{16}O proton density as obtained via a deconvolution from the proton charge density provided by De Vries [1] with a 3pF and a 12SoG parametrizations. Logarithmic scale is used to highlight the functional behaviour of the tails.

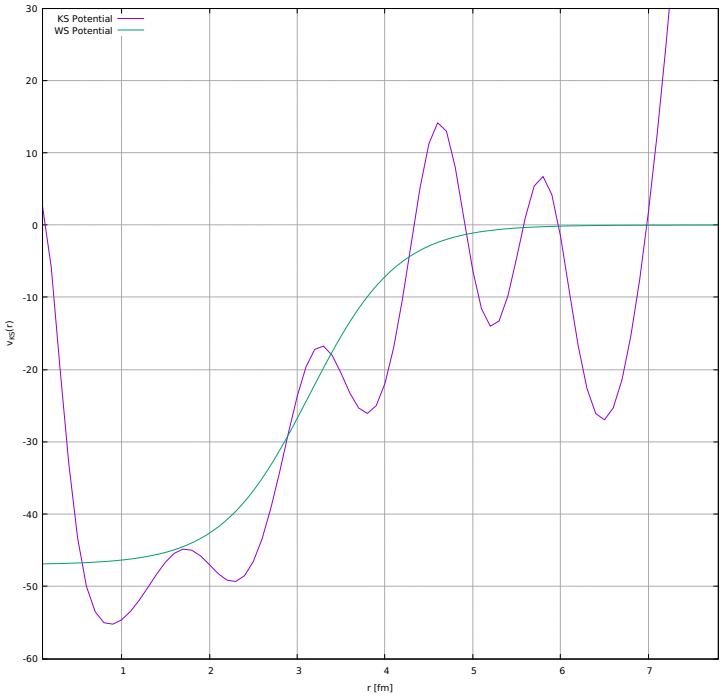

Figure 3.20: A comparison between the Kohn-Sham potential obtained by ^{16}O proton density (12SoG) through the constrained-variational method and a Woods-Saxon potential.

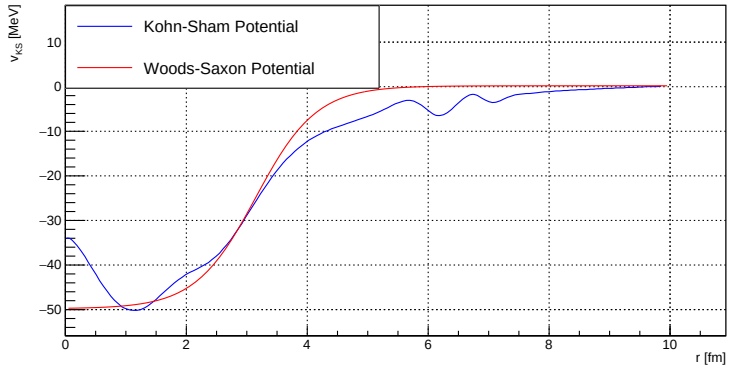

Figure 3.21: Comparison between the Kohn-Sham potential obtained by ^{16}O proton density (3pF) through the constrained-variational method and a Woods-Saxon potential.

3.4.3 The Calcium Nucleus

^{40}Ca proton density (figure 3.22) is provided by [1] in the 12SoG and 3pF parametrizations. Calcium is a medium-mass magic nucleus, with twenty protons and twenty neutrons, disposed in the six orbitals $1s_{1/2}$, $1p_{3/2}$, $1p_{1/2}$, $1d_{5/2}$, $2s_{1/2}$ and $1d_{3/2}$. The density of twenty particles in a harmonic oscillator trap is also shown in figure 3.22.

The box in which orbitals are defined is here $[0.1, 9]$ fm, with mesh $h = 0.1$ fm and penalty parameter $\delta = 0.1$.

In contrast with the case of Oxygen proton densities, the two different parametrizations appear to be more similar one another. However, it can be noticed that, again, the 12SoG choice predicts a more compact distribution of protons than 3pF. The 12SoG density presents a raise at the origin, while 3pF is flat by construction.

The radial extent of the densities is in both cases ($R = 3.8$ fm for 3pF and $R = 3.5$ fm for 12SoG) close to the expected value $R(^{40}\text{Ca}) = 3.4776(19)$ fm [6]. With the aid of figure 3.23, we remark again that the Sum of Gaussians density is more similar to an harmonic oscillator density than to a Fermi function.

Figure 3.24 shows the Kohn-Sham potential obtained from the 12SoG parametrization. An equivalent harmonic oscillator potential is depicted, too.

By comparison with a Woods-Saxon potential (see figure 3.25), we understand the the radial extent and the depth of the well are fairly well reproduced.

The non-physical oscillations in the intermediate radial interval of the potential, that characterized the Oxygen case, have here disappeared. This confirms the fact that oscillations were caused by the overlap of the two previously mentioned critical radial regions.

The potential at low r does not behave properly, since the dip in the density that was characterizing the Oxygen 12SoG density is here absent. The raise is not physical as that of the Oxygen potential, but, again, it has no physical explanation. The difference between the densities at the origin is remarkable. According to the discussion we have done in the first chapter, we know that the interior of the nuclear average potential can be well approximated by an harmonic oscillator potential. Also, we know from the three-dimensional test we have done in the previous section that

[6] `https://www-nds.iaea.org/radii/`

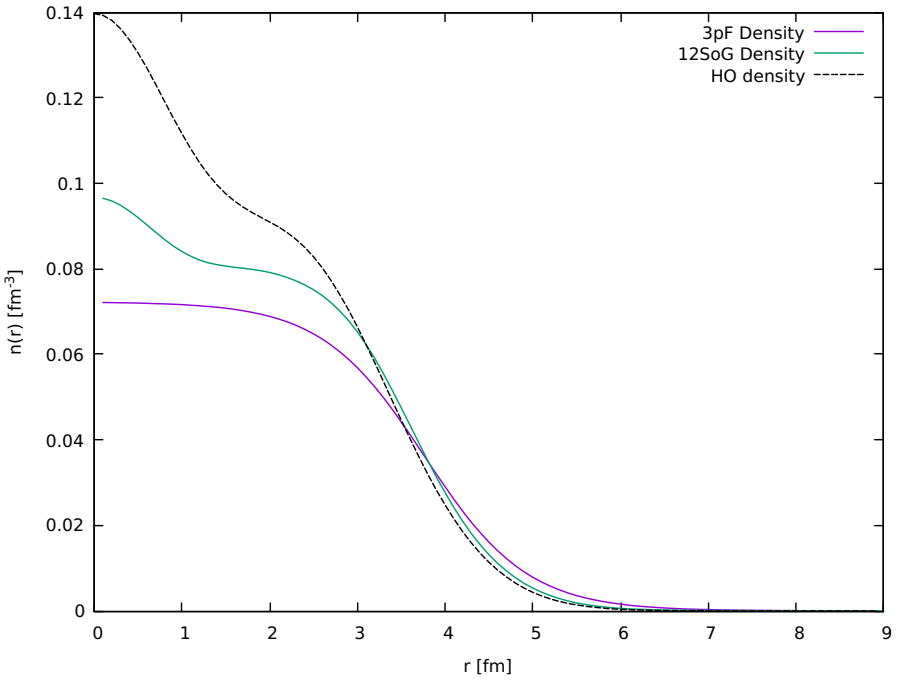

Figure 3.22: The ^{40}Ca proton density as obtained via a deconvolution from the proton charge density provided by De Vries [1] with a 3pF and a 12SoG parametrizations. The density of twenty particles in an isotropic harmonic oscillator trap is also depicted.

our inversion method works fine in the harmonic oscillator case. It seems that our inversion method misinterprets the that are values assumed by the experimental densities at the origin: when they are lower than the harmonic oscillator density, the inversion produces a non-physical raise that appears in many of our Kohn-Sham potentials.

An equivalent (in the sense specified above) harmonic potential is shown in figure 3.24; since such potential is an approximation of the nuclear average potential up to the radial extent of the potential well, we can read out from the figure what should be the expected form of the Calcium Kohn-Sham potential at the origin.

Figure 3.25 reports the Kohn-Sham potential deduced by the 3pF-parametrized density. The form of the effective potential in the intermediate region $[1.8, 5]$ fm is similar to that of the potential deduced by the 12SoG density.

The raise of the potential here is much more pronounced.

An asymptotic behaviour at large r is clear. This confirm the adequate functional assumption for the tail in 3pF densities.

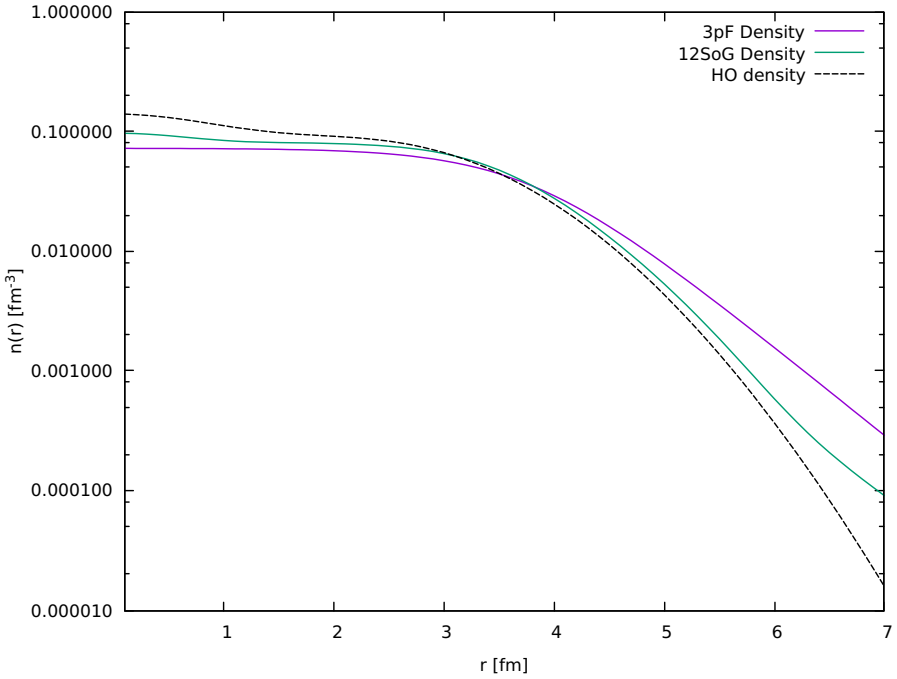

Figure 3.23: The ^{40}Ca proton density as obtained via a deconvolution from the proton charge density provided by De Vries [1] with a 3pF and a 12SoG parametrizations. The density of twenty particles in an isotropic harmonic oscillator trap is also depicted. Logarithmic scale is used to highlight the functional behaviour of the tails.

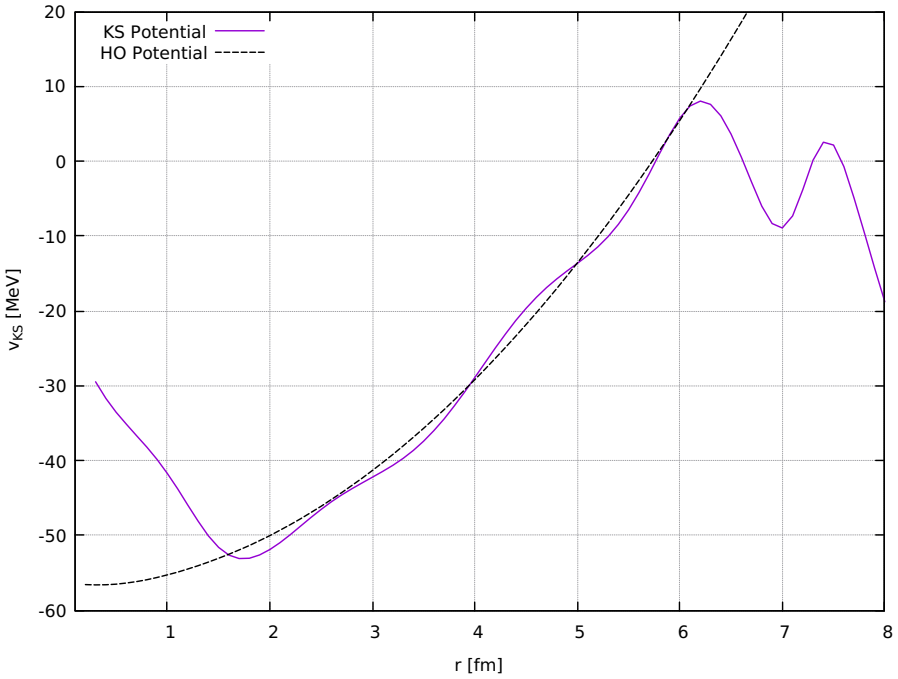

Figure 3.24: Comparison between Kohn-Sham potential deduced by the experimental 12SoG proton density of ^{40}Ca and that obtained from the density of twenty particles in an isotropic harmonic oscillator trap.

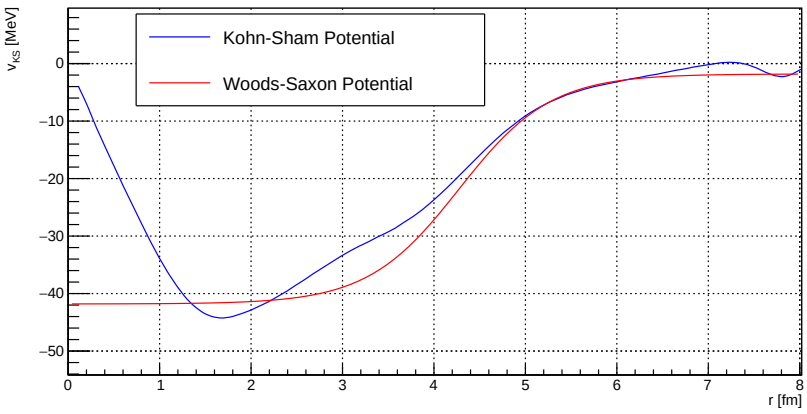

Figure 3.25: Comparison between the Kohn-Sham potential obtained by ^{40}Ca proton density (3pF) through the constrained-variational method and a Woods-Saxon potential.

3.4.4 Lead Nucleus

Lead is a heavy nucleus, with 82 protons and 126 neutrons. For the 22 orbital occupancy, we refer to figure 1.3.

Based on what we have discussed up to now, we expect the Kohn-Sham potential of ^{208}Pb to be more well-behaved than those of lighter nuclei, although its computational costs are higher. In fact, the radial extent of such nucleus, that is $R_{^{208}\mathrm{Pb}} = 7.4$ fm according to formula (1.2), is considerably bigger than in the other cases and we expect the two previously discussed critical radial intervals to stay well separated.

The literature makes available both the neutron [2] and the proton [1] density; we will limit our discussion to the former, because the absence of Coulomb effects will be likely to help us to better understand the inversion issues. Figure 3.26 shows the neutron density of Lead, as obtained by experimental measurements in the 12SoG parametrization. Again, the functional assumption for the tail of the density diverges from the expectations (see figure 3.27). In this figure we also report a theoretical density obtained via Hartree-Fock calculations; we will come back to this below. We choose the radial domain as $[0, 12]$ fm, with mesh $h = 0.1$ and $\delta = 0.1$.

Figure 3.28 shows the Kohn-Sham potential as deduced from the 12SoG neutron density, compared with a Woods-Saxon potential.

The interior part of the potential shows oscillations of amplitude of the order of 5 MeV; we ascribe those to similar reasons to those we have discussed while analysing the case of Helium.

The depth and the radial extent of the potential are slightly smaller than expected ($V_n \approx -45$ MeV and $R \approx 7$ fm), while the behaviour of the tail is, as expected, wrong.

Since we have clearly established that the tail divergence is caused by the wrong asymptotic of the experimental density parametrization, we are justified to extrapolate, through a fit, a more reasonable form of the tail. The idea is to search for the first inflexion point of the potential after the centre of the last Gaussian of the parametrization; in the case of Lead, this is at $R_i = 8.7$ fm. We assume that such inflexion point is the indication of where the tail of the density starts being extrapolated in a non-physical way. We substitute the tail of a Woods-Saxon potential (see equation (1.28)) to the divergent tail we have found. The depth of the Woods-Saxon potential is set to $V_0 \approx 50$ MeV, in agreement with the phenomenological expectation; we impose the two potentials to have the same value at the inflexion point r^* (continuity),

$$v_{KS}(r^*) = -\frac{V_0}{1 + e^{\frac{r^* - R}{a}}} + \epsilon, \tag{3.27}$$

and their first derivative to be equal there, too (differentiability),

$$v'_{KS}(r^*) = \frac{V_0}{a} \frac{e^{\frac{r^* - R}{a}}}{(1 + e^{\frac{r^* - R}{a}})^2}. \tag{3.28}$$

The two equations above determine $R[V_0, \epsilon]$ and $a[V_0, \epsilon]$. Finally, we fit the value of the arbitrary constant by assigning to it a value that makes the match of the potentials qualitatively as smooth as possible. A lower bound for ϵ is given by the value of the highest energy ϵ_j of the Kohn-Sham orbitals, that can be obtained by diagonalizing the matrix ϵ_{jk} of the orthonormality Lagrange multipliers. The potential with the corrected tail is shown in figure 3.29.

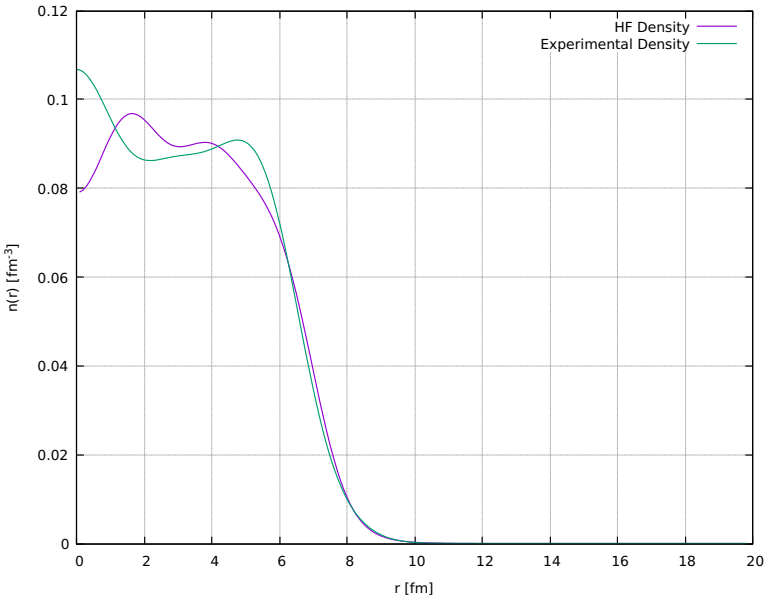

Figure 3.26: The neutron Lead density provided by Zenihiro [2] compared with the density obtained by solving a direct problem within Hartree-Fock approximation, in which a Skyrme force, SkP [3], is assumed.

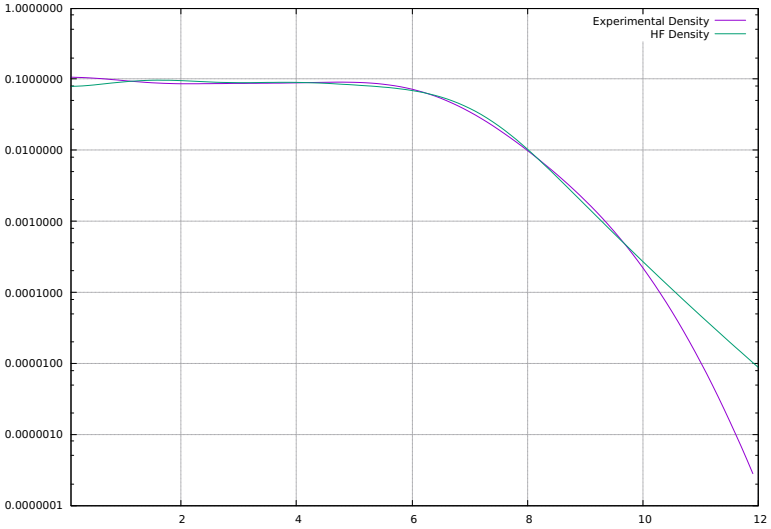

Figure 3.27: The neutron Lead density provided by Zenihiro [2] compared with the density obtained by solving a direct problem within Hartree-Fock approximation, in which a Skyrme force, SkP [3], is assumed. Logarithmic scale is used to better analyse the tails of the densities.

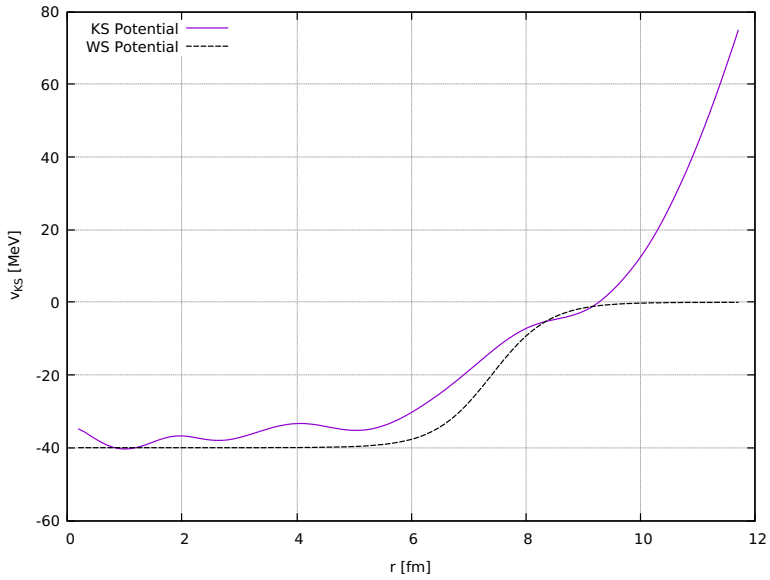

Figure 3.28: The Kohn-Sham potential as deduced from the experimental neutron density, compared with a Woods-Saxon potential.

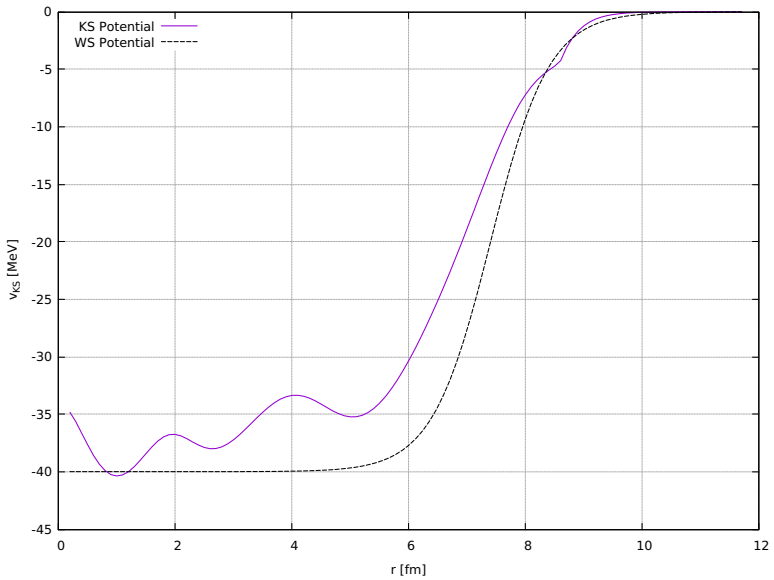

Figure 3.29: The Kohn-Sham potential as deduced from the experimental neutron density, with a corrected Woods-Saxon tail.

Qualitative Analysis of the Propagation of the Errors

We have defined a method for the correction of the model-dependent behaviour of the tail of the Kohn-Sham potential derived from a nSoG-parametrized density. Thus, we proceed to a qualitative analysis of the errors that characterized the inversion method itself.

In addition to what we have already shown, we studied the Kohn-Sham potential obtained from a theoretical density provided by Hartree-Fock calculations[7]

The theoretical density is depicted in figure 3.26 and 3.27. There is indeed a qualitative spread between the experimental and the theoretical density, that is especially visible ($\approx 30\%$) at the origin.

In order to understand if our correction to the tail of the Kohn-Sham potential is satisfactory, we study the inversion problem relatively to a density that is theoretically calculated. The tail of the latter density is indeed correct (see figure 3.27), since it is produced by a potential that go to zero correctly. A benchmark against which our corrected Kohn-Sham potential 3.29 can be compared is therefore available. Figure 3.30 illustrates the comparison between the potential obtained by the Hartree-Fock theoretical density, the Kohn-Sham potential obtained by the experimental density, and the original potential that has been used in HF calculations of the density. Results are in agreement in the central radial interval, let us say from 2 fm to 8.5 fm; the tails are in acceptable agreement only if we average the oscillations with amplitude of 5 MeV that characterize the Kohn-Sham potential obtained from the HF density at its large r interval. Although we have seen this is the typical magnitude of numerical noise, such feature does not let us understand the correct asympotic behaviour of the potential. In general, the absence of any clear asymptotic trend, combined with the fact that potentials are defined up to an arbitrary constant, renders the comparisons possible only at a qualitative level. The behaviour at the origin is clearly wrong, since it shows a non-physical growth. Again, the depth and the radial extent are compatible.

Another way to understand the level of correctness of our inversion method is given by a comparison with the results of another inversion scheme. Thus, we can fully understand which are the limitations of the input data and which are instead the limitations due to the implementation of a general algorithm to solve the inverse Kohn-Sham problem. In figure 3.31 we compare the Kohn-Sham potentials resulting from our Constrained Variational Method and the van Leeuween and Baerends method. The figure reports the potential assumed in Hartree-Fock calculations, too. It is remarkable to note that the two Kohn-Sham potentials envelop the theoretical potential. Two observations are in order.

- The results of the vLB method are highly dependent from the initial guess for the potential. Here, such starting guess is taken as a Woods-Saxon potential, with an adequate choice of the parameters.

[7] A very successful theoretical approach to nuclear structure is the self-consistent mean-field method. The approach is based on an independent particle picture, where nucleons are considered to be self-bound by the average of the two-body interactions over the states occupied by the other particles. The resulting field is created in a self-consistent way. Such a field is considered to be static, so that dynamical corrections are neglected. Specifically, this approach can be realized by means of an adopted effective interaction, solved at the level of the Hartree-Fock approximation. In the present case, the calculations have been carried out within a Skyrme-type force, SkP [3], in absence of a Coulomb term. The potential is used to solve the Schrödinger eigenvalue problem in Hartree-Fock approximation, in order to provide eigenfunctions that are used to compute the density of the nucleus.

- In the inner region, the spread between the results obtained with the two different methods is ≈ 25 MeV, that is about 50 % of the depth of the potential. Such spread diminishes to the value of ≈ 5 MeV (10 % of the depth) for intermediate radial coordinates, let us say $1.5 \leq r \leq 8.5$ fm.

A final possibility for understanding the level of the uncertainties in the density-to-potential inversion is to solve the direct problem with our Kohn-Sham potential. We do this by using the potential we retain to be more similar to the true solution of the corresponding inverse problem: the one deduced from the Lead experimental neutron density (12SoG-parametrized), with the corrected tail. We compare the density thus obtained with the input density of the inverse problem. A naive expectation would be to find exactly the density we have provided to the inversion method as an input. Clearly, this is not what happens, since the entire inversion plus direct process generates a certain amount of numerical noise in the quantities of interest. There is a main advantage in comparing densities instead of potentials. In the latter case, we must assume some asymptotic behaviour (the arbitrary constant of the potential) in order to be able to superpose the potentials and provide a quantitative comparison. Such problem is absent while contrasting densities. Figures 3.32 and 3.33 depict the original experimental neutron density and the one that we have deduced from the corresponding Kohn-Sham potential. Differences are evident, and 3.34 plots the relative spread between the two of them; at the origin the difference is, as we have already qualitatively estimated right above, around 40 %; in the intermediate region the spread decreases down to 5 %. The spread in the tail cannot be compared, since we have inserted an artificial correction to the tail of the potential.

It seems that, within the inversion process, the calculation of the Kohn-Sham orbitals is non-problematic; on the other hand, when one tries to deduce from those the form of the Kohn-Sham potential, the numerical uncertainties get incredibly magnified.

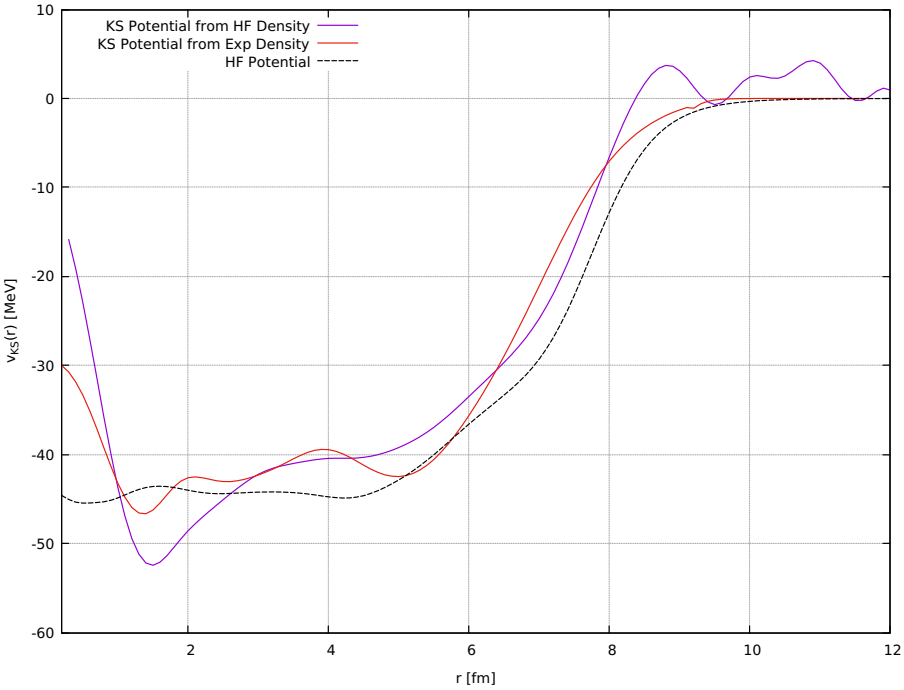

Figure 3.30: The Kohn-Sham potentials deduced from the Hartree-Fock theoretical and from the experimental neutron densities, compared with the potential assumed in the Hartree-Fock calculations of the density.

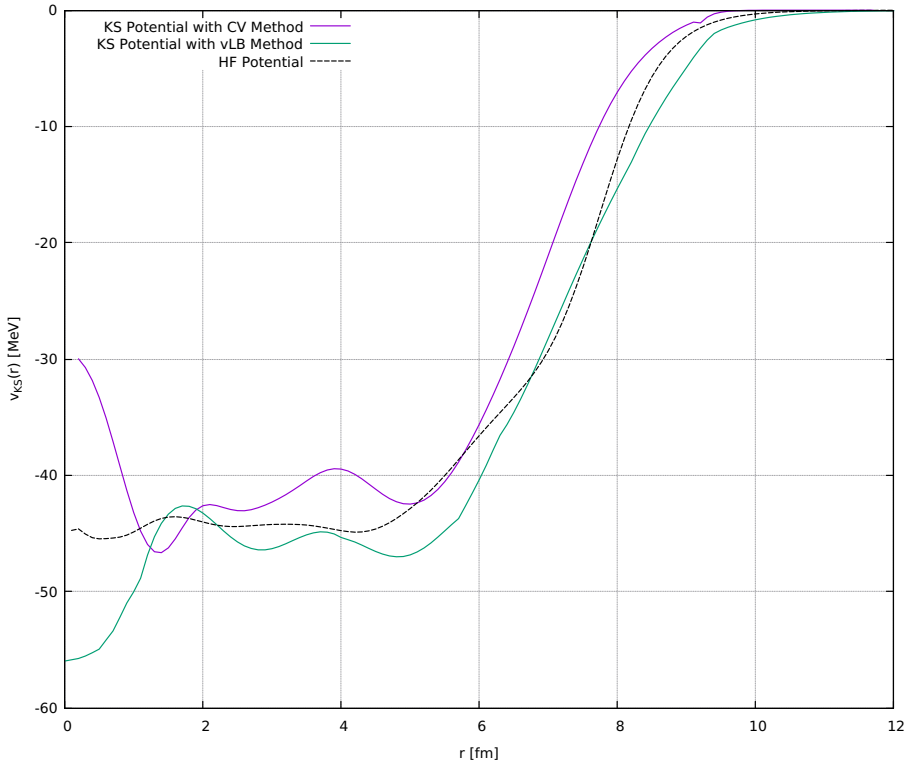

Figure 3.31: The Kohn-Sham potential deduced from experimental neutron density through two different inversion schemes, the CV method and the vLB method, compared with the potential assumed in the Hartree-Fock calculations of the density.

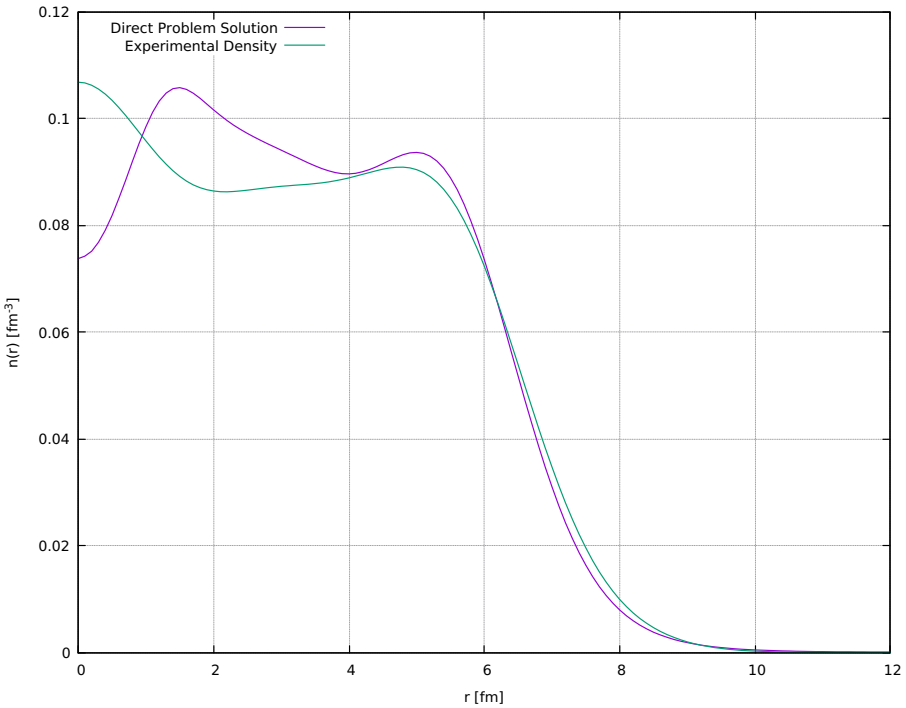

Figure 3.32: The density that is obtained by solving the Kohn-Sham direct problem using the Kohn-Sham potential deduced by experimental neutron density, compared with the experimental neutron density.

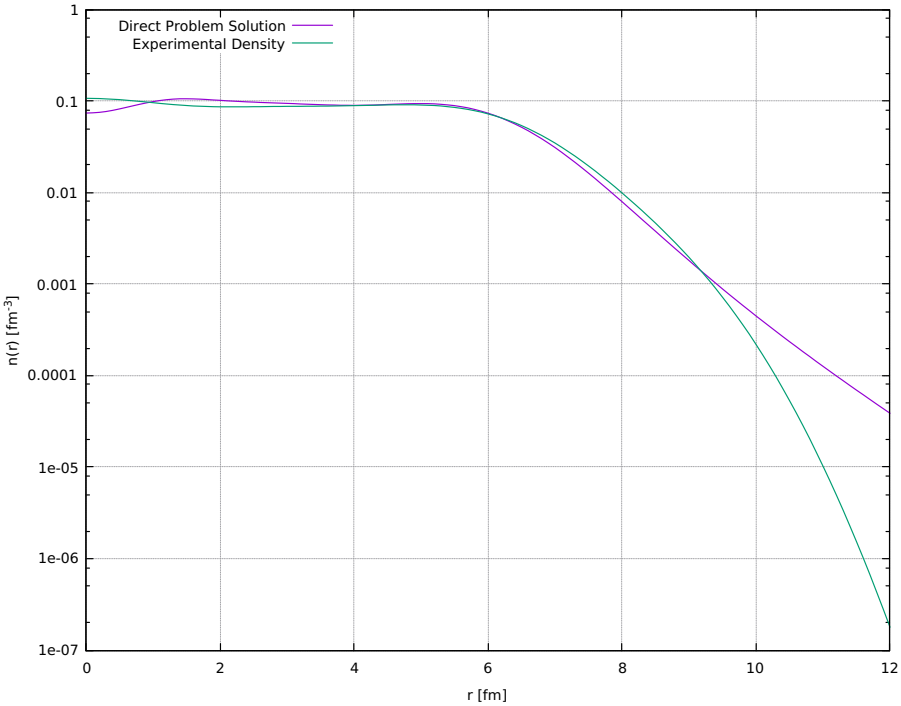

Figure 3.33: The density obtained by solving the Kohn-Sham direct problem using the Kohn-Sham potential deduced by experimental neutron density compare with the experimental neutron density. Logarithmic scale is used to analyse the tails of the densities.

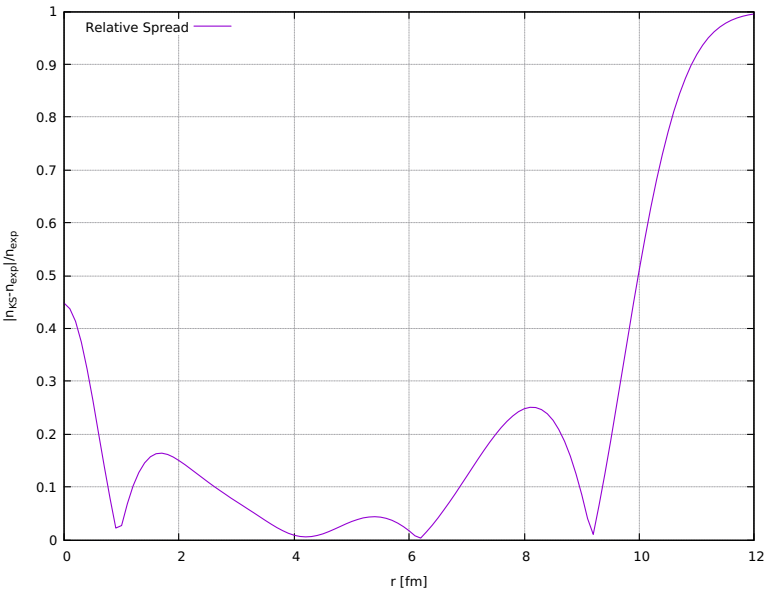

Figure 3.34: The relative spread between the density obtained by solving the Kohn-Sham direct problem using the Kohn-Sham potential deduced by experimental neutron density and the experimental neutron density.

Conclusions

The possibility of testing an exact functional through the knowledge of the exact effective potential that it should generate, is worth being investigated. This is especially true in the field of Nuclear Physics, where theoretical models are mostly based on phenomenology. The Hohenberg and Kohn DFT is indeed exact, but the ingredients of which the energy density functional consists cannot be obtained without relying on drastic approximations. In contrast, the construction of the exact Kohn-Sham potential from the nuclear density is in this sense promising and pioneering in Nuclear Physics, since it would provide a reliable benchmark against which the effective potentials assumed in energy density functional available on the market can be tested.

The original project of this thesis was to develop a numerical method to address the solution of the inverse Kohn-Sham problem in Nuclear Physics in the most general case. However, while encoding the first unidimensional tests, we have realized that the computational time necessary for calculations was a steep function (see figure 3.9) of the number of degrees of freedom in the problem. This feature suggested us to first proceed to the the application of our method on systems characterized by spherical symmetry. To this purpose, we have defined a new formalism for the Constrained Variational method, that has been presented in section 2.5.2. This formalism clearly sets a limitation to the range of the physical systems to be subject of investigation, but it follows the general idea to proceed step-by-step in the implementation of the inversion method.

The study of the Kohn-Sham potentials, as deduced by the experimental densities of a certain number of magic nuclei, has been treated in the bachelor's theses [12], [13] and [14], with a various level of detail and with different results. In all those works, however, a simple inversion method (the van Leeuwen and Baerends') has been used. As we have pointed out in this manuscript (in sections 3.4.1 and 3.4.4), such iterative method is highly biased by the initial guess on the potential, especially for which regards the behaviour of the tail of the Kohn-Sham potential. Our perspective has then been to build a method affected as least as possible by the initial assumptions on the solution of the non-linear inverse problem. We believe that the choice of our inversion method is particularly adequate to this aim.

The Constrained Variational method explores a much wider space in its search for the solution than what happens for iterative approaches. However, this somehow also represents a drawback of our implementation. In fact, whenever the input densities present some type of error or model-dependence, our scheme is not able to produce meaningful physical results. This is the case, for instance, for the tails of the experimental densities parametrized by nSoG, that are characterized by a wrong functional assumption. Moreover, our output is sensitive to small variations of the input density. Densities that should, at least in principle, be related to the same

effective potential, wind up in different results. This is what happens to our nuclear Kohn-Sham potential at small radii, where slight modifications of the occupancy of *s* orbital entail the appearance of non-physical behaviours. Since our procedure does not rely on a strong guidance towards the correct solution, such as a very valid initial guess for the potential, it does not produce physical results in some critical radial intervals, and there it is sensitive to numerical noise.

The application of the inversion Constrained Variational method on analytic systems has given acceptable results in all the cases. Such a wide testing procedure of the method represents itself a first objective of the thesis that we can consider fully accomplished.

On the other hand, we encountered a surprising amount of troubles when we considered as the input of the inversion process realistic densities, characterized by systematic physical uncertainties. The results we have presented in section 3.4 are not satisfactory. Although a partial justification is given by the high uncertainties and model-dependence that characterize the inner and the outer regions of the experimental nuclear densities, our method is not robust in those intervals, even when nuclear densities obtained theoretically are used. However, we believe that the sources of such non-physical behaviours of the nuclear effective potentials have been clearly identified in most of cases. Unluckily, we could not always find a practical and theoretically sound correction to those issues.

Further work must be done in this sense, and we have pointed to a clear possible direction for improvements: the exploitation of the different methods to address the solution of the inverse problem. In fact, none of the methods available on the market seems to be free of drawbacks that jeopardize the possibility of providing solid solutions to the Kohn-Sham inverse problem. For instance, our method could be used to provide an unbiased solution to the inverse Kohn-Sham problem; the parallel application of an iterative method could help instead to get physical corrections in those intervals where our solution is tainted by the uncertainties and model-dependence of the input density.

As a final observation, we would like to remark that our method is explicitly prepared in order to be generalized to more complex systems. The computational costs of each particular numerical method that is used in the inversion scheme represents the main obstacle to such generalizations. One could then think to face the inverse problem in a more generic way, without relying on assumptions about the symmetries of the problem.

Appendix A

The Method of Lagrange Multipliers

In general, some issues arise whenever one tries to perform a constrained multi-dimensional optimization. Just to mention the most trivial of those complications, derivatives cannot be defined properly on the borders of the regions in which the problem is defined, if those regions are not open spaces.

Let us consider a functional $F[f]$. A necessary condition for some function to be an extremum of such functional is that the variation of the functional vanishes for all $\delta f(x)$,

$$\delta F = \int dx \, \frac{\delta F}{\delta f(x)} \delta f(x) = 0 \tag{A.1}$$

It is then equivalent to require that the optimal solution satisfies

$$\frac{\delta F}{\delta f(x)} = 0. \tag{A.2}$$

Also, if one keeps in mind the particular case in which the functional is an action

$$F[f] = \int dx \, \mathscr{L}(f, f'; x) = 0, \tag{A.3}$$

then the condition (A.2) produces the well known *Euler-Lagrange equations*.

If some constraints are imposed to the optimization problem, such as

$$G_i[f] = 0, \tag{A.4}$$

it is often convenient to make use of the *method of Lagrange multipliers*. The method consists in building an auxiliary quantity, the so-called *Lagrangian*, defined as

$$\Lambda[f, \lambda_i] = F[f] + \sum_i \lambda_i G_i[f] = 0. \tag{A.5}$$

It is possible to proof that this new problem, namely the free optimization of the Lagrangian with respect to f and to the *Lagrange multipliers* λ_i is equivalent to the original constrained problem. Thereby, one finds a candidate extremal of (A.5), which will be parametrized by those λ_i, and afterwards imposes the constraints (A.4), fixes the values of the multipliers. Note that the method provides only a necessary

condition for functions to be an extremal of the functional investigated. Further information is required in order to understand if the extrema one finds are indeed minima, maxima or saddles. For more details on the method of Lagrange multipliers we address the reader to [50, 51].

Appendix B

Density Operators and Scalar/Vector Densities

B.0.1 Density Operators

One can consider a more fundamental definition of the density function, based on *density operators*. The quantity

$$\Psi_A(\vec{x}_1,\ldots,\vec{x}_A)\Psi_A^*(\vec{x}_1,\ldots,\vec{x}_A) \tag{B.1}$$

represents the probability distribution associated with a particular solution of the Schrödinger equation. Consider now quanties such as

$$\gamma_A = \Psi_A(\vec{x'}_1,\ldots,\vec{x'}_A)\Psi_A^*(\vec{x}_1,\ldots,\vec{x}_A). \tag{B.2}$$

It is natural to construct a *density matrix*, whose elements are the γ_A. The diagonal entries of the matrix are indeed the original (B.1). (B.2) can be also thought as the representation in the coordinates basis of the *density operator*

$$\hat{\gamma}_A = |\Psi_A\rangle\langle\Psi_A|. \tag{B.3}$$

The density operator is a projection operator, and

$$\mathrm{tr}(\hat{\gamma}_A) = \int d^A\,\vec{x}\,d^A\,\vec{x'}\Psi_A(\vec{x'}_1,\ldots,\vec{x'}_A)\Psi_A^*(\vec{x}_1,\ldots,\vec{x}_A) = 1 \tag{B.4}$$

if Ψ_A is normalized. Moreover, it is trivial to show that

$$\langle\hat{A}\rangle = \mathrm{tr}(\hat{\gamma}_A\hat{A}). \tag{B.5}$$

for each observable $\hat{A}$. The previous equation states a one-to-one mapping between the density operator and the obsevables of the system under investigation. In fact, by comparison with (1.7), one notices that the density operator does carry the same piece of information as any A-nucleon wave function $|\Psi_A\rangle$. Furthermore, while $|\Psi_A\rangle$ is defined up to an arbitrary phase factor, $\hat{\gamma}_A$ is unique. As well as each operator associated to some observable must be, $\hat{\gamma}_A$ is Hermitian, too.

The operator-like description becomes essential whenever the system under investigation is part of some enviroment, and it is not isolated from it. Indeed, in such a case the system does not have a complete Hamiltonian containing all its degrees of freedom. Then, the system is open, and this feature precludes any possibility of a wave function description [52].

B.0.2 Reduced Density Matrices

We are mainly interested in one- or two-particle operators operators. Let us recall that wave functions are antisymmetric. These two features allow to simplify the density matrix, to produce a *reduced density matrix* or, for a spin-compensated sysyem, a *spinless density matrix*. Let us call (B.1) A^{th}*-order density matrix*. One then defines the *reduced density matrix of order p* through

$$\begin{aligned}&\gamma_p(\vec{x'}_1,\vec{x'}_2\ldots\vec{x'}_p;\vec{x}_1,\vec{x}_2\ldots\vec{x}_p)\\&=\binom{A}{p}\int d\vec{x}_{p+1}\cdots\int d\vec{x}_A\,\gamma_A(\vec{x'}_1,\ldots\vec{x'}_A;\vec{x}_1,\ldots\vec{x}_A).\end{aligned}\tag{B.6}$$

In particular, second-order density matrix

$$\gamma_2(\vec{x'}_1,\vec{x'}_2;\vec{x}_1,\vec{x}_2)=\frac{A(A-1)}{2}\int d\vec{x}_3\cdots\int d\vec{x}_A\,\gamma_A(\vec{x'}_1,\ldots\vec{x'}_A;\vec{x}_1,\ldots\vec{x}_A)\tag{B.7}$$

integrates to the number of nucleon pairs $\frac{A(A-1)}{2}$, while the first-order density matrix

$$\gamma_1(\vec{x'}_1;\vec{x}_1)=A\int d\vec{x}_2\cdots\int d\vec{x}_A\,\gamma_A(\vec{x'}_1,\ldots\vec{x'}_A;\vec{x}_1,\ldots\vec{x}_A)\tag{B.8}$$

normalizes to the number of nucleons A. These operators are positive semi-definite and Hermitian, as well as $\hat{\gamma}_A$. Also, antisimmetry requires that interchange of two primed or two unprimed indices brings along a change of the sign of the density operators.

B.0.3 Spinless density matrices

It is natural, whenever the quantities of interest do not involve the spin coordinates, to further simplify the density matrices by a summation over σ_1 (and σ_2). The first-order and the second-order *spinless density matrices* read

$$n_1(\vec{r'}_1;\vec{r}_1)=\int d\sigma_1\,\gamma_1(\vec{x'}_1;\vec{x}_1),\tag{B.9}$$

$$n_2(\vec{r'}_1,\vec{r'}_2;\vec{r}_1,\vec{r}_2)=\int\int d\sigma_1\,d\sigma_2\,\gamma_2(\vec{x'}_1,\vec{x'}_2;\vec{x}_1,\vec{x}_2),\tag{B.10}$$

$$\tag{B.11}$$

and the two of them are linked by the relation

$$n_1(\vec{r'}_1;\vec{r}_1)=\frac{2}{A-1}\int d\vec{r}_2\,n_2(\vec{r'}_1,\vec{r}_2;\vec{r}_1,\vec{r}_2).\tag{B.12}$$

Note that the diagonal entries of $n_1(\vec{r'}_1;\vec{r}_1)$ provide just the nuclear density (1.29). One can write down an energy formula

$$\begin{aligned}E=&\int d\vec{r}\,\left[-\frac{\hbar^2}{2m}\nabla^2_{\vec{r}}n_1(\vec{r'};\vec{r})\right]_{\vec{r'}=\vec{r}}+\int d\vec{r}\;v(\vec{r})n_1(\vec{r})\\&+\int\int d\vec{r}_1\,d\vec{r}_2\;w(\vec{r}_1,\vec{r}_2)n_2(\vec{r}_1,\vec{r}_2).\end{aligned}\tag{B.13}$$

The three terms represent respectively the kinetic term, the external potential energy, and the nucleon-nucleon interaction energy. The main advantage of such formula is the fact that it involves only a function of three coordinates, $n(r)$, and two functions of six coordinates, namely $n_1(\vec{r'};\vec{r})$ and $n_2(\vec{r}_1,\vec{r}_2)$.

B.0.4 Scalar and Vector Densities

All along the thesis the term density means *barionic* density. In general, density functional theory, and therefore the inverse Kohn-Sham problem, other than being applicable to generic barionic system, can be considered in relation to other types of densities. In [53] and [54], a systematic construction of the energy-density functional, within local density approximation (LDA), is presented. If one considers the description of systems in which the time-reversal symmetry is broken, *e. g.* fast rotating nuclei [55], the density matrix and the resulting mean-field will be characterized by both time-even and time-odd components. While properties of time-even mean-field are known rather well, also thanks to experiments, the knowledge of time-odd mean-fields is fewer. The density of nuclear matter in the interior part of nuclei has a well known definite value, namely the saturation density, which is to some extent independent of the nuclear size. Because of that, a basic approximation is to consider the state of matter at some point in the nucleus as it would be given in in infinite matter at the corresponding density. In other words, the influence of different points of nuclear matter on properties that are calculated at some given point is rather little. It is such observation that justifies the adoption of local density approximation in nuclear systems and in other fields of Physics.

The finite nuclear size implies that corrections must be taken into account for the simplest version of LDA. Those corrections are implemented by local derivatives of the density. The total energy of the nucleus, in LDA, is given by the integral of a local energy density

$$E = \int d^3\vec{r}\, \mathscr{H}(\vec{r}) \tag{B.14}$$

and the energy density $\mathscr{H}$ depends on the one-body density matrix and on its derivatives, usually up to the second order.

The type of nucleon considered is accounted via the isospin degree of freedom; if we neglect it, the density matrix reads (compare the following with (B.8))

$$n(\vec{r}\sigma, \vec{r}'\sigma') = \langle \Psi | a^\dagger(\vec{r}'\sigma') a(\vec{r}\sigma) | \Psi \rangle \,. \tag{B.15}$$

One can separate the spin degrees of freedom by defining a scalar and a vector part of the density matrix, respectively

$$n(\vec{r}, \vec{r}') = \sum_\sigma n(\vec{r}\sigma, \vec{r}'\sigma') \tag{B.16}$$

$$\vec{s}(\vec{r}, \vec{r}') = \sum_{\sigma\sigma'} n(\vec{r}\sigma, \vec{r}'\sigma') \langle \sigma' | \vec{\sigma} | \sigma \rangle \,. \tag{B.17}$$

The density matrix is hermitian, and therefore its scalar and vector parts are symmetric under the exchange of the spatial arguments. Instead, the density matrix corresponding to time-reversed states read

$$n^T(\vec{r}, \vec{r}') = n^\dagger(\vec{r}, \vec{r}') = n(\vec{r}', \vec{r}) \tag{B.18}$$

$$\vec{s}^T(\vec{r}, \vec{r}') = -\vec{s}^\dagger(\vec{r}, \vec{r}') = -\vec{s}(\vec{r}', \vec{r}) \tag{B.19}$$

That means that the scalar density matrix is a real, symmetric, function of the spatial arguments. On the other hand, the vector density matrix is imaginary and antisymmetric. The local scalar and vector densities,

$$n(\vec{r}) = n(\vec{r}, \vec{r}), \tag{B.20}$$

$$\vec{s}(\vec{r}) = \vec{s}(\vec{r}, \vec{r}), \tag{B.21}$$

respectively do not and do change sign under time reversal. In other words, the barionic density is time-even, while the spin density is time-odd. In particular, one acts on the scalar and vector matrices with the operators $(\nabla - \nabla')/2i$, and afterwards sets $\vec{r} = \vec{r}'$. At the first order one obtains the *current density* $\vec{j}$ and the *spin current density* $J_{\mu\nu}(\vec{r})$. In the second order one applies the derivation above once again and gets the *kinetic density* and the *spin kinetic density*. According to some well-established rules, one constructs the local energy density as a sum of terms depending on the different densities just defined. In particular, each term must be quadratic in the local density; terms beyond the second order must be neglected; the energy must be invariant with respect to parity, time reversal, and rotations. By analysing all of such possible terms, it turns out that each density gives rise to one of the two main terms of the interactive part of energy density:

$$\mathscr{H}(\vec{r}) = \frac{\hbar^2}{2m}\tau_0 + \mathscr{H}^{\text{even}}(\vec{r}) + \mathscr{H}^{\text{odd}}(\vec{r}). \tag{B.22}$$

The scalar class of densities gives rise to the first interaction term, while the vector density and its local derivatives produce the second one.

To take into account the isospin quantum number, that is to consider different types of nucleons, the expression above must be labelled as $\mathscr{H}_t(\vec{r})$, with $t = 0$ standing for the isoscalar energy density and $t = 1$ for isovector one. Each of those quantities derives, respectively, by some n_0 or n_1. Those are defined as the sum and the difference of the proton and neutron contributions:

$$n_0 = n_n + n_p \tag{B.23}$$

$$n_1 = n_n - n_p, \tag{B.24}$$

and similar expression can be used to define other densities.

A variation of the energy density with respect to the possible six density functions produces mean fields $\Gamma_t^{\text{even,odd}}$, and the neutron or proton single-particle Hamiltonians can be obtained by combining the kinetic energy with the mean fields:

$$h_{n,p} = -\frac{\hbar^2\nabla^2}{2m_{n,p}} + \Gamma_0^{\text{even}} + \Gamma_0^{\text{odd}} \pm (\Gamma_1^{\text{even}} + \Gamma_1^{\text{odd}}) \tag{B.25}$$

Appendix C

Time-Independent Systems

As the time derivative in the Schrödinger equation appears linearly, one normally must consider complex fields [56] (or wave functions in the first-quantized picture). Those are obtained by the superposition of two independent real fields,

$$\psi = \frac{\psi_1 + i\psi_2}{\sqrt{2}}, \tag{C.1}$$

$$\psi^\dagger = \frac{\psi_1 - i\psi_2}{\sqrt{2}} \tag{C.2}$$

The Lagrangian density of a Schrödinger field is

$$\mathscr{L} = i\psi^\dagger\dot{\psi} - \frac{\hbar^2}{2m}\nabla\psi^\dagger\cdot\nabla\psi - \psi^\dagger V(\vec{r},t)\psi, \tag{C.3}$$

whence Euler-Lagrange equations

$$\frac{\delta\mathscr{L}}{\delta\psi} - \nabla\cdot\frac{\delta\mathscr{L}}{\delta\nabla\psi} = \left(\frac{\delta\mathscr{L}}{\delta\psi} - \nabla\cdot\frac{\delta\mathscr{L}}{\delta\nabla\psi}\right)^\dagger = 0 \tag{C.4}$$

return the Schrödinger equation and its complex conjugate

$$-\frac{\hbar^2}{2m}\nabla^2\psi^\dagger + V\psi^\dagger = -i\dot{\psi}^\dagger, \tag{C.5}$$

$$-\frac{\hbar^2}{2m}\nabla^2\psi + V\psi = i\dot{\psi}. \tag{C.6}$$

The conjugate variables are

$$\pi = \frac{\delta\mathscr{L}}{\delta\dot{\psi}} = i\psi^\dagger,$$

$$\pi^T = \frac{\delta\mathscr{L}}{\delta\dot{\psi}^\dagger} = 0, \tag{C.7}$$

so that the Hamiltonian density reads

$$\mathscr{H} = \pi\dot{\psi} + \pi^T\dot{\psi}^\dagger - \mathscr{L} = -i\frac{\hbar^2}{2m}\nabla\pi\cdot\nabla\psi - i\pi V\psi. \tag{C.8}$$

This leads to the usual Hamiltonian of a Schrödinger field,

$$H = \int_\Omega d\vec{r}\ \mathscr{H} = \int_\Omega d\vec{r}\ \psi^\dagger \Big[-\frac{\hbar^2}{2m}\nabla^2 + V \Big] \psi \tag{C.9}$$

If the fields are time-independent, the right hand side of Schrödinger equations (C.5) and (C.6) vanishes and the adjoint equation becomes trivial.

Appendix D

Deconvolution from Proton Charge Density to Proton Density

It is a matter of fact that experimental measurements are often limited to provide proton charge density distributions in nuclei, as it happens in De Vries [1], instead of nuclear densities. The reason is that in most of the experiments cross section data are obtained by using charged probes, such as electron beams, which does interact with protons, only.

Thus, the natural question that arises is how to move from some charge density distribution to the respective particle density distribution. The answer is rather simple, but it demands for some calculations.

Suppose one knows some radial proton charge density $n_{\text{ch}}(r)$. Then, the proton density $n(r)$ will be linked to the proton charge density by a convolution:

$$n_{ch}(r) = [F_{\text{proton}}(r - r') * n(r')](r) = \int dr'\, F_{\text{proton}}(r - r')n(r'), \tag{D.1}$$

where $F_{\text{proton}}(r - r')$ is the form factor of a proton with respect to the electric force. Such quantity represents the shape of the proton, which is not considered a point, as it would be deduced by the cross section obtained using beams that interact with it through the electric force. The form factor must normalize to the proton charge q_e. Therefore, it is necessary to apply a deconvolution on the above equation to reverse it with respect to $n(r)$. The key idea is that convolution operations are much more natural to be performed in the momentum space, where they correspond to the product of the Fourier transforms of the two functions involved,

$$\hat{n}_{\text{ch}}(q) = \hat{F}_{\text{proton}}(q)\hat{n}(q). \tag{D.2}$$

Once $\hat{n}(q)$ has been calculated, it is straightforward to get $n(r)$ via a backward Fourier transformation

$$n(r) = (\hat{n}(q))^{\vee} \tag{D.3}$$

As an example of such a deconvolution, consider a proton charge density given by a sum of Gaussians (nSoG). Here the parametrization is used just as an example to

show how to apply the deconvolution procedure.

$$n_{\rm ch}(r) = \sum_i \frac{A_i}{2\pi^{\frac{3}{2}}\gamma^3}\left[e^{\frac{(r-R_i)^2}{\gamma^2}} + e^{\frac{(r+R_i)^2}{\gamma^2}}\right], \tag{D.4}$$

where

$$A_i = \frac{q_e Z Q_i}{1+2\frac{R_i^2}{\gamma^2}}. \tag{D.5}$$

Q_i and R_i are parameters and $\sum_i Q_i = 1$, Z is the atomic number of the nucleus, and γ is a width parameter proportional to the rms radius of the nucleus. Let us recall some useful formulas, fundamental in order to perform the calculations below. First, in spherical coordinates the Fourier transformation and anti-transformation read

$$\hat{f}(q) = 4\pi\int_0^\infty r\,dr\,\frac{\sin(qr)}{q}f(r) \tag{D.6}$$

$$\check{f}(q) = \frac{1}{2\pi^2 r}\int_0^\infty q\,dq\,\frac{\sin(qr)}{r}f(q). \tag{D.7}$$

Another formula which is often used is the Gaussian integral

$$\int_{-\infty}^{\infty} dx\, e^{-ax^2+bx+c} = \sqrt{\frac{\pi}{a}}e^{\frac{b^2}{4a}+c}. \tag{D.8}$$

Thus, consider the Fourier transform of (D.4) in spherical symmetry,

$$\begin{aligned}
\hat{n}_{ch}(q) &= 4\pi\int_0^\infty dr\,\frac{\sin(qr)}{q}n_{ch}(r)\\
&= \sum_i \frac{4\pi}{q}\frac{A_i}{2\pi^{\frac{3}{2}}\gamma^3}\int_0^\infty r\,dr\,\sin(qr)\left[e^{\frac{(r-R_i)^2}{\gamma^2}} + e^{\frac{(r+R_i)^2}{\gamma^2}}\right]\\
&= -\sum_i \frac{A_i}{2q}\frac{\partial_q}{\sqrt{\pi}\gamma^2}\int_{-\infty}^\infty du\,\left[e^{iq(\gamma u\mp R_i)} + e^{-iq(\gamma u\mp R_i)}\right]\\
&= \sum_i A_i e^{-\frac{q^2\gamma^2}{4}}\left[\cos qR_i + \frac{2R_i}{q\gamma^2}\sin qR_i\right]
\end{aligned} \tag{D.9}$$

Now, it is reasonable to assume that the form factor of the proton is Gaussian-shaped [57],

$$F_{\rm proton}(r-r') = \frac{q_e}{\pi^{\frac{3}{2}}\alpha^3}e^{-\frac{(r-r')^2}{\alpha^2}}, \tag{D.10}$$

where α is proportional to the root mean squared radius of the proton. The calculation of the Fourier transform of the shape factor is a simpler version of the previous one; one finds

$$\hat{F}_{\rm proton}(q) = q_e e^{-\frac{q^2\alpha^2}{4}}. \tag{D.11}$$

We have all the ingredients necessary to use perform the deconvolution,

$$\hat{n}(q) = \sum_i \frac{A_i}{q_e}e^{-\frac{q^2\beta^2}{4}}\left[\cos qR_i + \frac{2R_i}{q\gamma^2}\sin qR_i\right], \tag{D.12}$$

where $\beta^2 = \gamma^2 - \alpha^2$. The final step consists in a reverse Fourier transformation of the nuclear density. Let us begin with the cosine term:

$$\begin{aligned} n_I(r) &= \sum_i \frac{A_i}{q_e} \frac{1}{2\pi^2 r} \int_0^\infty q\,dq\, \frac{\sin(qr)}{r} \cos qR_i e^{-\frac{q^2\beta^2}{4}} \\ &= \sum_i \frac{A_i}{16 q_e \pi^2 r} \partial_r \int_{-\infty}^\infty dq \left[e^{iq(r+R_i)} + e^{-iq(r+R_i)} + e^{iq(r-R_i)} + e^{-iq(r-R_i)} \right] e^{-\frac{q^2\beta^2}{4}} \\ &= \sum_i \frac{A_i}{2 q_e \pi^{\frac{3}{2}} \beta^3 r} \left[(r+R_i) e^{-\frac{(r+R_i)^2}{\beta^2}} + (r-R_i) e^{-\frac{(r-R_i)^2}{\beta^2}} \right]. \end{aligned} \tag{D.13}$$

As for the second term, a similar calculation gives

$$\begin{aligned} n_{II}(r) &= \sum_i \frac{A_i R_i}{q_e \gamma^2} \frac{1}{2\pi^2 r} \int_0^\infty q\,dq\, \frac{\sin(qr)}{r} \sin qR_i e^{-\frac{q^2\beta^2}{4}} \\ &= \sum_i \frac{A_i R_i}{2 q_e \pi^2 \gamma^2 r} \int_{-\infty}^\infty dq\, \frac{e^{iqr} - e^{-iqr}}{2i} \frac{e^{iqR_i} - e^{-iqR_i}}{2i} e^{-\frac{q^2\beta^2}{4}} \\ &= \sum_i \frac{A_i R_i}{2 q_e \pi^{\frac{3}{2}} \gamma^2 \beta r} \left[e^{-\frac{(r-R_i)^2}{\beta^2}} - e^{-\frac{(r+R_i)^2}{\beta^2}} \right]. \end{aligned} \tag{D.14}$$

The final result reads

$$n(r) = \sum_i \frac{A_i}{2 q_e \pi^{\frac{3}{2}} \beta r} \left[\left(\frac{r-R_i}{\beta^2} + \frac{R_i}{\gamma^2} \right) e^{-\frac{(r-R_i)^2}{\beta^2}} + \left(\frac{r+R_i}{\beta^2} - \frac{R_i}{\gamma^2} \right) e^{-\frac{(r+R_i)^2}{\beta^2}} \right]. \tag{D.15}$$

Appendix E

Discretization Methods

E.0.1 Discretized Derivative

The first and the second derivative are implemented through a symmetric five-points formula, which is obtained by solving the following system of Taylor series with respect to $f^{(1)}(x_0)$ and $f^{(2)}(x_0)$:

$$f(x_0 \pm h) = f(x_0) \pm h f^{(1)}(x_0) + \frac{h^2}{2} f^{(2)}(x_0) \pm \frac{h^3}{6} f^{(3)}(x_0) + \frac{h^4}{24} f^{(4)}(x_0) + O(h^5), \quad \text{(E.1)}$$

$$f(x_0 \pm 2h) = f(x_0) \pm 2h f^{(1)}(x_0) + \frac{4h^2}{2} f^{(2)}(x_0) \pm \frac{8h^3}{6} f^{(3)}(x_0) + \frac{16h^4}{24} f^{(4)}(x_0) + O(h^5). \quad \text{(E.2)}$$

The system is solved by

$$f^{(1)}(x_0) = \frac{-f(x_0+2h) + 8f(x_0+h) - 8f(x_0-h) + f(x_0-2h)}{12h} + O(h^4), \quad \text{(E.3)}$$

$$f^{(2)}(x_0) = \frac{-f(x_0+2h) + 16f(x_0+h) - 30f(x_0) + 16f(x_0-h) - f(x_0-2h)}{12h^2} + O(h^4). \quad \text{(E.4)}$$

It is plain that these formulas are very advantageous, since they require only four neighbours points, while the residuals wipe each other out and decay fast. On the other hand, the formulas cannot be used blindly on the borders of a spatial grid. The solution to this issue is to develop a non-symmetric derivative formula to be used on the outer points. This choice has the advantage of being precise, but the drawback of rendering the structure of the objective function, and of its gradient, very involved; moreover, it causes the loss of the symmetry of the Hessian of the Lagrangian. The asymmetric derivatives implementation can be found, at each order of approximation, in many references, e. g. in [58].

E.0.2 Discretized Integration

Integrations have been implemented through two different methods. The first single-particle test of this work uses a rectangles method, namely the Riemann formula. This integration has a very low impact on the objective structure, but it is

very rough, and potentially brings along non-negligible numerical errors.

$$\int dx\, f(x) = \sum_{i=2}^{n_r-1} h f(x_i) + \frac{h}{2}(f(x_1) + f(x_{n_r})) + O(h) \tag{E.5}$$

In order to improve the computation efficiency, we have implemented the Simpson's integration method, which interpolates the integrand through second order polynomials. This method is the one we have used in all of the test except the very first. This formula is symmetric, and it is advantageous for those same reasons of the symmetric derivative formula (E.3). Simpson's quadrature formula reads

$$\int dx\, f(x) = \frac{h}{3}\Big(f(x_0) + \cdots + 4f(x_{2k}) + 2f(x_{2k+1}) + \cdots + f(x_{nr-1})\Big) + O(h^5). \tag{E.6}$$

E.0.3 Linear Solver

Since the implementation of the discrete methods becomes more and more complicated, the direct extraction of the Kohn-Sham potential from the Lagrange multipliers becomes involved to be coded in a smart, general way. The correspondence between the Lagrange multiplier and the Kohn-Sham potential gets partially lost in the discretization of the space and of the numerical methods. Also, the combined usage of two scaling procedures of the problem (one is the redefinition of the orbitals according to the square root of the density, the second is an internal scaling performed by the IPOPT library) contributes to mask the direct relation between the numerical multipliers and the analytic ones. It is far better to separate the calculation of the Kohn-Sham potential and of the multipliers ϵ_{jk} from that of the Kohn-Sham orbitals.

Once IPOPT gives us the Kohn-Sham orbitals, we use them to solve directly the Euler-Lagrange equations with respect to the Lagrange multipliers. This is done via a sparse least-squares linear solver, that we have coded using the EIGEN [1] library's QR decomposition method. The idea is to decompose the matrix A of the equations' coefficients, which is actually a sparse one, as $A = Q * R$, where Q is orthogonal, that is straightforward to be inverted, and R is a sparse triangular or trapezoidal sparse matrix. The solution of the system $Ax = b$ is given by $x = R^{-1}Q^{-1}b = R^{-1}Q^t b$. The exploitation of the sparsity of the matrix improves the computational time.

E.0.4 Implementation

If we use the Riemann formula, together with the five-points derivatives, the objective function takes the form

$$\begin{aligned} J\{\varphi_j(x)\} \sim -\frac{1}{2}\sum_{i=0}^{n_r-1}\sum_{j=0}^{n_p-1} \varphi_{i+jn_r}\Big(\varphi_{i+jn_r}(-\frac{(\widetilde{n}_i')^2}{4n_i} + \frac{\widetilde{n}_i''}{2})h \\ + \widetilde{n}_i' \frac{-\varphi_{i+jn_r+2} + 8\varphi_{i+jn_r+1} - 8\varphi_{i+jn_r-1} + \varphi_{i+jn_r-2}}{12} \\ + \widetilde{n}_i \frac{-\varphi_{i+jn_r+2} + 16\varphi_{i+jn_r+1} - 30\varphi_{i+jn_r} + 16\varphi_{i+jn_r-1} - \varphi_{i+jn_r-2})}{12h} \\ - 2\delta \frac{-\varphi_{i+jn_r+2} + 16\varphi_{i+jn_r+1} - 30\varphi_{i+jn_r} + 16\varphi_{i+jn_r-1} - \varphi_{i+jn_r-2}}{12h}\Big), \end{aligned} \tag{E.7}$$

[1] `https://eigen.tuxfamily.org/`

where n_r is the number of points in the grid, while n_p is the number of particles of the system considered. The gradient of the objective reads

$$\begin{aligned}\frac{\partial f(\varphi_{i+jn_r})}{\partial \varphi_{l+mn_r}} = -\Big(&\varphi_{l+mn_r}\Big(-\frac{(\widetilde{n}_l')^2}{4n_l}+\frac{\widetilde{n}_l''}{2}\Big)h \\ &+\widetilde{n}_l\frac{-\varphi_{l+mn_r+2}+16\varphi_{l+mn_r+1}-30\varphi_{l+mn_r}+16\varphi_{l+mn_r-1}-\varphi_{l+mn_r-2})}{12h} \\ &+2\delta\frac{-\varphi_{l+mn_r+2}+16\varphi_{l+mn_r+1}-30\varphi_{l+mn_r}+16\varphi_{l+mn_r-1}-\varphi_{l+mn_r-2}}{12h}\Big),\end{aligned} \tag{E.8}$$

where $p = 0,\dots,n_r-1$ and $q = 0,\dots,n_p-1$. The constraints are

$$c_i^0 = \sum_{j=0}^{n_p-1}\varphi_{i+jn_r}^2 = 1, \tag{E.9}$$

$$c^{jk} = \sum_{i=0}^{n_r-1} h\widetilde{n}_i\varphi_{i+jn_r}\varphi_{i+kn_r} = \delta_{jk}, \tag{E.10}$$

with $j = 0,\dots,np-1$ and $k = 0,\dots,j$.

The Jacobian of the constraints is a rectangular $(n_r + \frac{n_p(n_p+1)}{2}\times n_r n_p)$ matrix, and reads

$$\begin{bmatrix} 2\varphi_{mn_r} & & & & & \\ & \ddots & & & & \\ & & 2\varphi_{l+mn_r} & & & \\ & & & \ddots & & \\ & & & & 2\varphi_{n_r-1+mn_r} & \\ \dots & & h\widetilde{n}_i(\delta_{i+jn_r,l+mn_r}+\delta_{i+kn_r,l+mn_r}) & & \dots & \end{bmatrix} \tag{E.11}$$

Note that the matrix is always wider than taller, and therefore the system of Euler-Lagrange equations is never under-determined. By further deriving the results obtained right above, we obtain the Hessian of the Lagrangian as a $nr\times np$ square matrix:

$$\begin{bmatrix} & \ddots & & & \\ & \ddots & (-\frac{(\widetilde{n}_i')^2}{4n_i}+\frac{\widetilde{n}_i''}{2})h+\frac{5\widetilde{n}_i+2\delta}{2h}+2\lambda_i^0+2\lambda^{ii} & & \\ & \ddots & -\frac{4(\widetilde{n}_i+2\delta)}{3h} & \ddots & \\ \ddots & & \frac{\widetilde{n}_i+2\delta}{12h} & \ddots & \\ & \lambda^{ij}\widetilde{n}_i h & & \ddots & \\ & & \ddots & & \end{bmatrix} \tag{E.12}$$

Bibliography

[1] H. De Vries, C.W. De Jager, and C. De Vries. Nuclear charge-density-distribution parameters from elastic electron scattering. *Atomic Data and Nuclear Data Tables*, 36(3):495 – 536, 1987.

[2] J. Zenihiro, H. Sakaguchi, T. Murakami, M. Yosoi, Y. Yasuda, S. Terashima, Y. Iwao, H. Takeda, M. Itoh, H. P. Yoshida, and M. Uchida. Neutron density distributions of ^{204,206,208}Pb deduced via proton elastic scattering at E_p = 295 mev. *Phys. Rev. C*, 82:044611, Oct 2010.

[3] J. Dobaczewski, H. Flocard, and J. Treiner. Hartree-fock-bogolyubov description of nuclei near the neutron-drip line. *Nuclear Physics A*, 422(1):103 – 139, 1984.

[4] Richard M. Martin. *Electronic Structure: Basic Theory and Practical Methods*. Cambridge University Press, 2004.

[5] X. Roca-Maza and N. Paar. Nuclear equation of state from ground and collective excited state properties of nuclei. *Progress in Particle and Nuclear Physics*, 101:96 – 176, 2018.

[6] Michael Bender, Paul-Henri Heenen, and Paul-Gerhard Reinhard. Self-consistent mean-field models for nuclear structure. *Rev. Mod. Phys.*, 75:121–180, Jan 2003.

[7] P.-G. Reinhard and W. Nazarewicz. Nuclear charge and neutron radii and nuclear matter: Trend analysis in skyrme density-functional-theory approach. *Phys. Rev. C*, 93:051303, May 2016.

[8] P. Hohenberg and W. Kohn. Inhomogeneous electron gas. *Phys. Rev.*, 136:B864–B871, Nov 1964.

[9] W. Kohn and L. J. Sham. Self-consistent equations including exchange and correlation effects. *Phys. Rev.*, 140:A1133–A1138, Nov 1965.

[10] R. Newton. Inverse problems in physics. *SIAM Review*, 12(3):346–356, 1970.

[11] Ashley H. Carter. A class of inverse problems in physics. *American Journal of Physics*, 68(8):698–703, 2000.

[12] I. Macocco. *Costruzione Del Potenziale Nucleare Efficace Di Kohn-Sham Dalle Densità Empiriche*. Bachelor Thesis. Not Published, 2015.

[13] A. Porro. *Potenziali nucleari da densità e distribuzioni di spin microscopiche*. Bachelor Thesis. Not Published, 2017.

[14] N. Martinez Cuenca. *Deduzione di potenziale medio e massa efficace dei nucleoni dalle densita nucleari*. Bachelor Thesis. Not Published, 2018.

[15] Weitao Yang and Qin Wu. Direct method for optimized effective potentials in density-functional theory. *Phys. Rev. Lett.*, 89:143002, Sep 2002.

[16] Qin Wu and Weitao Yang. A direct optimization method for calculating density functionals and exchange–correlation potentials from electron densities. *The Journal of Chemical Physics*, 118(6):2498–2509, 2003.

[17] Qingsheng Zhao, Robert C. Morrison, and Robert G. Parr. From electron densities to kohn-sham kinetic energies, orbital energies, exchange-correlation potentials, and exchange-correlation energies. *Phys. Rev. A*, 50:2138–2142, Sep 1994.

[18] R. van Leeuwen and E. J. Baerends. Exchange-correlation potential with correct asymptotic behavior. *Phys. Rev. A*, 49:2421–2431, Apr 1994.

[19] Yue Wang and Robert G. Parr. Construction of exact kohn-sham orbitals from a given electron density. *Phys. Rev. A*, 47:R1591–R1593, Mar 1993.

[20] Qingsheng Zhao and Robert G. Parr. Quantities t_s[n] and t_c[n] in density-functional theory. *Phys. Rev. A*, 46:2337–2343, Sep 1992.

[21] Andreas Görling. Kohn-sham potentials and wave functions from electron densities. *Phys. Rev. A*, 46:3753–3757, Oct 1992.

[22] Daniel S. Jensen and Adam Wasserman. Numerical density-to-potential inversions in time-dependent density functional theory. *Phys. Chem. Chem. Phys.*, 18:21079–21091, 2016.

[23] M.G. Mayer and J.H.D. Jensen. *Elementary Theory of Nuclear Shell Structure*. Structure of matter series. John Wiley & Sons, 1955.

[24] A. L. Fetter and J. D. Walecka. *Quantum Theory of Many-Particle Systems (Dover Books on Physics)*. Dover Publications, June 2003.

[25] P. Ring and P. Schuck. *The Nuclear Many-Body Problem (Theoretical and Mathematical Physics)*. Springer, May 2005.

[26] A. Bohr and B.R. Mottelson. *Nuclear Structure*. Number v. 1 in Nuclear Structure. World Scientific, 1998.

[27] T. H. R. Skyrme. The effective nuclear potential. *Nuclear Physics*, 9(4):615 – 634, 1958–1959.

[28] J. Dechargé and D. Gogny. Hartree-fock-bogolyubov calculations with the $d1$ effective interaction on spherical nuclei. *Phys. Rev. C*, 21:1568–1593, Apr 1980.

[29] T. Nikšić, D. Vretenar, and P. Ring. Relativistic nuclear energy density functionals: Mean-field and beyond. *Progress in Particle and Nuclear Physics*, 66(3):519 – 548, 2011.

[30] W. Kohn. v-representability and density functional theory. *Phys. Rev. Lett.*, 51:1596–1598, Oct 1983.

[31] H. Englisch and R. Englisch. Hohenberg-kohn theorem and non-v-representable densities. *Physica A: Statistical Mechanics and its Applications*, 121(1):253 – 268, 1983.

[32] T. L. Gilbert. Hohenberg-kohn theorem for nonlocal external potentials. *Phys. Rev. B*, 12:2111–2120, Sep 1975.

[33] R.G. Parr and Y. Weitao. *Density Functional Theory of Atoms and Molecules*. International Series of Monographs on Chemistry. Oxford University Press, 1994.

[34] Mel Levy. Electron densities in search of hamiltonians. *Phys. Rev. A*, 26:1200–1208, Sep 1982.

[35] Elliott H. Lieb. *Density Functionals for Coulomb Systems*, pages 269–303. Springer Berlin Heidelberg, Berlin, Heidelberg, 2002.

[36] Klaus Capelle. A bird's-eye view of density-functional theory. *Brazilian Journal of Physics*, 36(4A):1318–1343, 2006.

[37] J. Kaipio and E. Somersalo. *Statistical and Computational Inverse Problems*. Applied Mathematical Sciences. Springer New York, 2006.

[38] V. I. Arnold. *Catastrophe Theory*. Springer-Verlag Berlin Heidelberg, 1984.

[39] Jari Kaipio and Erkki Somersalo. Statistical inverse problems: Discretization, model reduction and inverse crimes. *Journal of Computational and Applied Mathematics*, 198(2):493 – 504, 2007. Special Issue: Applied Computational Inverse Problems.

[40] A. N. Tikhonov. On the solution of ill-posed problems and the method of regularization. *Dokl. Akad. Nauk SSSR*, 151:501–504, 1963.

[41] O. Scherzer. The use of morozov's discrepancy principle for tikhonov regularization for solving nonlinear ill-posed problems. *Computing*, 51(1):45–60, Mar 1993.

[42] J. T. Chayes, L. Chayes, and Mary Beth Ruskai. Density functional approach to quantum lattice systems. *Journal of Statistical Physics*, 38(3):497–518, Feb 1985.

[43] M. E. Rose. The charge distribution in nuclei and the scattering of high energy electrons. *Phys. Rev*, 73:279 – 284, Feb 1948.

[44] Robert Hofstadter. Electron scattering and nuclear structure. *Rev. Mod. Phys.*, 28:214–254, Jul 1956.

[45] J. Negele. *Advances in Nuclear Physics*. Number v. 15 in Advances in Nuclear Physics. Springer US, 2013.

[46] Andreas Wächter and Lorenz T. Biegler. On the implementation of an interior-point filter line-search algorithm for large-scale nonlinear programming. *Mathematical Programming*, 106(1):25–57, Mar 2006.

[47] Philip M. Morse. Diatomic molecules according to the wave mechanics. ii. vibrational levels. *Phys. Rev.*, 34:57–64, Jul 1929.

[48] S. Wilson. *Handbook of Molecular Physics and Quantum Chemistry: Molecules in the physico-chemical environment: spectroscopy, dynamics and bulk properties*. Handbook of Molecular Physics and Quantum Chemistry: Spectroscopy, Dynamics and Bulk Properties. Molecules in the Physico-chemical Environment. Wiley, 2003.

[49] Jens Peter Dahl and Michael Springborg. The morse oscillator in posititon space, momentum space, and phase space. *Journal of Chemichal Pysics*, 88(7):4535–4547, 1988.

[50] J. Lafontaine. *An Introduction to Differential Manifolds*. Springer International Publishing, 2015.

[51] D.P. Bertsekas and W. Rheinboldt. *Constrained Optimization and Lagrange Multiplier Methods*. Computer science and applied mathematics. Elsevier Science, 2014.

[52] H. P. Breuer and F. Petruccione. *The theory of open quantum systems*. Oxford University Press, Great Clarendon Street, 2002.

[53] J. Dobaczewski and J. Dudek. Time-odd components in the rotating mean field and identical bands. *Acta Phys.Polon. (1996)*, B27:45–58, Oct 1995.

[54] J. Dobaczewski and J. Dudek. Time-odd components in the mean field of rotating superdeformed nuclei. *Phys. Rev. C*, 52:1827–1839, Jan 1995.

[55] K. Heyde. *Basic Ideas and Concepts in Nuclear Physics: An Introductory Approach, Second Edition*. Taylor & Francis, 1998.

[56] D.S. Koltun and J.M. Eisenberg. *Quantum mechanics of many degrees of freedom*. Wiley-Interscience publication. Wiley, 1988.

[57] Zhihong Ye, John Arrington, Richard J. Hill, and Gabriel Lee. Proton and neutron electromagnetic form factors and uncertainties. *Physics Letters B*, 777:8 – 15, 2018.

[58] W. H. Press, S. A. Teukolsky, W. T. Vetterling, and B. P. Flannery. *Numerical Recipes 3rd Edition: The Art of Scientific Computing*. Cambridge University Press, New York, NY, USA, 3 edition, 2007.